Cuffless Blood Pressure Estimation Using Cardiovascular Dynamics

Hamed Samimi

Thesis submitted to the University of Ottawa
in partial Fulfillment of the requirements for the degree of
Doctor of Philosophy in Electrical and Computer Engineering

School of Electrical Engineering and Computer Science
Faculty of Engineering
University of Ottawa

Abstract

Blood pressure (BP) monitoring is an important tool for management of hypertension, which is a significant risk for cardiovascular disease and premature death. Since cuff-based BP measurement can be uncomfortable and does not provide continuous readings, several cuffless methods that are typically based on within-beat information or on the pulse transit time (PTT) have recently been investigated. This work proposes a novel cuffless BP estimation approach that mainly uses the information from cardiovascular dynamics of photoplethysmogram (PPG) waveforms.

This work is divided into three parts. The first part proposes a calibration-free approach that uses dynamic changes in the pulse waveform. Results from 200 patients showed that the method achieved grade B, in terms of accuracy, for diastolic blood pressure (DBP) based on the British Hypertension Society (BHS) standard and complied with the accuracy requirements of the Association for Advancement of Medical Instrumentation/European Society of Hypertension/International Organization for Standardization (AAMI/ESH/ISO) standard. The second part presents a method based on calibrated cardiovascular dynamics, achieved through a mathematical model that relates reflective PTT (R-PTT) to BP. Results from 30 patients showed a mean error (ME) of 0.58 mmHg, standard deviation of the error (SDE) of 8.13 mmHg, and a mean absolute error (MAE) of 4.93 mmHg for DBP and an ME of 2.52 mmHg, SDE of 12.28 mmHg, and an MAE of 8.82 mmHg for systolic blood pressure (SBP). The third part proposes a calibration-free method that combines morphology features and dynamic changes of the pulse waveform over short intervals. In this method a neural network was trained on 200 patients and tested on never-seen data from 25 other patients and provided an ME of -0.31 mmHg, SDE of 4.89 mmHg, and MAE of 3.32 mmHg for DBP and an ME of -4.02 mmHg, SDE of 10.40 mmHg, and MAE of 7.41 mmHg for SBP. Overall, the results show that cardiovascular dynamics may contribute useful information for cuffless estimation of BP.

Acknowledgements

I would like to thank my supervisor, Dr. Hilmi Dajani for allowing me to work on this project, and for his mentorship, guidance and continuous support throughout this work. I am also grateful for the advice that I received from the members of my supervisory committee, Dr. Miodrag Bolic and Dr. Adrian Chan.

My gratitude also goes to my family, for their unwavering patience and kindness without whose support completing this work would have been much more difficult if not impossible.

Table of Contents

List of Figures

List of Tables

List of Acronyms and Abbreviations

AAMI	Association for Advancement of Medical Instrumentation
ABP	Arterial Blood Pressure
AC	Alternating Current
ANN	Artificial Neural Network
ANS	Autonomic Nervous System
BHS	British Hypertension Society
BP	Blood Pressure
BPV	Blood Pressure Variability
BRS	Baroreflex Sensitivity
CVD	Cardiovascular Disease
DBP	Diastolic Blood Pressure
DC	Direct Current
DCT	Discrete Cosine Transform
DFA	Detrended Fluctuation Analysis
ECG	Electrocardiogram
ESH	European Society of Hypertension
HF	High Frequency
HRV	Heart Rate Variability
HRVAS	Heart Rate Variability Analysis Software
IBI	Inter-Beat Interval
ICU	Intensive Care Unit
ISO	International Organization for Standardization
LSP	Lomb-Scargle Periodogram
LSTM	Long Short-Term Memory
MAE	Mean Absolute Error
ME	Mean Error
MIMIC	Multiparameter Intelligent Monitoring in Intensive Care
MLR	Multiple linear regression
mPTP	Mean Point-to-Point Pairing
MRI	Magnetic Resonance Imaging
oPTP	One Point-to-Point Pairing
PAT	Pulse Arrival Time
PCA	Principal Component Analysis
PPG	Photoplethysmogram
PRVti	Pulse Rate Variability Triangular Index
PSD	Power Spectral Density
PTT	Pulse Transit Time
PWV	Pulse Wave Velocity
R-PTT	Reflective PTT

SA	Sino Arterial
SAFE	Sensitivity Analysis For Everyone
SBP	Systolic Blood Pressure
SDE	Standard Deviation of Error
SNA	Sympathetic Nerve Activity
SVM	Support Vector Machine
TINN	Triangular Interpolation of IBI Histogram
TPOT	Tree Based Pipeline Optimization Tool
UCI	University of California Irvine
VLF	Very Low Frequency

Chapter 1: Introduction

1.1 Motivation

Cardiovascular disease (CVD) is the leading cause of mortality worldwide. According to the World Health Organization, 32% of deaths in 2019 were related to cardiovascular issues. This accounts for 17.9 million people (World Health Organization, 2021). Two important factors that contribute to CVD are hypertension and long-term variability in blood pressure (BP) (Chao et al., 2021; Yang et al., 2021). In order to reduce the effect of the above-mentioned two elements and consequently reduce mortality due to CVD, BP monitoring over extended periods is necessary and is currently practiced by doctors (Pandey et al., 2021). However, conventional BP measurement that relies on inflating and deflating a cuff to measure BP is not convenient and only provides intermittent readings. BP is a quasi-periodic signal that swings between an upper and a lower bound. The maximum value is called systolic blood pressure (SBP) and the minimum value is called diastolic blood pressure (DBP). A person is diagnosed with hypertension if at rest condition his/her systolic or diastolic blood pressure exceeds 130 or 80 mmHg respectively based on the American College of Cardiology and the American Heart Association updated definition in 2017. At the same time, SBP between 120 and 129mmHg is considered elevated (Tamura, 2021).

Accurate measurement of blood pressure is achieved by either invasive or non-invasive methods. The invasive method is usually performed in clinical settings by placing a cannula needle directly in an artery. This is the most accurate way to measure blood pressure and provides a continuous reading of changes in BP; however, because of the nature of this method, it could cause infection and other serious complications. On the other hand, the commonly-used non- invasive method eliminates the requirement of direct access to the artery, but it cannot provide continuous measurement due to periodic cuff inflation and deflation. It is also less accurate compared to the invasive method. In addition, cuff inflation

applies pressure on the measuring limb and that results in discomfort and can disturb sleep when making nocturnal measurements (Zambrana-Vinaroz et al., 2019). Due to above mentioned limitations for both invasive and non-invasive monitoring, there is a need for a different method that provides the possibility of collecting continuous blood pressure measurement in a more comfortable way.

In recent years, cuffless blood pressure monitoring has been researched as a potential candidate approach to overcome some of the problems that were discussed earlier. Among different methods, most cuffless BP monitoring is based on the photoplethysmogram (PPG) and the electrocardiogram (ECG). The PPG is an optical method that measures changes in blood volume each time that heart pumps blood to the body. On the other hand, the ECG is a measure of electrical activity of the heart. Many studies have considered both of these signals together to determine pulse transit time (PTT) or pulse arrival time (PAT) and use them as the main indicator to monitor blood pressure without a cuff. There are also other studies that have used morphology of individual beats in PPG to estimate blood pressure (Sagirova et al., 2021). These methods among others are discussed in more detail in the coming sections. Although the majority of cuffless blood pressure monitoring research has been conducted using PTT/PAT or the morphology of individual beats in PPG, they both have limitations. Most PTT based devices (such as healthwatches) do not perform continuous measurement, and PPG based methods have been limited to experimental models that were investigated on small groups of people (Sagirova et al., 2021).

Since the cardiovascular system is dynamic and whose hemodynamic parameters depend on the properties and health of the system, including the blood pressure, we hypothesized that the information contained in the oscillations and in the changes of the parameters of the system may aid in the estimation of the blood pressure. Furthermore, most cuffless methods aim to provide beat-by-beat estimates of BP. However, in most situations, this density of estimates is not needed and estimates every few minutes would be sufficient. This possibility

to work over intervals of a few minutes allows us to measure various dynamic parameters and use them in BP estimation as will be shown in the thesis.

Therefore, the key difference between our approach and most currently-used approaches for cuffless BP estimation is that we rely on dynamic changes in cardiovascular parameters over consecutive intervals of a few minutes, instead of relying on beat-by-beat changes in PTT or morphology.

1.2 Objectives

Our main objective, unlike other works, is to use dynamics of cardiovascular system for estimation of blood pressure. In this research, we investigate the relationship between pulse waveform oscillation and blood pressure. The main difference between our work and previous studies is that not only will we be using the PPG signal without accompanying ECG, but also we will be focusing on dynamics of the signal by analysing intervals over a number of beats.

There have been many studies done on the subject of cuffless blood pressure estimation over the last few years; however, despite the claims of high accuracy (that is, having estimated and the reference BP values being close to each other) in laboratory studies, this remains an unsolved problem as evidenced by the lack of commercially available cuffless devices that accurately and reliably estimate BP and which have been validated in accordance with the 2014 IEEE Standard for Wearable, Cuffless BP measuring Devices (IEEE Standard Association, 2014) or the 2019 amendment to it (IEEE Standard Association, 2019) (Cox, et at., 2022). With all the advancements that have taken place so far in this field, the need for an accurate cuffless blood pressure monitoring system is still on top of many clinicians' wish list (Ando, 2014; Stergiou et al., 2022; Chrysant, 2022).

In continuous monitoring of BP (measuring blood pressure without interruptions even as one sleeps), beat-by-beat estimation is rarely required (and possibly only during complex operations). Instead, obtaining estimates every few minutes (e.g. 5 minutes) would be

sufficient for most needs (Sola et al., 2016). This opens up the possibility of using signal dynamics and statistics over consecutive intervals whose duration is a few minutes each. We propose that information about the PPG dynamics and statistics may be useful for estimating BP either on its own or in combination with standard approaches that have been used in the past (e.g. morphology features within individual pulses or averaged over several pulses). This is a novel approach to cuffless blood pressure estimation and to our knowledge there is no previous work that has systematically investigated this approach. As a result, this work could help us to provide an accurate and reliable non-invasive cuffless blood pressure monitoring that only relies on collection of the PPG signal.

In this research, we discuss our methodologies for cuffless blood pressure measurement in detail along with estimation results that have been obtained. Our work consists of three distinct sections that are all built on the idea of using information from cardiovascular dynamics obtained from a single PPG sensor to estimate blood pressure without use of a cuff. In this study we use the terms cardiovascular dynamics and cardiovascular oscillations interchangeably to refer to alterations over time in arterial blood pressure or the PPG. These three sections, written in the form of articles, describe the following proposed approaches:

1. Calibration-free cuffless blood pressure estimation using cardiovascular dynamics.

2. Calibrated cuffless blood pressure estimation using a combination of cardiovascular dynamics and a mathematical calibration model.

3. Calibration-free cuffless blood pressure estimation using a combination of cardiovascular dynamics and pulse morphology.

1.3 Thesis Organization

This thesis is divided into six chapters which include the introduction (Chapter 1), a background review on cardiovascular system and blood pressure measurement methods (Chapter 2), a concluding chapter (Chapter 6) and three chapters (Chapters 3, 4 and 5)

representing each of the three sections that were mentioned in the section above on the objectives. This thesis is presented as a series of independent articles that have been submitted to peer reviewed scientific publications. As a result, some overlap in the information provided in the papers may be observed. In more detail, the following chapters are:

Chapter 2: Background

This chapter provides a comprehensive background on human cardiovascular system as well as different methods that are used for blood pressure measurement.

Chapter 3: Cuffless blood pressure estimation using cardiovascular dynamics, Samimi, H., & Dajani, H.R. (2022). In Proceedings of the International Conference on Electrical, Computer and Energy Technologies (ICECET), Prague, Czech Republic. Available from: https://ieeexplore.ieee.org/document/9872800.

This chapter presents the result of the proposed methodology for cuffless blood pressure estimation through cardiovascular dynamics.

Chapter 4: Cuffless blood pressure estimation using calibrated cardiovascular dynamics in the photoplethysmogram, Samimi, H., & Dajani H.R. (2022), *Bioengineering*, Special Issue on Machine Learning for Biomedical Applications, 9(446).

This chapter proposes new technique to calibrate the cuffless blood pressure estimation system to achieve a higher accuracy and summarizes the results of the experiments conducted to evaluate the proposed method.

Chapter 5: A PPG-based calibration-free cuffless blood pressure estimation method using cardiovascular dynamics, Samimi, H., & Dajani, H.R. (2023), Sensors, Special Issue on Recent Advancements in Sensor Technologies for Healthcare and Biomedical Applications (Volume II), 23(4145).

In this chapter, the possibility of using information from waveform morphology in addition to the information from cardiovascular dynamics for cuffless blood pressure estimation is investigated. The results of experiments for a calibration-free method are presented and discussed.

Chapter 6: Conclusions and Future Work

This is a final chapter and presents a discussion related to all aspects of the thesis. It also summarizes the work that was done and proposes avenues for future work.

Addendum

This section contains several notes and clarifications related to material found in the chapters mentioned above.

1.4 References

Ando, S. (2014). What does a perfect blood pressure meter look like from a clinician point of view? *IEEE Instrumentation & Measurement Magazine*, *17*(3), 15-20.

Chao, P.C.P., Wu, C.C., Nguyen, D.H., Nguyen, B.S., Huang, P.C., & Le, V.H. (2021). The machine learnings leading the cuffless PPG blood pressure sensors into the next stage. *IEEE Sensors Journal, 21*(11), 12498-12510.

Chrysant, S.G. (2022). Relatability of blood pressure monitoring with wearable cuffless devices. *American Journal of Cardiology, 169*, 145-147.

Cox, J., Louka, K., Avolio, A.P., Tan, I., & Butlin, M. (2022). Are commercial cuffless blood pressure devices being validated? *Journal of Hypertension, 40*(Suppl 1), e104.

IEEE Standard Association. (2014). *IEEE Standard for Wearable Cuffless Blood Pressure Measuring Devices (1708-2014)*, 1-38.

IEEE Standard Association. (2019). *IEEE Standard for Wearable Cuffless Blood Pressure Measuring Devices: amendment 1 (1708a-2019)*.

Pandey, R.K., Lin, T.Y., & Chao, P.C.P. (2021). Design and implementation of a photoplethysmography acquisition system with an optimized artificial neural network for accurate blood pressure measurement. *Microsystem Technologies, 27*(3), 1-23.

Sagirova, Z., Kuznetsova, N., Gogiberidze, N., Gognieva, D., Suvorov, A., Chomakhidze, P., Omboni, S., Saner, H., & Kopylov, P. (2021). Cuffless blood pressure measurement using a smartphone-case based ECG monitor with photoplethysmography in hypertensive patients. *Sensors*, 21(10), 3525.

Sola, J., Proenca, M., Braun, F., Pierrel, N., Degiorgis, Y., Verjus, C., Lemay, M., Bertschi, M., & Schoettker, P. Continuous non-invasive monitoring of blood pressure in the operating room: a cuffless optical technology at the fingertip. *Current Directions in Biomedical Engineering, 2*(1), 267-271.

Stergiou, G.S., Mukkamala, R., Avolio, A., Kyriakoulis, K.G., Mieke, S., Murray, A., Parati, G., Schutte, A.E., Sharman, J.E., Asmar, R., McManus, R.J., Asayama, K., De La Sierra, A., Head, G., Kario, K., Kollias, A., Myers, M., Niiranen, T., Ohkubo, T., Wang, J., Wuerzner, G., O'Brien, E., Kreutz, R., Palatini, P. (2022). Cuffless blood pressure measuring devices: review and statement by the European Society of Hypertension Working Group on Blood Pressure Monitoring and Cardiovascular Variability. *Journal of Hypertension, 40*(8), 1449-1460.

Tamura, T. (2021). Cuffless blood pressure monitors: principles, standards and approval for medical use. *IEICE Transactions on Communications, E104B*(6).

Yang, S., Sohn, J., Lee, S., Lee, J., & Kim, H.C. (2021). Estimation and validation of arterial blood pressure using photoplethysmogram morphology features in conjunction with pulse arrival time in large open databases. *IEEE Journal of Biomedical and Health Informatics, 25*(4), 1018-1030.

World Health Organization. (2021, June 11). *Cardiovascual Diseases (CVD)*. https://www.who.int/news-room/fact-sheets/detail/cardiovascular-diseases-(cvds).

Zambrana-Vinaroz, D., Vicente-Samper, J.M., Juan, C.G., Esteve-Sala, V., & Sabater-Navarro, J.M. (2019). Non-invasive device for blood pressure wave acquisition by means of mechanical transducer. *Sensors*, *19*(19), 4311-4323.

Chapter 2: Background

2.1 The Cardiovascular System

The human body consists of many component systems such as the nervous system, digestive system, and cardiovascular (circulatory) system. Each system itself is divided into a number of subsystems that carry out different physiological tasks. For example, by pumping blood from the heart the cardiovascular system oversees transporting nutrients to the cells and transporting waste products from cells. At the same time, it carries deoxygenated blood to the lungs and the oxygenated blood back to the tissues. The result of this circulation is purification of the metabolic waste and carbon dioxide contained in the blood. It also allows the body tissues to receive nutrients and oxygen (Acharya et al., 2007). Figure 2-1 shows a simplified block diagram of the cardiovascular system related to blood pressure (Fossion et al., 2020). It is important to note that this system is dynamic, even at rest. That is, the different hemodynamic parameters (e.g. heart rate, blood pressure) fluctuate constantly over time, as the system seeks to maintain adequate blood supply to the tissues.

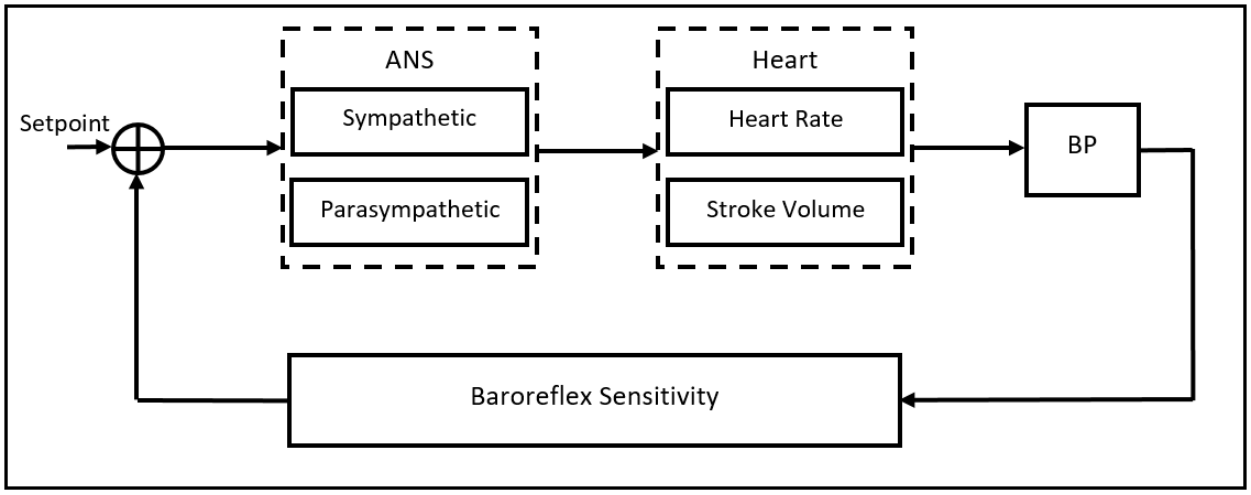

Figure 2-1. Simplified block diagram of human cardiovascular system considering BP. In this diagram setpoint is the targeted (ideal) BP value and ANS is the autonomic nervous system**.** This diagram is created based on the work done by Fossion et al., 2020.

2.1.1 The Autonomic Nervous System

The autonomic nervous system (ANS) (a division of the nervous system that non-voluntarily controls systems of the body) consists of two branches: sympathetic and parasympathetic. The sympathetic branch stimulates functioning of an organ and is associated with low frequency oscillations in the cardiovascular system (0.04-0.15Hz), whereas the parasympathetic branch constrains functioning of the same organ and is associated with higher frequency oscillations (0.15-0.4Hz). An increase in sympathetic stimulation results in heart rate increase whereas an increase in parasympathetic stimulation results in heart rate decrease. Although both sympathetic and parasympathetic systems are active at rest, to maintain the heart rate below 70 beats per minute, parasympathetic stimulation dominates (Acharya et al., 2007).

2.1.2 The Heart

The heartbeat originates at the sino-atrial (SA) node in the right atrium of the heart. This is where an electrical impulse that leads to heart muscle contraction is generated. At rest, the electrical impulses are generated at the rate of 100 to 120 pulses per minute by the SA node. However, since the autonomic nervous system has continuous control over the SA node firing, the heart rate at rest for a healthy heart will not approach this value, and generally remains between 50 to 70 beats per minute (Acharya et al., 2007). Figure 2-2 below illustrates various parts of the human heart.

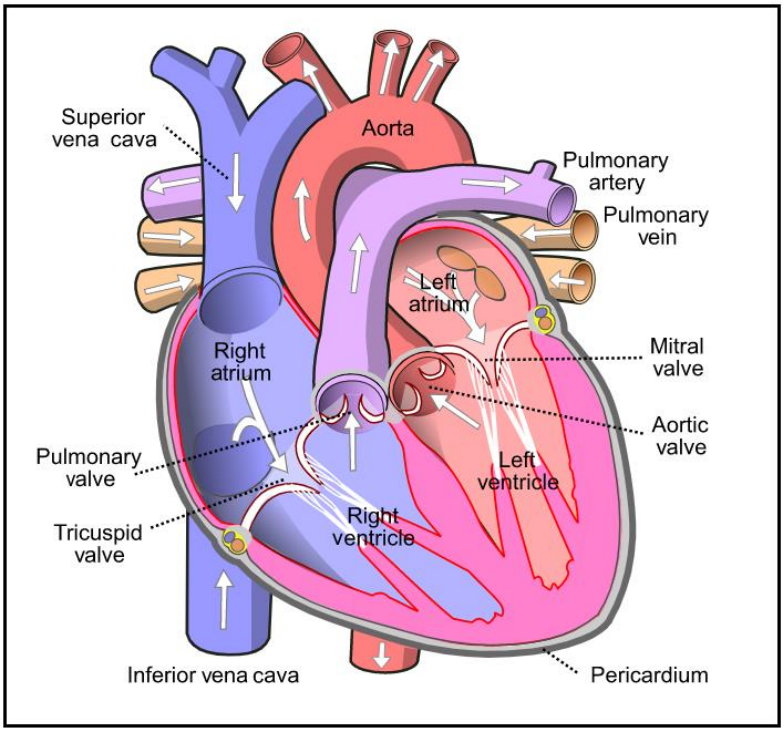

Figure 2-2. Anatomy of the human heart (adapted from Wikimedia Commons at https://upload.wikimedia.org/wikipedia/commons/e/e5/Diagram_of_the_human_heart_%28cropped%29.svg).

The heart is responsible to circulate blood in the body. The amount of blood that heart pumps through the systemic circulation is measured in liters per minute and it is called cardiac output, which is equal to the product of the heart rate by the stroke volume. Cardiac output is one of the physiological factors that affects BP and is directly proportional to it (Chaudhry et al., 2020). Every time that the systolic cardiac contraction happens, a certain amount of blood pumps out of the left ventricle of the heart. The amount of blood that is pumped out through this action is called the stroke volume (Ortiz-Rangel et al., 2021). Stroke volume is used to assess cardiac pump function and organ perfusion as well as for assessment of cardiac dysfunction in patients with congestive heart failure (Bruss and Raja, 2021). Stroke volume and as a result cardiac output need to be sustained in a healthy hemodynamically stable person to minimize a mismatch between the supply and demand for oxygen by an organ. Any increase in demand for oxygen by an organ (due to exercise, etc.) will require an increase of

the cardiac output which leads to an increase of the stroke volume and the heart rate (Vieira et al., 2016).

2.1.3 Blood Pressure

The arterial system circulates blood throughout the body. It delivers oxygenated blood to the tissues through continuous capillary flow. With each contraction of the ventricle, a pulsatile pressure and a pulsatile flow is created. The pressure pulse gets transmitted to the most peripheral arteries right after the contraction, while the blood flow takes number of cardiac cycles to get to the same distance (Ranganathan et al., 2007). As the blood flow reaches arteries, their diameter increases to accommodate the volume surge. The arteries then contract as the generated elastic energy is released. The distention and contraction of the arteries generate a beating effect or a pulse. Since the arterial pulse follows the heartbeat and propagates in the form of waves it is referred to as arterial pulse waves (Alastruey et al., 2012). Figure 2-3 below shows examples of such waveforms. As shown in this figure, blood pressure can be measured in different places along the arterial path; however, the location where the measurement is taken makes a difference in the waveform due to different factors such as volume effect, pressure in the vessels, or reflection.

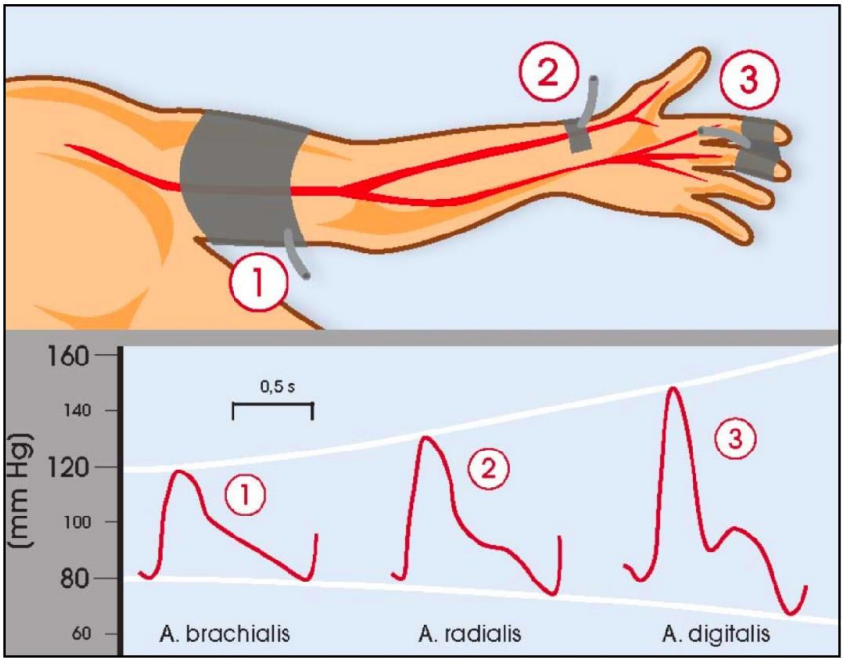

Figure 2-3. Blood pressure waves measured along the arterial pathway (adapted from Wikimedia Commons at: https://commons.wikimedia.org/wiki/File:Arterial_Pathway.jpg).

Vessels have different elasticity depending on their distance from the heart, and the ones closer to the heart are more elastic. This can be explained by Laplace's law, which states that the volume has a direct effect on the tension or in other words tension is in direct relation to pressure and radius:

$$\mathbf{Tension} = \mathbf{Pressure} \times \mathbf{Radius} \qquad \textbf{Equation 2-1}$$

for a thin-walled cylinder and

$$\mathbf{Tension}\ \boldsymbol{\alpha}\ \mathbf{Pressure} \times \left({}^{\boldsymbol{Radius}}/_{\boldsymbol{2h}}\right) \qquad \textbf{Equation 2-2}$$

for a thick-walled cylinder, where $\mathbf{h}$ is thickness of the wall.

As the vessels get further from the heart, they become narrower but the total cross section of multiple vessels increases. As a result, each vessel receives a smaller volume of the blood and therefore does not need to handle the same amount of tension. This is the reason that the peripheral vessels have thicker walls (relative to the cross section) and are

less elastic; hence to get the same amount of change in the diameter of the peripheral vessels, they require much more pressure (Ranganathan et al., 2007).

As was mentioned earlier, the pressure pulse is different from the blood flow. As the pressure pulse travels to the peripheral vessels it changes in shape. Even though the mean pressure decreases as the vessels get further and further from the heart, the pulse pressure - which is the difference between the systolic and diastolic pressures - increases and consequently the peak pressure increases as the wave propagates (Ranganathan et al., 2007). This effect is shown in Figure 2-3 where the amplitude of the curve of the pulse wave increases as a result of wave propagation.

Another factor that affects the shape and amplitude of the pulse wave contour is reflection. Studies have shown that if an artificial pressure pulse wave is applied to a closed tube filled with fluid, it gets reflected. In the arterial tree, this reflection happens at the branching points (Ranganathan et al., 2007). The fact that the pulse pressure increases at the peripheral arteries despite the decrease in the mean pressure, is another reason to believe that the reflection contributes to this effect.

In general, the shape of the arterial pressure waveform depends on the incident wave, the intensity and the timing of the reflection, and the ejection time. Figure 2-4 below illustrates a typical arterial pulse waveform. In this figure, wave A is the arterial pulse waveform and wave B is the corresponding recorded ECG. In a healthy person, the reflected wave appears in the diastolic phase, which occurs at the end of systolic phase and after the closure of the aortic valve. The closing of the aortic valve marks the dicrotic notch and the time interval between dicrotic notch and the following diastolic pressure point is referred to as the diastolic phase (Singh and Sunkaria, 2017). The intensity and timing of reflection becomes important since the reflected wave can enter the systolic phase and affect the systolic peak. The speed of reflection is directly related to the stiffness of the vessels (the stiffer the arteries, the faster is the reflection velocity).

Monitoring arterial pulse pressure is important since it can reveal information about underlying cardiovascular conditions. Low pulse pressure could indicate that there is not sufficient blood flow in the body and this could ultimately cause heart failure. On the other hand, a high arterial pulse pressure could point to a malfunctioning heart valve or some other conditions.

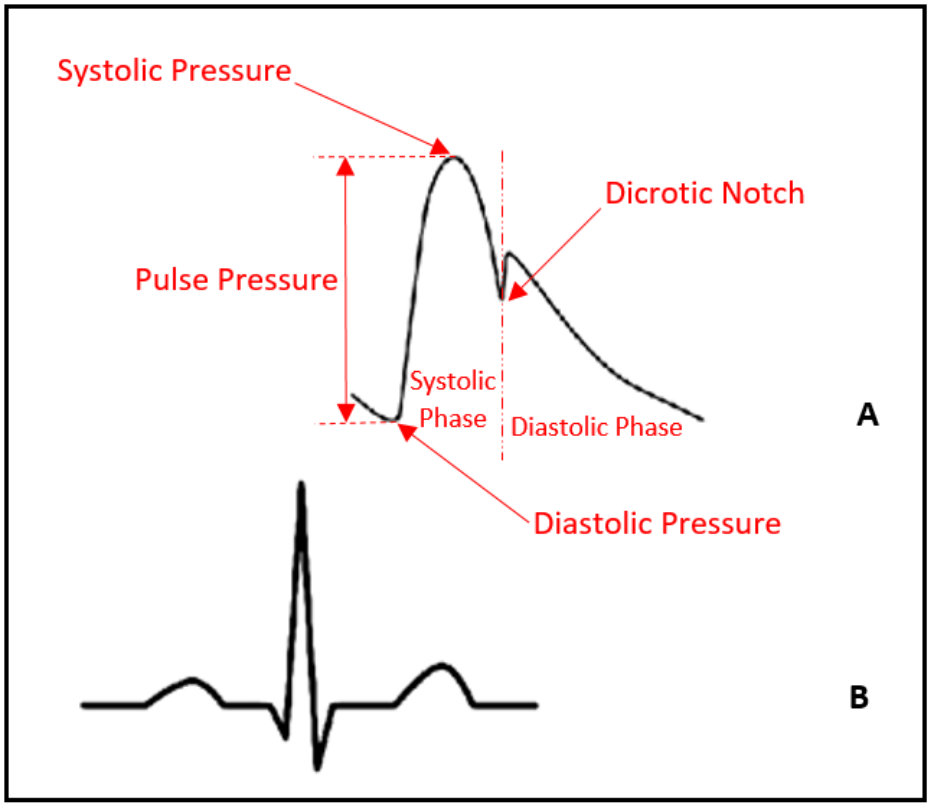

Figure 2-4. Arterial pulse waveform and related ECG signal (adapted with modification from Wikimedia Commons at https://upload.wikimedia.org/wikipedia/commons/8/85/Arterial-blood-pressure-curve.svg and https://upload.wikimedia.org/wikipedia/commons/9/9e/SinusRhythmLabels.svg).

2.1.4 Baroreflex Sensitivity

The baroreflex is a basic mechanism that regulates blood pressure in the short term. Baroreceptors provide the autonomous nervous system (ANS) with continuous information on changes in blood pressure. The ANS in return provides two feedback responses to this information. If baroreceptors report an increase in blood pressure, then the ANS responds with a decrease in heart rate (increase in the pulse intervals) and also decrease in arterial

stiffness resulting in lowering the blood pressure as a feedforward effect. Conversely, if baroreceptors register a decrease in blood pressure, the ANS increases the heart rate and arterial stiffness resulting in an increase of the blood pressure (Bogachev et al., 2015). Figure 2-5 represents a simplified mechanism of the arterial baroreflex system.

Baroreflex sensitivity is defined as the change in inter-beat intervals per unit change of blood pressure (Swenne, 2013). Impairment of baroreflex mechanism often is the cause for cardiovascular diseases; it can result in hypertension, coronary artery disease, myocardial infarction and heart failure (La Rovere et al., 2008).

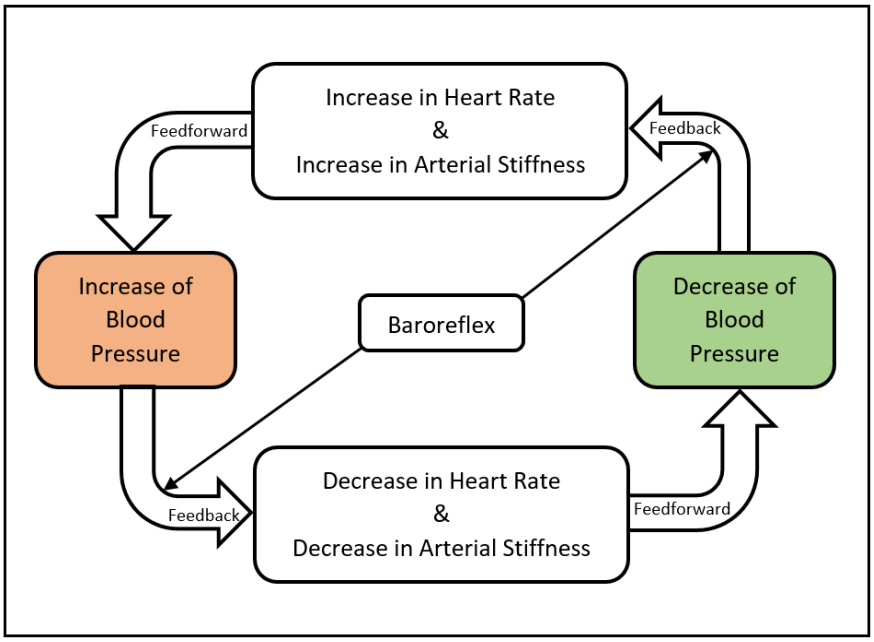

Figure 2-5. Simplified Baroreflex model (adapted with modification from Bogachev et al., 2015).

2.1.5 Cardiovascular Oscillations

Cardiovascular oscillations can be measured in arterial blood pressure, heart rate variability, blood flow, near infrared spectroscopy, and retinal arterial vessel diameters (Rieger et al., 2018). Heart rate variability (HRV) and blood pressure variability (BPV) are considered as useful measures that carry information about the cardiovascular control mechanism. HRV corresponds to the changes in heart rate over time. HRV analysis is important as it reveals

the state of the sympathetic and parasympathetic branches of the ANS and the overall cardiac health. HRV is age and gender dependent, as it decreases with age and variation is higher in females compared to males. There are other factors that could affect HRV such as respiration (HRV increases with decreasing respiration frequency), drugs, smoking (HRV decreases with smoking), alcohol (HRV decreases with acute ingestion of alcohol), etc. (Acharya et al., 2007). Figure 2-6 below illustrates heart rate variability.

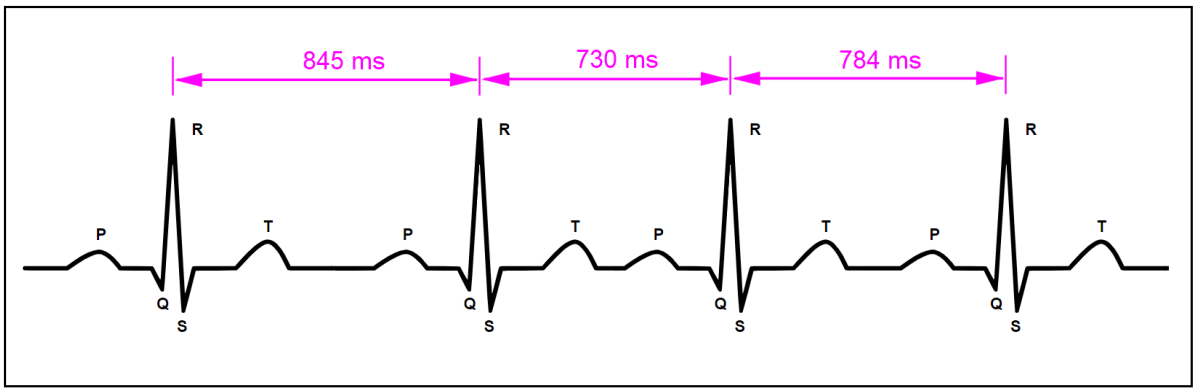

Figure 2-6. Demonstration of heart rate variability by showing beat to beat variation of R-R interval in ECG signal.

HRV can be analyzed using a number of different methods such as time domain analysis including geometrical method, Poincaré geometry, and frequency domain analysis. Time domain analysis is used to distinguish two types of heart rate variability; fast changes in heart rate (short term variability) and slow changes in heart rate (long term variability). Both changes are determined using the R-R intervals over a certain time window. The geometrical method uses R-R intervals and takes advantage of various geometrical approaches such as the triangular index. Poincaré geometry is another approach related to the geometrical method where the Poincaré plot is used to plot each R-R interval against the next interval. This plot provides beat to beat information as well as summary information (Acharya et al., 2007). Frequency domain analysis on the other hand is used to obtain the heart rate variability in a specific frequency range. Cardiac signals are usually expressed as beats per minute (that is a unit of frequency) rather than based on the duration of a beat or the interval between beats (that is a unit of time) (Rangayyan, 2001).

Spectral analysis of HRV can be performed on both the short term, typically with signal durations of a few minutes as well as on the long term, which involves dividing a 24 hours ECG recording into consecutive epochs of a few minutes and averaging parameters over all the epochs. However, to obtain a better evaluation of HRV and cardiovascular function, other signals such as respiratory activity can also be simultaneously analyzed (Ando et al., 1997; Lombardi, 1997; Li et al., 2019). Spectral analysis of HRV is characterized by three components, very low frequency (VLF) that corresponds to frequencies below 0.04 Hz, low frequency (LF) that corresponds to frequencies between 0.04 Hz and 0.15 Hz and high frequency (HF) that represents frequencies between 0.15 Hz to 0.4 Hz (Acharya et al., 2007).

It is believed that the high frequency oscillation is connected to respiration, the low frequency oscillation (the Mayer wave) is based on sympathetic activity and the closed loop regulation of the cardiovascular system, and the very low frequency oscillation is caused by vascular tone to control blood flow for thermal or humoral regulation. However, the sources for LF and VLF components, unlike those for HF are still controversial (Seydnejad and Kitney, 2001; Pham et al., 2021). It is observed that the center frequency of slow oscillation (both LF and VLF) decreases with age for both R-R intervals (i.e. HRV) and arterial pressure (i.e. BPV). Other factors that can cause lowering the center frequency of the oscillation are diabetes and hypertension and that can be caused by an increased delay in baroreflex loop. At the same time, patients with recent myocardial infarction can have increase of center frequency for slow oscillation in R-R intervals caused by progressive heart failure (Kiviniemi et al., 2010).

While these three components (VLF, LF and HF) account for almost all the power of the variability signal, the LF and HF components account for up to 65% of the total power in short term HRV analysis. In addition, an increase in LF or LF/HF ratio is associated with conditions such as acute phase of myocardial infarction, while an increase in HF with LF/HF ratio smaller than one is related to strong vagal modulation. The analysis of short term HRV can be used

for non-invasive evaluation of sympatho-vagal balance as well as evaluation of the effects of different pharmacological and non-pharmacological interventions on autonomic control of sinus node (Lombardi, 1997).

Spectral analysis of 24-hour recordings is more complex compared to the analysis of short term recordings. The spectrum of the long-term method is completely different from the one in short term method. In the 24-hour method, LF and HF components account for less than 10% of the total power. Most of the energy is distributed below 0.04 Hz and therefore the spectrum cannot provide much of information on autonomic regulatory mechanisms (Lombardi, 1997), unless the analysis is performed in consecutive shorter intervals over the 24-hour period. Table 2-1 shows advantages and disadvantages of each of these two methods (Li et al., 2019).

Table 2-1. Advantages and disadvantages of short term and long term HRV spectral analysis.

Analysis Method	Advantages	Disadvantages
Short term	Low computation complexity	Cannot be used for VLF analysis
	Easy to perform	Not stable
Long term	Stable	High computation complexity
	Can be used for VLF analysis	Affected by environmental factors
		Can be noisy

Dynamic changes in the heart rate, expressed through heart rate variability and also in blood pressure, expressed through blood pressure variability, in response to physiological perturbations guarantee constant and adequate blood flow to all organs and tissues (Shin et al., 2011). Many studies have focused on BPV and its correlation to a number of different pathologies in the autonomic nervous system because it provides independent information about autonomic cardiovascular regulation (Ma and Zhang, 2005). Blood pressure is continuously affected by external stimuli, but as patterns of change show, it always has the tendency to go back toward a reference set point (Parati et al., 1995). Similar to blood

pressure regulation, heart rate regulation is also affected by different factors such as respiration, physical activity, stress, etc. (Tikhonova et al., 2021). Studies have shown that the dynamic behavior caused by fluctuation in each of these signals contains valuable information about the state of the cardiovascular system (Parati et al., 1995).

In addition to linear dynamics of cardiovascular system, non-linear dynamics also need to be considered when studying cardiovascular regulation. Studies in this field are mainly focused on HRV, and to a lesser degree on BPV, and provide a useful tool for in-depth evaluation of the function of the cardiovascular system (Papaioannou et al., 2006). However, some studies have shown that under certain conditions there are differences between HRV and BVP characteristics such as:

- The response of BPV-HF is completely different from the response of HRV-HF during anesthesia and hemorrhage (Kawasi et al., 2001).
- After spinal cord injury, frequency specific differences exist between HRV and BPV (Solinsky et al., 2021).
- Impairment of autonomic nerve function leads to increase in BPV and decrease in HRV (Zhang et al., 2020).

2.1.6 Cardiovascular Dynamics and Blood Pressure

The study of heart rate variability and blood pressure variability is important for understanding cardiovascular function in health and disease, including in conditions such as heart failure, diabetes and hypertension. These oscillations were identified over 100 years ago and over the years it has been understood that cardiovascular dynamics can be used as diagnostic tools (Malpas, 2002). Cardiovascular oscillation could give information about blood pressure. There have been studies showing that during periods of stress the cardiovascular system displays more oscillations (Harris et al., 2009) and we know that stress causes temporary blood pressure elevation (Kulkarni et al., 1998). The oscillation can also occur in the presence of hypoxia which can result in higher blood pressure (Harris et al., 2009).

Although it is not known exactly how the fluctuations happen in cardiovascular control loops (Takalo et al., 1994), they provide useful information regarding one's blood pressure condition. A study by Takalo et al. has shown that cardiovascular dynamics are different for normotensive, borderline hypertensive, and mildly hypertensive people (Takalo et al., 1994). In addition to relationship between cardiovascular oscillation and blood pressure, a study on piglets has shown that the intensity of cardiovascular fluctuations is gender dependent and large changes happen less frequently in males compared to females (Harris et al., 2009).

2.2 Blood Pressure Measurement Methods

Blood pressure is a force that is applied to the sides of vessels by blood while it circulates in the body to deliver oxygen to organs. Each heart beat generates a maximum and a minimum blood pressure that is measured in millimeters of mercury (or mmHg). These maximum and minimum values are referred to as systolic blood pressure and diastolic blood pressure respectively. Blood pressure varies from person to person, and it also changes in the same individual based on many factors such as activity, stress level, diet, etc. Table 2-2 shows blood pressure classification for adults (Fortino and Giampa, 2010).

Both high and low blood pressure can cause health complications. Low blood pressure (hypotension) is the result of heart pumping blood through arteries with less force in comparison to normal pumping. As a result, a person with hypotension could experience damage to heart, brain or other vital organs due to inadequate blood flow (Bhargave et al., 2013). On the other hand, high blood pressure (hypertension) is caused by excessive force exerted on blood vessels during pumping of the heart. Hypertension is a major health risk and the risk increases as a person lives longer with the condition without treatment. Hypertension increases risk of chronic and coronary heart disease, stroke, visual impairment, heart failure, retinal hemorrhage, etc. (Singh et al., 2017).

Table 2-2. Blood Pressure Classification for Adults as recommended by the American Heart Association. The BP values are based on measurements taken from patient's upper arm. (adapted from Whelton et al., 2018).

Category	Systolic BP, mmHg	Diastolic BP, mmHg
Hypotension	Lower than 90	Lower than 60
Normal	90-119	60-79
Prehypertension	120-129	60-79
Stage 1 Hypertension	130-139	80-89
Stage 2 Hypertension	140 or higher	90 or higher
Hypertension Crisis	Higher than 180	Higher than 120

Any physical activity, stress, or emotional reaction can cause rapid changes to blood pressure for people with high blood pressure. Therefore, it is very important for people who are diagnosed with or at substantial risk for hypertension to have their blood pressure monitored continuously for chronic management of this condition and to be able to get proper medical attention promptly when needed (Xing and Sun, 2016). Blood pressure can be measured invasively or non-invasively. Below, we discuss each of these methods in more detail.

2.2.1 Invasive Method

In clinical practice, invasive blood pressure measurement is conducted using an intra-arterial line such as a thin catheter that is inserted into an artery. This method is often considered as the gold standard for arterial pressure measurement (Ding et al., 2016) and the procedure can only be done by licensed practitioners. Every time that the heart contracts, mechanical motion is generated within the catheter due to blood flow. A rigid fluid filled tube is used to transmit this motion to a transducer, which converts its input to an electrical signal that gets displayed on a monitor as both beat-to-beat arterial waveform and numerical pressure (Nguyen and Bora, 2021). Although the intra-arterial method is continuous in nature and could be a good fit for diagnosing hypertension, it imposes an elevated risk on the patient of complications such as infection (Ghosh et al., 2016) or in instances of disconnection of the

line, severe bleeding. As a result, this method is not an ideal choice for blood pressure monitoring (Fortino and Giampa, 2010).

2.2.2 Non-Invasive Method

Another method for blood pressure measurement is non-invasive and it can be categorized into intermittent and continuous measurement. While intermittent measurement is done through inflatable cuff, the continuous method can be done using tonometry, volume clamp, or cuffless methods (Meidert and Saugel, 2018). Figure 2-7 shows a classification of blood pressure measurement methods according to their types and abilities.

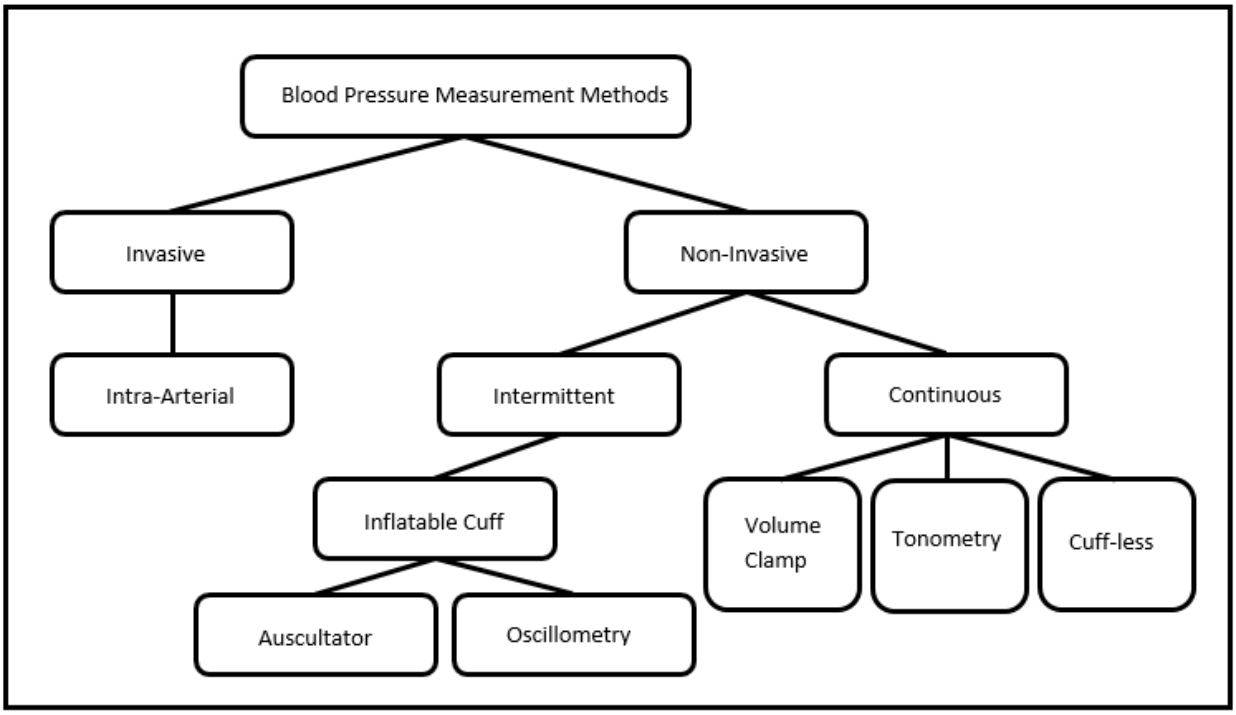

Figure 2-7. Blood pressure monitoring methods (adapted with permission from Meidert and Saugel, 2018).

2.2.2.1 Inflatable Cuff Method

One of the commonly used methods that uses inflatable cuff to measure blood pressure is the auscultatory technique. This method is based on Korotkoff sounds (Ogedegbe and Pickering, 2010), which are tapping-like sounds that can be heard using a stethoscope while releasing pressure in a cuff. These sounds are divided into five categories. Category one is a distinct

tapping sound follow by category two where the tapping gets softened. Then comes category three that is characterized as being like category one, but with sharper sound. Category four is where the sound gets faded and muffled and finally category five where there is complete silence (Campbell and Pillarisetty, 2019).

The auscultatory method is a manual way of measuring blood pressure. In this method a trained practitioner wraps a cuff around patient's arm and inflates the cuff. Inflation in the cuff blocks the brachial artery in a way that there would be no blood flow through the artery. Then while listening to the sound from the artery using a stethoscope, the practitioner slowly deflates the cuff. When phase one of Korotkoff sounds is heard, the pressure indicated by a sphygmomanometer corresponds to the systolic blood pressure. The cuff is deflated more till Korotkoff sounds enter phase five. At this point the sphygmomanometer pressure corresponds to the diastolic blood pressure (Ogedegbe and Pickering, 2010 and Campbell and Pillarisetty, 2019). Figure 2-8 shows blood pressure measurement using the auscultatory method.

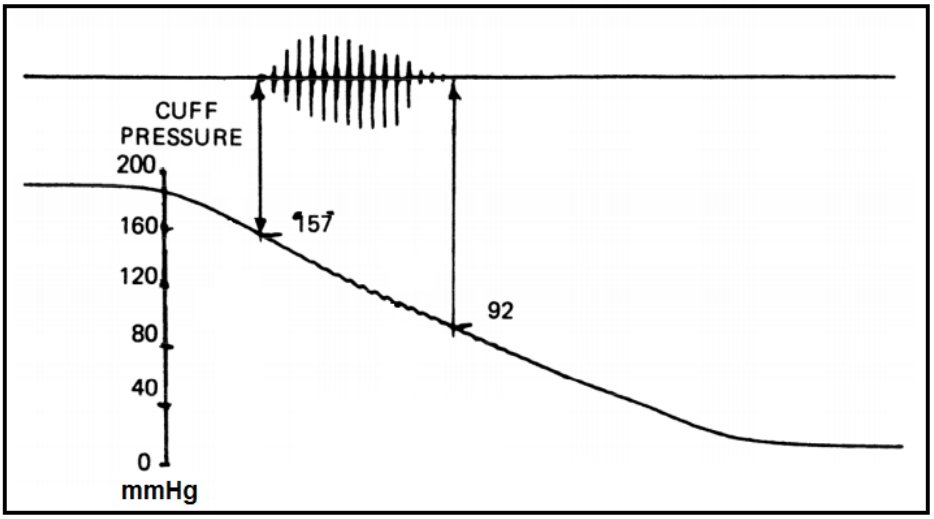

Figure 2-8. Changes appearing a sphygmomanometer during cuff deflation. The top waveform is the Korotkoff sounds and the lower curve is the decreasing cuff pressure accompanied with pressure value in mmHg indicated by a sphygmomanometer. Korotkoff sounds start at cuff pressure of 157 mmHg and stop when pressure reaches 92 mm/Hg. These numbers correspond to systolic and diastolic blood pressure respectively (adapted with permission from Ogedegbe and Pickering, 2010).

Another method that uses an inflatable cuff to measure blood pressure is the oscillometric technique. This method takes advantage of arterial pulsation and detects them as small

pressure oscillations superimposed on the deflating cuff pressure. The most common automated devices that have been used in the past few decades to measure blood pressure non-invasively are based on oscillometry (Sharma et al., 2017). They are easy to operate by an untrained person, and so they can be used at home to monitor blood pressure (Sharma et al., 2017).

In the oscillometric method, a cuff is usually placed around the upper arm and inflated to the point that the air pressure in the cuff exceeds the intra-arterial pressure in brachial artery (there is another less common version of the oscillometric method where the cuff is placed around the wrist, but it is based on the same principle). As a result, arterial flow stops at the cuff location. At this point the cuff is deflated gradually and a sensor in the cuff starts to record the arterial pulsation (pressure inside the cuff). This pulsation, also referred to as oscillation, starts at approximately systolic pressure and increases in amplitude as the cuff pressure is reduced. The pulsation exists past the diastolic pressure point and then fades away. Between the first appearance of the pressure oscillations and their disappearance, the point at which the amplitude of the oscillation is maximum corresponds to the mean arterial pressure. The mean arterial pressure is then used in a different algorithm (depending on the manufacturer of the monitor) to estimate systolic and diastolic blood pressure (Ogedegbe and Pickering, 2010). An algorithm that is commonly used is based on coefficients experimentally determined from population studies that relate the amplitude of the systolic and diastolic oscillation to the mean arterial pressure oscillation. Figure 2-9 demonstrates the oscillometric blood pressure measurement method.

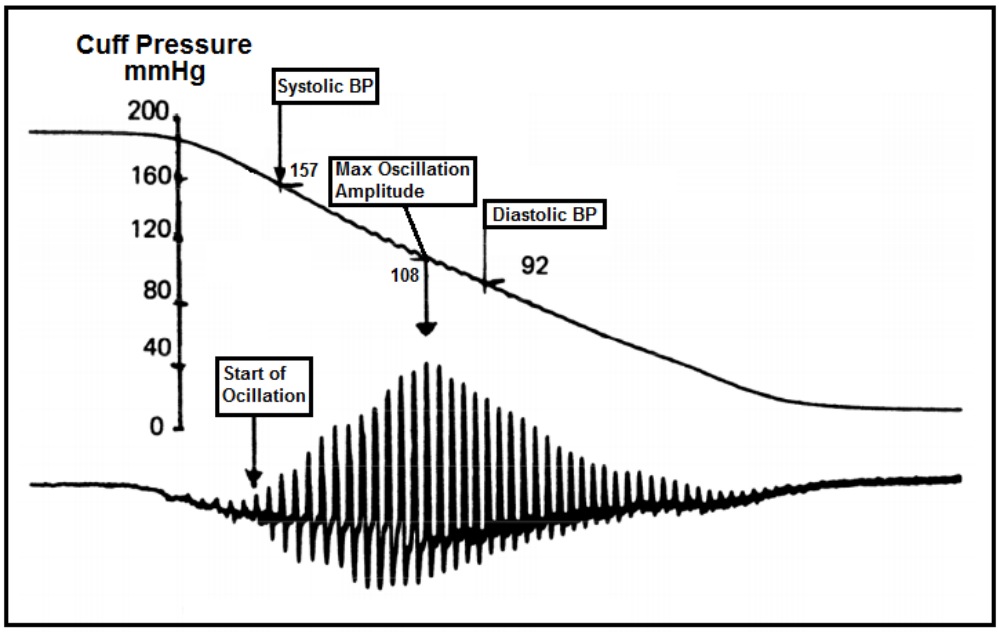

Figure 2-9. Demonstration of the oscillometric blood pressure measurement method. The top curve is the decreasing cuff pressure in mmHg. Oscillation starts before systolic pressure of 157 mmHg and increases in amplitude till reaches the maximum amplitude at cuff pressure of 108 mmHg. The oscillation then decreases in amplitude and fades away past the diastolic pressure point. The maximum amplitude of the oscillation (108 mmHg) corresponds to the mean arterial pressure that is used in an algorithm to estimate systolic and diastolic blood pressure values (adapted with permission from Ogedegbe and Pickering, 2010).

The major advantage of using oscillometry-based devices is that since they can be used at home, blood pressure can be regularly monitored (Ding et al., 2016). However, the drawback is that these devices provide only intermittent blood pressure values, not continuous readings. As mentioned earlier, continuous estimation of blood pressure would help doctors diagnose and control hypertension in patients (Kachuee et al., 2017 and Ding et al., 2016). In addition, cuff inflation and deflation in oscillometric devices can cause discomfort especially at night during sleep (Ding et al., 2016).

2.2.2.2 Tonometry Method

As was mentioned earlier, the intra-arterial method provides the most accurate continuous blood pressure measurement; however, it can only be applied in a clinical environment. Therefore, researchers have developed non-invasive methods that can correlate with the intra-arterial method. One of early methods that was developed by Pressman and Newgard

in 1963 was arterial tonometry. In this method, a transducer is placed externally on the skin above one of the shallow arteries and it pushes the artery down to the bone below it. Then the transducer measures the arterial displacement that is caused by arterial pulsation. This displacement is proportional to intra-arterial pressure and can be represented as:

$$\delta = \frac{F_a}{K} \qquad \textbf{Equation 2-3}$$

where δ is arterial displacement, F_a is the force caused by arterial pressure, and K represents spring rate of the transducer (Ding, et al., 2016). With advancement in tonometry, this method is now used to measure mean arterial pressure and subsequently calculate systolic and diastolic pressure (Meidert and Saugel, 2018). However, this method requires calibration by another method (e.g. cuff-based oscillometry) and is currently only used in specialized settings. Figure 2-10 shows a sphygmograph that is based on arterial tonometry.

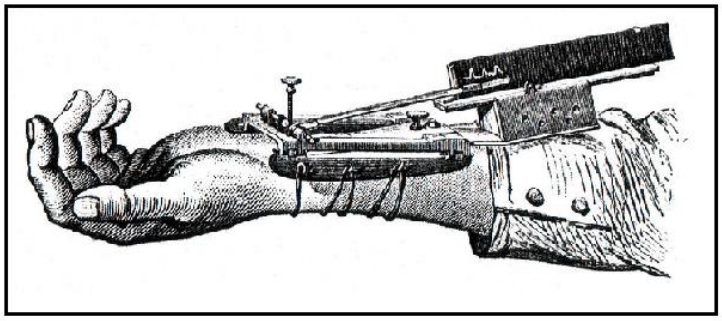

Figure 2-10. Marey's Sphygmograph (adapted from Wikimedia Commons at https://upload.wikimedia.org/wikipedia/commons/a/ac/Marey_Sphygmograph.jpg).

2.2.2.3 Volume Clamp Method

Another method for measuring continuous blood pressure non-invasively is the volume clamp technique that was developed by Penaz. In this method, as shown in Figure 2-11, a photodiode is used to measure the diameter of the artery in the finger. At the same time, the finger is wrapped by an inflatable cuff. The job of the cuff is to adjust its inflation level to ensure that the diameter of the artery in the finger stays constant. Based on the pressure change in the cuff, a blood pressure curve for the artery can be calculated (Meidert and

Saugel, 2018). Devices that implement the volume clamp method are usually expensive, and they are currently used only in laboratory or clinical settings.

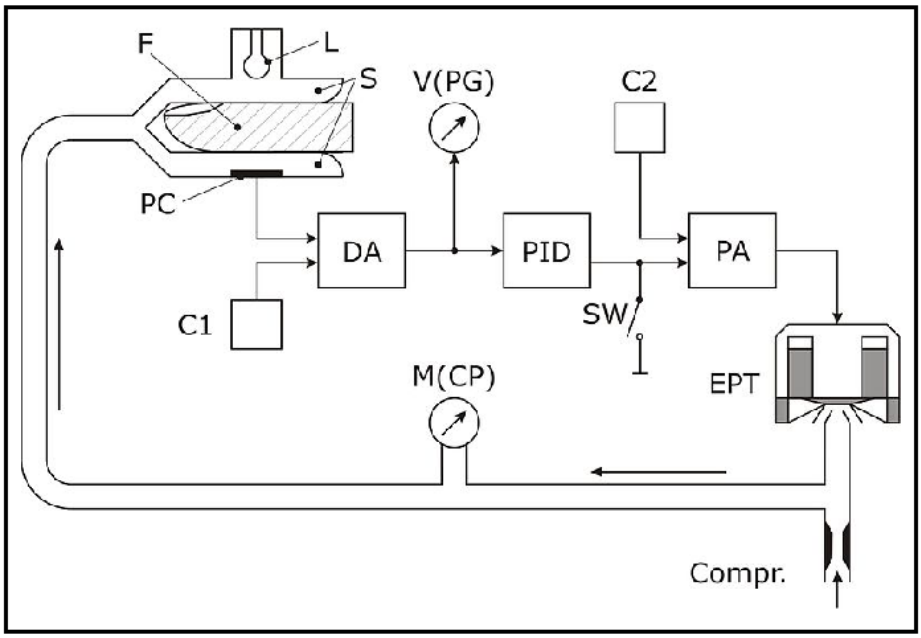

Figure 2-11. Block diagram of the volume clamp system used by Penaz containing a single control loop. "F" is finger that is under test, "L" is lamp, "PC" is photocell, "S" are segments of transparent pressure cuff, "C1" is average of photocell signal, "DA" is difference amplifier, "V(PG)" is plethysmographic signal, "PID" is correcting network, "C2" is set point, "SW" is switch between open and closed loop, "PA" is power amplifier, "EPT" is electro-pneumatic transducer, and "M(CP)" is pressure measured with manometer. (adapted from Wikimedia Commons at https://upload.wikimedia.org/wikipedia/commons/4/43/Penaz_principle.jpg).

2.2.2.4 Cuffless Method

In recent years, there has been a lot of interest in developing cuffless techniques for blood pressure measurement, as they can allow for continuous monitoring of blood pressure. Forces driving the increase in demand for such methods can be summarised in profound need and feasibility. Since hypertension is a serious problem that does not have a high rate of detection, cuffless blood pressure monitoring methods can improve the detection rate by providing out-of-clinic measurements and offering patients continuous feedback. As a result, hypertension detection rate can be improved, and more cases can be treated that otherwise would have been at great cardiovascular risk. In addition, with the latest technological advancements in

wearable sensing, computational power and size optimization, developing such techniques now seems more achievable (Mukkamala et al., 2015). Methods based on ultrasound signals, the photoplethysmogram (PPG), along with analysis based on machine learning are among popular unobtrusive techniques that are being used in the development of cuffless blood pressure monitoring devices.

The ultrasound method is based on the fact that ultrasound can be used to visualize blood flow and measure its velocity. It can also reveal information about arterial wall motion, cross section area and flow area. The gathered information then can be used to estimate the pressure waveform (Ding et al., 2016).

In recent years, photoplethysmography (PPG) based methods have shown a lot of promise in cuffless blood pressure measurement (Xing and Sun, 2016). PPG is used to measure blood volume changes in microvascular tissue noninvasively (Challoner, 1979). This volume change is caused by the pulsatile characteristics of the circulatory system. Although PPG uses a simple technique, the origin of different components of the collected signal is not fully understood. However, despite the limited understanding of the signal, there is a general agreement that PPG can provide valuable information about the function of the cardiovascular system (Kamal et al., 1989).

To collect the PPG signal, a light source and a photodetector are used. The light is placed on the skin beside or across from the photodetector. When the source illuminates the skin and tissues beneath it, the photodetector can measure changes in blood volume, blood vessel wall movement, and the orientation of red blood cells by sensing variations in reflected or transmitted light intensity (Allen, 2007 and Sun and Thakor, 2016). Figure 2-12 illustrates PPG signal collection in two different modes, reflectance mode and transmittance mode. It is worth mentioning that the PPG signal can be obtained from various body locations.

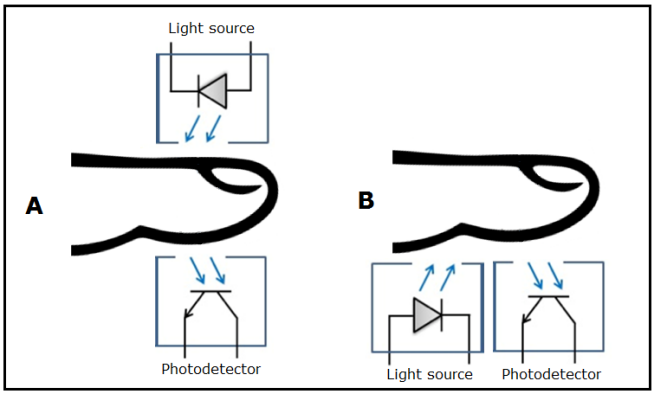

Figure 2-12. Different methods for collecting the PPG signal. A) Collecting PPG signal by using a transmission light configuration. B) Collecting the PPG signal by reflection light configuration (adapted with permission from Elsamnah et al., 2018).

The optical technique used in PPG is based on variation in sensitivity of blood and tissue components to individual light wavelengths. Since change in blood volume is measured in PPG, the selected wavelength needs to have greater absorbance with blood compared to tissue. Based on this, ultraviolet and longer infrared wavelengths that have high absorbance in liquid are used in PPG. When the heart pumps blood to the body, the volume of blood under the skin increases resulting in absorption of more light and so a weaker signal measured by the photodetector. Conversely as blood goes back to the heart, blood volume decreases leading to less absorption of the light and so a stronger signal measured by the photodetector. As a result, the photodetector records a pulsatile waveform that is usually referred to as the alternating current (AC) part of the PPG, which is superimposed on a slow varying offset or direct current (DC) part that carries information about respiration, venous flow, sympathetic nervous system activity and thermoregulation (Sun and Thakor, 2016). Since there is a similarity between the PPG waveform and arterial blood pressure (ABP) waveform morphologies, using PPG signal in cuffless methods to estimate blood pressure is very promising (Martinez et al., 2018). Figure 2-13 shows the different components of PPG signal.

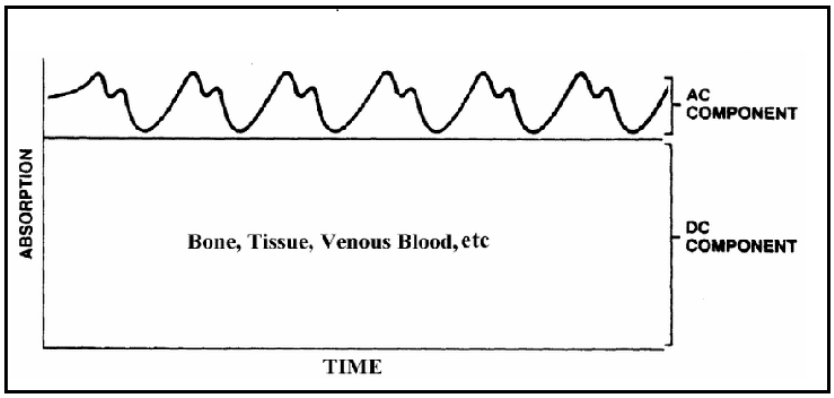

Figure 2-13. PPG signal along with its DC and AC components (adapted from everipedia at https://everipedia-storage.s3-accelerate.amazonaws.com/ProfilePics/ppg-signal-analysis__24651.png).

Among different PPG based methods, pulse transit time (PTT) and related pulse wave velocity (PWV) approaches have been the most widely used techniques (Ding et al., 2016). PTT is defined as the time delay it takes a pulse wave to travel from one arterial site to another (Mukkamale et al., 2015) and may be measured using two photoplethysmogram (PPG) sensors located at two distant sites on the body (Le et al., 2020). PTT can be calculated in a few different ways such as time delay between the proximal and distal PPG waveforms (Le et al., 2020), the time difference from mid-point of the falling edge of the proximal PPG pulse to the peak of the peripheral PPG pulse (Chen at el., 2012), or as the time difference from the dicrotic notch of the proximal PPG pulse and the peak of the peripheral PPG pulse (Kao et al., 2019). It is also worth mentioning that many studies refer to pulse arrival time (PAT) as PTT and the use of the true PTT is not greatly researched (Le et al., 2020). So, in this study, we also use the terms PTT and PAT interchangeably. The PAT that is widely used as a surrogate for PTT is defined as the time interval between electrical activation of the heart and arrival of the pulse wave to the periphery (Thambiraj et al., 2020) and it is usually measured as time interval between the R-peak in electrocardiogram (ECG) and peak of the pulse waveform in PPG recorded at the fingertip (Ding et al., 2016). Figure 2-14 shows the definition of PAT. The pulse wave velocity (PWV) is defined as the distance traveled by the pulse waveform between two arterial sites divided by the travel time (PTT or PAT).

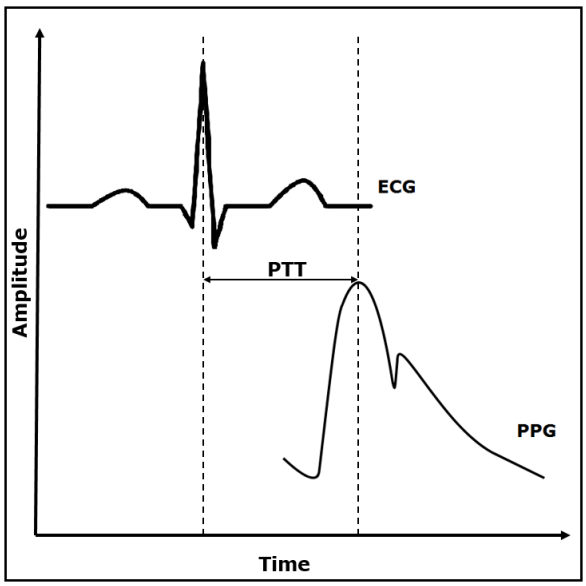

Figure 2-14. Definition of the pulse arrival time (adapted with modification from Wikimedia Commons at https://upload.wikimedia.org/wikipedia/commons/8/85/Arterial-blood-pressure-curve.svg and https://upload.wikimedia.org/wikipedia/commons/9/9e/SinusRhythmLabels.svg).

The PTT/PWV modeling approach for blood pressure estimation is mostly based on the Moens-Korteweg equation:

$$\mathbf{PWV} = \sqrt{\frac{\mathbf{Eh}}{\boldsymbol{\rho}\mathbf{D}}} \qquad \textbf{Equation 2-4}$$

where E is the modulus of elasticity of the artery, h is the thickness of the arterial wall, ρ is the blood density and D is the diameter of the artery. In addition, the modulus of elasticity of the artery is related to mean arterial pressure:

$$\mathbf{E} = \mathbf{E_0}.\,\mathbf{e^{\gamma P}} \qquad \textbf{Equation 2-5}$$

where E_0 is the zero-pressure modulus, γ is a coefficient depending on the artery and P is the mean arterial pressure. When Equation 2-5 is substituted in Equation 2-4 and given the following relationship between PTT and PWV:

$$\mathbf{PWV} = \mathbf{L}/\mathbf{PTT} \qquad \textbf{Equation 2-6}$$

where L is the distance between the heart and a peripheral site, the mean arterial pressure can be calculated as:

$$\mathbf{P = \frac{1}{\gamma}\left(\ln \frac{L^2 \rho D}{E_0 h} - 2 \ln PTT\right)}$$ **Equation 2-7**

Equation 2-7 demonstrates that blood pressure can be estimated from PTT. Although more advanced research has been done that includes other variables in the estimation of blood pressure based on PTT, the baseline for such estimation is as shown in this equation (Ding et al., 2016).

Variations of this method (PTT/PWV) are the most common techniques used for PPG based cuffless blood pressure estimation (Kachuee et al., 2017). For example, in one study, an algorithm was developed to estimate systolic blood pressure, diastolic blood pressure and mean arterial pressure based on PAT. Two types of features were considered in this study. One was based on physiological parameters such as heart rate, arterial stiffness index etc. and the other one was based on PPG morphology within individual pulses. Physiological parameters included measurement of the time differences between R-peak from the ECG and three points on the PPG signal that led to the measurement of PAT parameters. The three points on PPG that were considered for these measurements are: PPG maximum peak (resulting in PATp), PPG minimum (providing PATf) and the point of maximum slope for PPG (giving PATd). All collected features were then passed through a dimensionality reduction process (principal component analysis - PCA) to reduce the number of features. Estimation was done using different machine learning algorithms in both calibration-free and calibrated modes. The study concluded that this method can be used for non-invasive, cuffless blood pressure measurement (Kachuee, et al., 2017).

A different approach was used in another study where a secondary peak detection method was deployed in order to minimize false PTT estimation. This study mainly focused on ECG and PPG signals to determine PTT and concluded that the proposed method could be used in continuous, non-invasive cuffless blood pressure measurement (He, et al., 2014). Shriram et al. conducted another study in which they used the PTT/PWV method for continuous cuffless

blood pressure measurement and compared the results with the ones obtained from a sphygmomanometer. They concluded that reliable estimation can be obtained based on the proposed method. The study also found that PPG signal amplitude generally is lower in females compared to males (Shriram et al., 2010).

There are also several of studies that have used the PPG signal by itself as the source of information to develop cuffless blood pressure monitoring technique. As has been described by Elgendi et al., the studies that have been done so far on cuffless blood pressure estimation based solely on the PPG signal (as opposed to being based on the PTT for example) can be mainly divided into two categories based on waveform morphology theory (using a single PPG waveform) and waveform propagation theory (using multiple pulse signals) (Elgendi et al., 2019). They may use a single pulse or average over multiple pulses, gathering information in time domain or frequency domain, but the selected features are mostly based on the morphology of the signal.

One of many such studies that has analysed a single pulse and collected features based on that is the work done by Teng and Zhang. They used width of 1/2 and 2/3 pulse amplitude along with systolic upstroke time (the time for the pulse to reach maximum peak) and diastolic time (duration of time from peak to trough of the signal) of a single pulse as features to be passed to linear regression for estimating blood pressure. The signals were collected from 15 people and the estimation results were compared with the ones obtained from PTT method. They concluded that PPG-based estimation had better performance compared to PTT-based estimation for DBP, but this was not the case for SBP where PTT resulted in better estimation (Teng and Zhang, 2003).

Datta et al. used a similar approach by using widths at 25%, 50% and 75% of the pulse amplitude, in addition to cycle duration, systolic upstroke time, diastolic time, trough to notch time, notch to trough time, peak to notch time and some demographic features such as age, height and weight. Their study focused on preprocessing the signal for better feature selection

and ultimately better performance of cuffless blood pressure measurement (Datta et al., 2016). Khalid et al., and Hassani and Foruzan, also used width of a PPG pulse at different amplitudes as features for their machine learning algorithms. Khalid et al. also used other features such as pulse area and pulse rise time (Khalid et al., 2018), whereas Hassani and Foruzan added systolic time and diastolic time information at each of the marked amplitudes to their feature set (Hassani and Foruzan, 2019). In another study, Wang et al. used spectral information of PPG pulse for low frequencies (below 10 Hz) in 0.5 Hz intervals to generate 20 features. Systolic upstroke time and diastolic time were two morphological features that were also added to the feature set (Wang et al., 2018). In a different study, Shin and Min used velocity (first derivative) and acceleration (second derivative) of PPG signals collected from 25 subjects to develop a new pressure index to be used alongside some physical characteristics of subjects such as age, height, and weight as features in estimating blood pressure (Shin and Min, 2017). Atomi et al. also used a similar approach of using information from acceleration of PPG signal along with some physical characteristics of subjects as a feature set (Atomi et al., 2017).

Pan and Zhang used a series of models and performed averaging to determine detection accuracy. In this method, they randomly created multiple subsets of the training data. Each of these training sets were used in a separate estimation model (either stepwise regression or back propagation neural network) and the results from the models were averaged (after going through clustering analysis) to obtained final BP estimation value. They used time domain features from the PPG signal that were based on amplitudes of the peak, the foot, the dicrotic notch, and the dicrotic peak (Pan and Zhang, 2017). Bersano and Sanson looked at time domain features of PPG signal; however, they considered the blood pressure estimation as a classification problem and tried to divide the data into different bins corresponding to ranges of blood pressure. In addition to temporal features, they added some demographic characteristics such as age, height, weight and gender and concluded that the demographic

features carry a significant weight in algorithm learning. They also noted that the size of hidden layers in their neural network had negligible impact on the result (Bersano and Sanson, 2018).

Xing et al. estimated blood pressure based on the PPG signal with no calibration involved. They split their data population based on the subjects' age (below 50 years old and above 50 years old), since age is correlated with an increase in arterial stiffness. They noted that in the older group PPG lost some of its key features and resulted in less accurate estimation of blood pressure. They also used temporal features such as perfusion index, stiffness index (ratio of height of the subject to the time lapse between systolic peak and dicrotic notch), heart rate, and area under PPG pulse. Xing et al. concluded that their achieved result was somewhat improved, relative to the ones reported by Ruiz-Rodriguez et al. in 2013 and Shin et al. in 2017, for calibration-free blood pressure estimation (Xing et al., 2019).

Contrary to what has been described so far (defining features within a single pulse), there have been some other studies that have worked with multiple pulses and averaged information over the duration of the signal. In one such study, four features were extracted from PPG signals that were collected from 40 subjects, along with standard SBP and DBP values that were used as target values. Standard SBP was considered to be in the range of 98-138 mmHg and standard DBP to be in the range of 60-95 mmHg. The PPG as well as SBP and DBP were measured using a BP handheld device with reflective PPG bio-sensor developed by Sensor IC Laboratory (SiL) at the National Chiao Tung University (NCTU). After preprocessing PPG signal using a bandpass filter with a 0.5 Hz to 30 Hz passband, the pulse duration, systolic upstroke time, diastolic time and reflective pulse transit time (distance between first peak and the second peak in one cycle) were selected as features. The average of each feature over the duration of the signal was then used as input to an artificial neural network with two hidden layers. This study concluded that proposed method provided high accuracy in estimating both SBP and DBP (Priyanka et al., 2018).

In another study, PPG was collected from five healthy subjects and a number of features were extracted from accelerated PPG. Accelerated plethysmography was generated by differentiating the PPG signal twice and this provided six peaks whose amplitudes were considered as features. In addition, time intervals between any one of the peaks and each of the others were considered as another set of 15 features. There were also some compound features that were generated using accelerated PPG information. Another feature that was considered in this study was related to sympathetic nerve activity (SNA). This feature was obtained by transforming heart rate variability data from accelerated PPG to frequency domain and determining the ratio between low frequency band and high frequency band of the signal. The last feature that was used in this study was drift rate which was calculated as:

$$\mathbf{D} = \frac{\int_{0.2}^{0.7} \mathbf{P(f)df}}{\int_{0.7}^{2} \mathbf{P(f)df}} \qquad \textbf{Equation 2-8}$$

where $\mathrm{P(f)}$ is the power spectrum of the PPG signal.

The collected features were then used to estimate blood pressure using a stepwise multiple regression analysis. The study concluded that the proposed method resulted in similar performance to a previously measured blood pressure using a cuff, based on observed correlation between estimated and actual result (Fukushima et al., 2013).

In addition to features extracted in the time domain, some researchers have proposed feature collection in the frequency domain. Xing and Sun used amplitude and phase characteristics of PPG signals from 69 patients to train an artificial neural network for estimating blood pressure. They found good correlation between the reference and estimated values (Xing and Sun, 2016). Wang and Zhang also used the frequency domain to extract features from the PPG signal. They used a dataset with 300 PPG records and collected the first 15 points of the discrete cosine transform (DCT) sequence as the features to train a neural network. They also achieved a good estimation result based on this method (Wang and Zhang, 2017).

Table 2-3 lists a number of different studies that have been done in the field of cuffless blood pressure estimation.

Table 2-3. A list of some of the research that has been done for cuffless blood pressure estimation. This table indicates the authors' names as well as publication year, the dataset, the type of signal that was used in the study, and the analysis method.

Author	Publication Year	Signal	Method	Database	Best Result Achieved (mmHg)
					SBP/DBP
Teng and Zhang	2003	PPG	Linear regression - Based on morphology theory	Private - 15 people	ME:0.21/0.02 STD:7.32/4.39
Shriram et al.	2010	ECG-PPG	PWV/PTT - Mathematical model	Private - 23 people	ME: -0.34/- STD: 3.1/-
Ruiz-Rodriguez et al.	2013	PPG	Regression based on deep belief network-restricted Boltzmann machine - Based on morphology theory	Private - 572 people	ME: -2.98/-3.65 STD:19.35/8.69
Fukushima et al.	2013	PPG	Stepwise multi regression - Based on waveform propagation theory	Private - 5 people	r: 0.71 for MBP
Kurylyak et al.	2013	PPG	ANN - Based on morphology theory	MIMIC II – 15000 periods	ME: 3.80/2.21 SDE: 3.46/2.09
He et al.	2014	ECG-PPG	PWV/PTT - Linear regression, quadric regression and cubic regression	MIMIC II - 100 people	ME: 3.06/- SDE: 3.69/-
Dastmalchi	2015	PPG	ANN and PCA - Based on	MIMIC II – 11 hypertensive and 11	ME: 0.07/-0.07 SDE: 4.64/3.21

Author	Publication Year	Signal	Method	Database	Best Result Achieved (mmHg)
					SBP/DBP
			morphology theory	normotensive with 10 periods	
Xing and Sun	2016	PPG	Multi layer feed forward back propagation ANN - Based on waveform propagation theory	MIMIC II - 69 people. Private - 23 people	ME: 0.06/0.01 SDE: 7.08/4.66
Datta et al.	2016	PPG	Linear regression and Windkessel model - Based on morphology theory	Private - No information on population	MAE: ~13/~8 SDE: ~17/~9
Kachuee et al.	2017	ECG-PPG	PAT - Linear regression, random forest, decision tree, support vector machine (SVM) and adaboost	MIMIC II - 3663 signals from 1000 records	Calibration-Free: MAE: 11.17/5.35 SDE: 10.09/6.14 Calibration Based: MAE: 8.21/4.31 SDE: 5.45/3.52
Wang and Zhang	2017	PPG	Discrete cosine transform - SVM and adaboost with ten ANNs - Based on morphology theory	PhysioNet CinC Challenge 2010 - 300 records	ME: 1.8707/1.0339 SDE: 2.9425/1.6507
Shin and Min	2017	PPG	Linear regression - Based on morphology theory	Private - 25 people	r: 0.818 for SBP
Atomi et al.	2017	PPG	Multiple regression analysis - Based on	Private - 25 people	ME: 2.13/- SDE: 5.32/-

Author	Publication Year	Signal	Method	Database	Best Result Achieved (mmHg)
					SBP/DBP
			morphology theory		
Pan and Zhang	2017	PPG	Ensemble model based on stepwise regression and ANN - Based on waveform propagation theory	University of Queensland vital signs - 12 people	Multiple results comparing ensemble model to single model.
Priyanka et al.	2018	PPG	ANN - Based on morphology theory	Private - 40 people	ME: 0.17/0.3 SDE: 3.9/1.8
Khalid et al.	2018	PPG	Regression tree, multiple linear regression and SVM - Based on morphology theory	University of Queensland vital signs - 32 people	ME; -0.1/-0.6 SDE: 6.5/5.2
Wang et al.	2018	PPG	ANN - Based on morphology theory	MIMIC - 72 people	MAE: 4.02/2.27 SDE: 2.79/1.82
Bersano and Sanson	2018	PPG	Softmax regression, SVM and ANN - Based on morphology theory	Private - 52 people	Multiple results comparing proposed method to other (previous) methods based on output BP range.
Hassani and Foruzan	2019	PPG	ANN and support vector regression (SVR) - Based on morphology theory	MIMIC II - 120 people	ME: -0.14/0.25 SDE: 5.75/5.76
Xing et al.	2019	PPG	Random forest - Based on morphology theory	Private - 2079 measurements	Multiple results based on age group (old/young) and BP group (low/medium/high)

Author	Publication Year	Signal	Method	Database	Best Result Achieved (mmHg)
					SBP/DBP
Slapnicar et al.	2019	PPG	Spectro-temporal deep neural network - Based on morphology theory	MIMIC III - 510 people	MAE: 9.43/6.88
Chen et al.	2019	ECG-PPG	PTT and pulse waveform characteristics - SVR	MIMIC III - 772 sets of waveform	ME: 3.27/1.16 SDE: 5.52/1.97
Mohebbian et al.	2020	PPG	Optimized inductive group method of data handling - Based on morphology theory	MIMIC 12000 subjects training - Private 25 subjects testing	MAE: 2.40/3.33 SDE: 1.01/1.61
Soh et al.	2020	ECG	Convolutional neural network	MIT-BIH 18 subjects - SHAREE 139 subjects	Classification accuracy of 99.99%
Jain et al.	2020	ECG	Deep convolutional neural network	SHAREE 139 subjects - PTB Diagnostic ECG Database 73 subjects	Classification accuracy of 90.98%
Sagirova et al.	2021	ECG-PPG	PWV/PTT - Linear regression classical method	Private - 512 people	ME: 0.32/0.61 SDE: 3.63/2.95
Fati et al.	2021	PPG	Auto ML tree based pipeline optimization tool (TPOT) - Based on waveform propagation theory	PhysioNet - 1000 people	MAE: 6.52/4.19
Yamakoshi et al.	2021	PPG	Mathematical model - Based on morphology theory	Private - 13 people	r: 0.934 for SBP 0.844 for DBP

Author	Publication Year	Signal	Method	Database	Best Result Achieved (mmHg)
					SBP/DBP
Li and Laleg-Kirati	2021	PPG	SVM, Multiple linear regression and decision tree - Based on morphology theory	MIMIC II - 8000 records	MAE: 7.44/5.09 SDE: 7.37/5.66
Agham and Chaskar	2021	PPG	Long short term memory network and sequential genetic feature algorithm - Based on waveform propagation theory	MIMIC II - 2780 people	MAE: 1.04/1.02 For normal BP MAE: 0.96/0.42 For hypertension
El-Hajj and Kyriacou	2021	PPG	Four recurrent NN models (MLR, feed forward, LSTM and GRU) - Based on morphology theory	MIMIC II - 500 people	MAE: 2.58/1.26 SDE: 3.35/1.63
Haddad et al.	2022	PPG	Multiple linear regression, network-Based on morphology theory	MIMIC I – data from 28 people	MAE: 6.10/4.65 SDE: 8.08/6.22
Wang et al.	2022	PPG	Convolution neural network (CNN) - Based on morphology theory	UCI from MIMIC II – 348 people	ME: 0/-0.04 SDE: 8.46/5.36
Byfield et al.	2022	PPG	PWV - Gaussian process regressor	Private - 26 people	R^2: 0.8814 for SBP 0.6246 for DBP

In conclusion, to the best of our knowledge, previous studies have not systematically investigated the information related to cardiovascular dynamics over short intervals for cuffless estimation of blood pressure using PPG alone. While some studies have explored the relationship between PPG waveform features and blood pressure, these have primarily focused on features extracted from the pulse morphology and have not investigated the effect of cardiovascular dynamics. This represents an important gap in the literature, as accurate and reliable estimation of blood pressure is critical for monitoring cardiovascular health and detecting potential dangerous fluctuations in blood pressure. Further research in this area is needed to develop more accurate and reliable methods for cuffless estimation of blood pressure based on PPG. This will be explored in the following chapters.

2.3 References

Acharya, U.R., Suri, J.S., Spaan, J.A.E., & Krishnan, S.M. (2007). *Advances in Cardiac Signal Processing*. Springer.

Agham, N.D., & Chaskar, U.M. (2021). An advanced LAN model based on optimized feature algorithm: towards hypertension interpretability. *Biomedical Signal Processing and Control, 68*, 102760.

Alastruey, J., Parker, K., & Sherwin, S. (2012). Arterial pulse wave hemodynamics. *Proceedings of the eleventh International Conference on Pressure Surges*, Lisbon, Portugal, 401-442.

Allen, J. (2007). Photoplethysmography and its application in clinical physiological measurement. *Physiological Measurement*, *28*(3), R1-R39.

Ando, S., Dajani, H.R., & Floras, J.S. (1997). Frequency domain characteristics of muscle sympathetic nerve activity in heart failure and healthy humans. *American Journal of Physiology - Regulatory Integrative and Comparative Physiology, 273*, R205-R212.

Atomi, K., Kawanaka, H., Bhuiyan, S., & Oguri, K. (2017). Cuffless blood pressure estimation based on data-oriented continuous health monitoring system. *Computational and Mathematical Methods in Medicine, 2017*(37), 1-10.

Bersano, N., & Sanson, H. (2018). Non-invasive blood pressure estimation from photoplethysmography signals using artificial neural networks. *2018 20th International Conference on Advanced Communications Technology (ICACT)*, Chuncheon, South Korea.

Bhargave, A., Gangwar, L., & Grewal, H. S. (2013). To study the effect of holy basil leaves on low blood pressure (hypotension) women aged 18-30 years. *International Conference on Food and Agricultural Sciences (IACSIT)*, Singapore, *55*(16), 83-86.

Bogachev, M.I., Markelov, O.A., Pyko, N.S., & Pyko, S.A. (2015). Blood pressure – heart rate synchronization coefficient as a complementary indicator of baroreflex mechanism efficiency. *XVIII International Conference on Soft Computing and Measurements (SCM)*, St. Petersburg, Russia, 173-175.

Bruss, Z.S., & Raja, A. (2022, September 12). *Physiology, Stroke Volume*. StatPearls. https://www.ncbi.nlm.nih.gov/books/NBK547686.

Byfield, R., Miller, M., Miles, J., Guidoboni, G., & Lin, J. (2022). toward robust blood pressure estimation from pulse wave velocity measured by photoplethysmography sensors. *IEEE Sensors Journal, 22*(3), 2475-2483.

Campbell M., & Pillarisetty L.S. (2022, September 07). *Physiology, Korotkoff Sound*. StatPearls. https://www.ncbi.nlm.nih.gov/books/NBK539778.

Challoner, A.V.J. (1979). Photoelectric plethysmography for estimating cutaneous blood flow. *Non-Invasive Physiological Measurements, 19*(3), 317-328.

Chaudhry, R., Miao, J. H., & Rehman, A. (2022, October 16). *Physiology, Cardiovascular*. StatPearls. https://www.ncbi.nlm.nih.gov/books/NBK493197.

Chen, S., Ji, Z., Wu, H., & Xu, Y. (2019). A non-invasive continuous blood pressure estimation approach based on machine learning. *Sensors*, *19*(11), 2585.

Chen, Y., Wen, C., Tao, G., & Bi, M. (2012). Continuous and noninvasive measurement of systolic and diastolic blood pressure by one mathematical model with the same model parameters and two separate pulse wave velocities. *Annals of Biomedical Engineering*, *40*(4), 871-882.

Dastmalchi, A. (2015). *Beat-to-beat Estimation of Blood Pressure by Artificial Neural Network* [MASc thesis, Department of Mechanical Engineering, University of Ottawa].

Datta, S., Banerjee, R., Choudhury, A.D., Sinha, A., & Pal, A. (2016). Blood pressure estimation from photoplethysmogram using latent parameters. *IEEE International Conference on Communications*, Kuala Lumpur, Malaysia, 1-7.

Ding, X.R., Zhao, N., Yang, G.Z., Pettigew, R.I., Lo, B., Miao, F., Li, Y., Liu, J., & Zhang, Y.T. (2016). Continuous blood pressure measurement from invasive to unobtrusive: celebration of 200th birth anniversary of Carl Ludwig. *IEEE Journal of Biomedical and Health Informatics, 20*(6), 1455-1465.

Elgendi, M., Fletcher, R., Liang, Y., Howard, N., Lovell, N.H., Abott, D., Lim, K., & Ward, R. (2019). The use of photoplethysmography for assessing hypertension. *Nature Partner Journals Digital Medicine, 2*(60).

El-Hajj, C., & Kyriacou, P.A. (2021). Deep learning models for cuffless blood pressure monitoring from PPG signals attention mechanism. *Biomedical Signal Processing and Control*, *65*, 102301.

Elsamnah, F., Hattori, R., Affiq, M., Shim, C.H., Bilgaiyan, A., & Sugawara, R. (2018). Reflection-based monolithic organic pulsemeter device for measuring photoplethysmogram signal. *IEEE International Instrumentation and Measurement Technology Conference,* 1-5.

Fati, S.M., Munner, A., Akbar, N.A., & Taib, S.M. (2021). A continuous cuffless blood pressure estimation using tree-based pipeline optimization tool. *Symmetry*, *13*(686), 1-22.

Fortino, G., & Giampa, V. (2010). PPG-based methods for non invasive and continuous blood pressure measurement: an overview and development issues in body sensor networks. *IEEE International Workshop on Medical Measurements and Applications (MeMeA)*, Ottawa, Canada, 10-13.

Fossion, R., Saenz-Burrola, A., & Zapata-Fonseca, L. (2020). On the stability and adaptability of human physiology: Gaussians meet heavy-tailed distributions. *INTERdisiplina*, *8*(20), 55-81.

Fukushima, H., Kawanaka, H., Bhuiyan, S., & Oguri, K. (2013). Cuffless blood pressure estimation using only photoplethysmography based on cardiovascular parameters. *35th Annual International Conference of the IEEE EMBS,* Osaka, Japan, 2123-2135.

Ghosh, S., Banerjee, A., Ray, N., Wood, P.W., Boulanger, P., & Padwal, R. (2016). Continuous blood pressure prediction from pulse transit time using ECG and PPG signals. 2016 IEEE *Healthcare Innovation Point-Of-Care Technologies Conference (HI-POCT)*, Cancun, Mexico, 188-191.

Haddad, S., Boukhayma, A., & Caizzone, A. (2022). Continuous PPG-based blood pressure monitoring using multi linear regression. *IEEE Journal of Biomedical and Health Informatics, 26*(5), 2096-2105.

Harris, T.A., Healy, G.N., Colditz, P.B., & Lingwood, B.E. (2009). Oscillations in cardiovascular function during acute hypoxia in the newborn piglet are associated with less neurological damage and occur more frequently in females. *Pediatric Research*, *65*(5), 504-508.

Hassani, A., & Foruzan, A.H. (2019). Improved PPG-based estimation of the blood pressure using latent space features. *Signal, Image and Video Processing, 13*, 1141-1147.

He, X., Goubran, R.A., & Liu, X.P. (2014). Secondary peak detection of PPG signal for continuous cuffless arterial blood pressure measurement. *IEEE Transactions on Instrumentation and Measurement*, *63*(6), 1431-1439.

Jain, P., Gajbhiye, P., Tripathy, R.K., & Acharya, U.R. (2020). A two-stage deep CNN architecture for the classification of low-risk and high-risk hypertension classes using multi-lead ECG signals. *Informatics in Medicine Unlocked*, *21*, 100479.

Kachuee, M., Kiani, M.M., Mohammadzade, H., & Shabany, M. (2017). Cuffless blood pressure estimation algorithms for continuous health-care monitoring. *IEEE Transactions on Biomedical Engineering*, *64*(4), 859-869.

Kamal, A.A., Harness, J.B., Irving, G., & Mearns, A.J. (1989). Skin photoplethysmography—a review. *Computer Method and Programs in Biomedicine,* 28(4), 257-269.

Kao, Y.H., Chao, P.C.P., & Wey, C.L. (2019). Design and validation of a new PPG module to acquire high-quality physiological signals for high-accuracy biomedical sensing. *IEEE Journal of Selected Topics in Quantum Electronics*, *25*(1), 69000210.

Kawase, M., Komatsu, T., Nishiwaki, K., Kobayashi, M., Kimura, T., Shimada, Y. (2001). Heart rate variability and arterial blood pressure variability show different characteristic changes during hemorrhage in isoflurane-anesthetized, mechanically ventilated dogs. *Anesthesia & Analgesia, 94*(1), 16-21.

Khalid, S.G., Zhang, J., Chen, F., & Zheng, D. (2018). Blood pressure estimation using photoplethysmography only: comparison between different machine learning approaches. *Journal of Healthcare Engineering, 2018*(1).

Kiviniemi, A.M., Tiinanen, S., Hautala, A.J., Seppanen, T., Makikallio, T.H., Huikuri, H.V., & Tulppo, M.P. (2010). Frequency of slow oscillations in arterial pressure and R–R intervals during muscle metaboreflex activation. *Autonomic Neuroscience: Basic and Clinical*, *152*(1-2), 88-95.

Kulkarni, S., O'Farrel, I., Erasi, M., & Kochar, M.S. (1998). Stress and hypertension. *WMJ: Official Publication of the State*, *97*(11), 34-38.

Kurylyak, Y., Lamonaca, F., & Grimaldi, D. (2013). A neural network-based method for continuous blood pressure estimation from a PPG signal. *2013 IEEE International Instrumentation and Measurement Technology Conference (I2MTC),* Minneapolis, USA, *12*, 280.

La Rovere, M.T., Pinna, G.D., & Raczak, G. (2008). Baroreflex sensitivity: measurement and clinical implications. *Ann Noninvasive Electrocardiol, 13*(2), 191-207.

Le, T., Ellington, F., Lee, T.Y., Vo, K., Khine, M., Krishnan, S.K., Dutt, N., & Cao, H. (2020). Continuous non-invasive blood pressure monitoring: a methodological review on measurement techniques. *IEEE Access*, *8*, 212478-212498.

Li, P., & Laleg-Kirati, T.M. (2021). Central blood pressure estimation from distal PPG measurement using semiclassical signal analysis features. *IEEE Access*, *9*, 44963-44973.

Li, K., Rudiger, H., & Ziemssen, T. (2019). Spectral analysis of heart rate variability: time window matters. *Frontiers in Neurology*, *10*(545), 1-12.

Lombardi, F. (1997). Spectral Analysis of Heart Rate Variability. *Cardiac Electrophysiology Review*, *1*(3), 335-337.

Ma, T., & Zhang, Y.T. (2005). A correlation study on the variabilities in pulse transit time, blood pressure, and heart rate recorded simultaneously from healthy subjects. *Proceedings of the 2005 IEEE Engineering in Medicine and Biology 27th Annual Conference*, Shanghai, China, 996-999.

Malpas, S.C. (2002). Neural influences on cardiovascular variability: possibilities and pitfalls. *American Journal of Physiology-Heart and Circulatory Physiology*, *282*(1), H6-H20.

Martinez, G., Howard, N., Abbott, D., Lim, K., Ward, R., & Elgendi, M. (2018). Can photoplethysmography replace arterial blood pressure in the assessment of blood pressure? *Journal of Clinical Medicine, 7*(10), 316.

Meidert, A.S., & Saugel, B. (2018). Techniques for non-invasive monitoring of arterial blood pressure. *Frontiers in Medicine, 4*(231).

Mohebbian, M.R., Dinh, A., Wahid, K., & Alam, M.S. (2020). Blind, cuff-less, calibration-free and continuous blood pressure estimation using optimized inductive group method of data handling. *Biomedical Signal Processing and Control*, *57*, 101682.

Mukkamala, R., Hahn, J.O., Inan, O.T., Mestha, L.K., Kim, C.S., Toreyin, H., & Kyal, S. (2015). Toward ubiquitous blood pressure monitoring via pulse transit time: theory and practice. *IEEE Transactions on Biomedical Engineering, 62*(8), 1879-1901.

Nguyen, Y., & Bora, V. (2022, September 18). *Arterial Pressure Monitoring*. StatPearls. https://www.ncbi.nlm.nih.gov/books/NBK556127.

Ogedegbe, G., & Pickering, T. (2010). Principles and techniques of blood pressure measurement. *Cardiol Clinic,* 28(4), 571-586.

Ortiz-Rangel, E., Guerrero-Ramirez, G.V., Garcia-Beltran, C.D., Guerrero-Lara, M., Adam-Medina, M., Astorga-Zaragoza, C.M., Reyes-Reyes, J., & Posada-Gomez, R. (2021). Dynamic modeling and simulation of the human cardiovascular system with PDA. *Biomedical Signal Processing and Control*, *71*, 103151.

Pan, J., & Zhang, Y. (2017). Improved blood pressure estimation using photoplethysmography based on ensemble method. *In Proceedings of the 14th International Symposium on Pervasive Systems, Algorithms and Networks & 11th International Conference on Frontier of Computer Science and Technology & Third International Symposium of Creative Computing,* Exeter, UK, 105-111.

Pham, T., Lau, Z.J., Chen, S.H.A., Makowski, D. (2021). Heart rate variability in psychology: a review of HRV indices and an analysis tutorial. *Sensors*, *21*(12), 3998.

Papaioannou, T.G., Vlachopoulos, C., Loakeimidis, N., Alexopoulos, N., & Stefanadis, C. (2006). Nonlinear dynamics of blood pressure variability after caffeine consumption. *Clinical Medicine and Research*, *4*(2), 114-118.

Priyanka, K.N.G., Chao, P.C.P., Tu, T.Y., Kao, Y.H., Yeh, M.H., Pandey, R., & Eka, F.P. (2018). Estimating blood pressure via artificial neural networks based on measured photoplethysmography waveforms. *2018 IEEE Sensors,* New Delhi, India, 1-4.

Ranganathan, N., Sivaciyan, V., & Saksena, F.B. (2007). *The Art and Science of Cardiac Physical Examination with Heart Sounds and Pulse Wave Forms on CD*. Humana Press.

Rangayyan, R.M. (2002). *Biomedical Signal Analysis: A Case-Study Approach*. Wiley-IEEE Press.

Rieger, S., Klee, S., & Baumgarten, D. (2018). Experimental characterization and correlation of mayer waves in retinal vessel diameter and arterial blood pressure. *Frontiers in Physiology,* 9(892).

Ruiz-Rodriguez, J.C., Ruiz-Sanmartin, A., Ribas, V., Caballero, J., Garcia-Roche, A., Riera, J., Nuvials, X., de Nadal, M., de Sola-Morales, O., Serra, J., & Rello, J. (2013). Innovative continuous non-invasive cuffless blood pressure monitoring based on photoplethysmography technology. *Intensive Care Medicine*, *39*(9), 1618–1625.

Sagirova, Z., Kuznetsova, N., Gogiberidze, N., Gognieva, D., Suvorov, A., Chomakhidze, P., Omboni, S., Saner, H., & Kopylov, P. (2021). Cuffless blood pressure measurement using a smartphone-case based ECG monitor with photoplethysmography in hypertensive patients. *Sensors*, *21*(10), 3525.

Seydnejad, S.R., & Kitney, R.I. (2001). Modeling of Mayer waves generation mechanisms. *IEEE Engineering in Medicine and Biology Magazine*, *20*(2), 92-100.

Sharma, M., Barbosa, K., Ho, V., Griggs, D., Ghirmai, T., Krishnan, S., Hsiai, T.K., Chiao, J.C., & Cao, H. (2017). Cuff-less and continuous blood pressure monitoring: a methodological review. *Technologies, 5*(2), 21.

Shin, W.J., Kang, S.J., Kim, Y.K., Seong, S.H., Ham, S.M., & Hwang, G.S. (2011). Link between heart rate and blood pressure Mayer wave during general anesthesia. *Clinical Autonomic Research*, *21*(5), 309-317.

Shin, H., & Min, S.D. (2017). Feasibility study for the non-invasive blood pressure estimation based on PPG morphology: normotensive subject study. *BioMedical Engineering Online, 16*(1), 10.

Shriram, R., Wakankar, A., Daimiwal, N., & Ramdasi, D. (2010). Continuous cuffless blood pressure monitoring based on PTT. *2010 International Conference on Bioinformatics and Biomedical Technology,* Chengdu, China, 51-55.

Singh, S., Shankar, R., & Singh, G.P. (2017). Prevalence and associated risk factors of hypertension: a cross-sectional study in urban Varanasi. *International journal of hypertension*, *2017*, 5491838.

Singh, O., & Sunkaria, R.K. (2017). Detection of onset, systolic peak and diastolic notch in arterial blood pressure pulses. *Measurement and Control*, *50*(7-8), 170-176.

Slapnicar, G., Mlakar, N., Lustrek, M. (2019). Blood pressure estimation from photoplethysmogram using a spectro-temporal deep neural network. *Sensors*, *19*(15), 3420.

Soh, D.C.K., Ng, E.Y.K., Jahmunah, V., Oh, S.L., Tan, R.S., & Acharya, U.R. (2020). Automated diagnostic tool for hypertension using convolutional neural network. *Computers in Biology and Medicine*, *126*, 103999.

Solinsky, R., Vivodtzev, I., Hamner, J.W., Taylor, J.A. (2021). The effect of heart rate variability on blood pressure is augmented in spinal cord injury and is unaltered by exercise training. *Clinical Autonomic Research, 31*(2), 293-301.

Sun, Y., & Thakor, N. (2016). Photoplethysmography revisited: from contact to noncontact, from point to imaging. *IEEE Transactions on Biomedical Engineering*, *63*(3), 463-477.

Swenne, C.A. (2013). Baroreflex sensitivity: mechanisms and measurement. *Netherlands heart journal: monthly journal of the Netherlands Society of Cardiology and the Netherlands Heart Foundation*, *21*(2), 58-60.

Takalo, R., Korhonen, I., Turjanmaa, V., Majahalme, S., Tuomisto, M., & Uusitalo, A. (1994). Short-term variability of blood pressure and heart rate in borderline and mildly hypertensive subjects. *Hypertension*, *23*(1), 18-24.

Teng, X.F., & Zhang, Y.T. (2003). Continuous and noninvasive estimation of arterial blood pressure using a photoplethysmographic approach. *Proceedings of the 25th Annual International Conference of the IEEE EMBS,* Cancun, Mexico, *17*(21), 3153-3156.

Thambiraj, G., Gandhi, U., Mangalanathan, U., Jose, V.J.M., & Anand, M. (2020). Investigation on the effect of Womersley number, ECG and PPG features for cuff less blood pressure estimation using machine learning. *Biomedical Signal Processing and Control*, *60*, 101942.

Tikhonova, I.V., Grinevich, A.A., & Tankanag, A.V. (2021). Analysis of phase interactions between heart rate variability, respiration and peripheral microhemodynamics oscillations of upper and lower extremities in human. *Biomedical Signal Processing and Control*, *71*, 103091.

Vieira, S.S., Lemes, B., de Carvalho, P.D.T.C., de Lima, R.N., Bocalini, D.S., Junior, J.A.S., Arsa, G, Casarin, C.A, Andrade, E.L., & Serra, A.J. (2016). Does stroke volume increase during an incremental exercise? a systematic review. *Open Cardiovasc Medicine Journal*, *10*, 57-63.

Wang, W., Mohseni, P., Kilgore, K.L., & Najafizadeh, L. (2022). Cuff-less blood pressure estimation from photoplethysmography via visibility graph and transfer learning. *IEEE Journal of Biomedical and Health Informtics, 26*(5), 2075-2085.

Wang, Z., & Zhang, Y. (2017). A novel frequency domain method for estimating blood pressure from photoplethysmogram. *Proceedings of the 9th International Conference on Signal Processing System,* Auckland, New Zealand, 201-206.

Wang, L., Zhou, W., Xing, Y., & Zhou, X. (2018). A novel neural network model for blood pressure estimation using photoplethesmography without electrocardiogram. *Journal of Healthcare Engineering, 2018*, 7804243.

Whelton, P.K., Carey, R.M., Aronow, W.S., Casey, D.E., Collins, K.J., Himmelfarb, C.D., Depalma, S.M., Gidding, S., Jamerson, K.A., Jones, D.W., MacLaughlin, E.J., Munter, P., Ovbiagele, B., Smith, S.C., Spencer, C.C., Stafford, R.S., Taler, S.J., Thomas, R.J., Williams, K.A., Williamson, J.D., & Wright, J.T. (2018). 2017 ACC/AHA/AAPA/ABC/ACPM/AGS/APhA/ASH/ASPC/NMA/PCNA guideline for the prevention, detection, evaluation, and management of high blood pressure in adults: a report or the American college of cardiology/ American heart association task force on clinical practice guidelines. *Journal of the American College of Cardiology*, *71*(19), e127-e248.

Xing, X., & Sun, M. (2016). Optical blood pressure estimation with photoplethysmography and FFT-based neural networks. *Biomedical Optics Express, 7*(8), 3007-3020.

Xing, X., Ma, Z., Zhang, M., Zhou, Y., Dong, W., & Song, M. (2019). An unobtrusive and calibration-free blood pressure estimation method using photoplethysmography and biometrics. *Scientific Reports, 9*(1), 8611.

Yamakoshi, T., Rolfe, P., & Yamakoshi, K.I. (2021). Cuffless blood pressure estimation based on haemodynamic principles: progress towards mobile healthcare. *PeerJ*, *9*(8476), e11479.

Zhang, Y., Zhou, C., Huang, Z., Ye, X. (2021). Study of cuffless blood pressure estimation method based on multiple physiological parameters. *Physiological Measurement, 42,* 055004.

Chapter 3: Cuffless Blood Pressure Estimation Using Cardiovascular Dynamics

---

Samimi, H., Dajani, H.R. (2022). Cuffless blood pressure estimation using cardiovascular dynamics. In Proceedings of the International Conference on Electrical, Computer and Energy Technologies (ICECET 2022), Prague, Czech Republic, available in IEEE Xplore: https://ieeexplore-ieee-org.proxy.bib.uottawa.ca/document/9872800.

Abstract: Noninvasive estimation of blood pressure is important in preventing and managing cardiovascular disease. The cuffless technique has captured a lot of attention in recent years to unobtrusively provide continuous monitoring of blood pressure. This paper proposes a calibration-free approach, which makes use of dynamic changes of the pulse waveform over brief time intervals. Experimental results from two studies, the first using normalized intra-arterial blood pressure waveforms from 390 patients and the second using photoplethysmogram (PPG) waveforms from 200 patients, show that the accuracy of the proposed method for estimating the diastolic blood pressure (DBP) falls within the accuracy criteria of the Association for Advancement of Medical Instrumentation/European Society of Hypertension/International Organization for Standardization (AAMI/ESH/ISO) standard and achieves grade B based on the British Hypertension Society (BHS) standard. In addition, a correlation of 99.4% was found between the inter-beat intervals (IBIs) obtained from the PPG and the intra-arterial waveforms in 390 patients. This paper demonstrates the possibility of using the PPG signal for estimation of blood pressure based on analysis of dynamic changes in the IBI.

3.1 Introduction

Cardiovascular disease (CVD) is the most frequent cause of death worldwide. According to the World Health Organization, 32% of deaths in 2019 were related to cardiovascular

ailments. This accounts for 17.9 million people (World Health Organization, 2021). A common condition leading to CVD is high blood pressure or hypertension (Sharma et al., 2017). Hypertension mostly develops without any sign in preliminary stages and that is why most hypertension patients do not know about their condition (Kachuee et al., 2017). Hypertension, or as some call it, the silent killer, is also associated with harming other internal body organs such as kidney, brain, eyes, etc. (Kachuee et al., 2017). To diagnose hypertension, accurate blood pressure (BP) measurement is necessary.

BP is a force that is applied to the walls of vessels by blood while it is circulating in the body to deliver oxygen and nutrients to organs. Each heartbeat generates a maximum, called systolic blood pressure (SBP), and a minimum, called diastolic blood pressure (DBP) that are measured in millimeters of mercury. Traditionally, a person is diagnosed with hypertension if at rest condition his/her SBP exceeds 140 or the DBP exceeds 90 mmHg (Kachuee et al., 2017). However, recent guidelines from the American Heart Association suggest that a diagnosis of hypertension should be made if the SBP or DBP exceed 130 mmHg or 80 mmHg, respectively (Cifu and Davis, 2017).

At present, direct (invasive) and indirect (noninvasive) methods are used for measuring blood pressure. The direct technique is mostly used in a clinical setting for patients with unstable condition or under vasoactive treatments and it allows for continuous collection of data with higher accuracy in comparison to indirect techniques. The drawback of this method is that it is invasive and requires cannulating an artery to obtain the intra-arterial blood pressure measurement (Esmaelpoor et al., 2020). Commonly used indirect methods on the other hand cannot provide continuous measurement due to periodic cuff inflation and deflation. In addition, cuff inflation applies pressure on the measuring limb and this results in discomfort (Zambrana-Vinaroz et al., 2019), which can be particularly problematic during sleep (Fong et al., 2019). These limitations underline the need for development of new

methods that can measure blood pressure accurately and continuously in a more comfortable way.

One such method that has seen increasing interest in recent years is the cuffless technique. The increase in demand for this technique is primarily due to significant need and increased feasibility. Since hypertension is a serious problem that does not have a high rate of detection, cuffless blood pressure monitoring methods could improve the detection rate by providing out of clinic measurements and offering patients and clinicians with continuous feedback. As a result, hypertension detection rate might be improved, and cases could be treated that otherwise would have been at great cardiovascular risk. In addition, with the latest technological advancement in wearable sensing, computational power, and size optimization, developing such techniques seems more achievable now (Mukkamala et al., 2015).

Currently, the two most popular types of approaches for cuffless estimation of blood pressure are based on either the pulse transit time or on features extracted from pulse morphology within individual heartbeats (Soltan-Zadi et al., 2018; Yan et al., 2019; Hosanee et al., 2020). However, previous research has shown that oscillations in heart rate and blood pressure are due to sympathetic and parasympathetic activity of the autonomic nervous system (Tobaldini et al., 2013; Goldoozian et al., 2017). We also know that blood pressure is a function of cardiac output and vascular resistance that are both controlled by the autonomic nervous system (Guyenet et al., 2006). This suggests that there is a link between cardiovascular dynamics and blood pressure (Fong et al., 2019). One study on hypertensive patients has reported increase of sympathetic tone and a small reduction in parasympathetic tone by analyzing the heart rate variability (HRV) for these patients in the frequency domain (Chen et al., 2018). The power spectral density (PSD) of the HRV showed clear peaks at high frequency (HF, 0.15-0.4 Hz) and low frequency (LF, 0.04-0.15 Hz) for people with normal blood pressure while there was only one peak at LF for hypertensive patients. Another study,

after analyzing heart rate variability (HRV) and changes in blood pressure level, concluded that the increase in BP is related to three factors in HRV: reduction of overall short term HRV, increased power of high frequency components, and reduction in nonlinear heartbeat dynamics (Sannino et al., 2015).

In this work, we investigated the relationship between cardiovascular dynamics expressed in the arterial pulse waveform oscillations and the blood pressure level. We systemically studied dynamic changes over brief intervals and not changes in the morphology of the pulse waveform in each heartbeat. This paper also addresses the question of whether the photoplethysmogram (PPG) can be used as surrogate for the arterial pulse waveform for estimation of BP based on analysis of dynamic changes.

This is a novel approach to cuffless blood pressure monitoring and is based on the hypothesis that the cardiovascular oscillatory dynamics change with the blood pressure level.

3.2 Methodology

Figure 3-1 shows the high-level methodology used in this work for estimation of blood pressure.

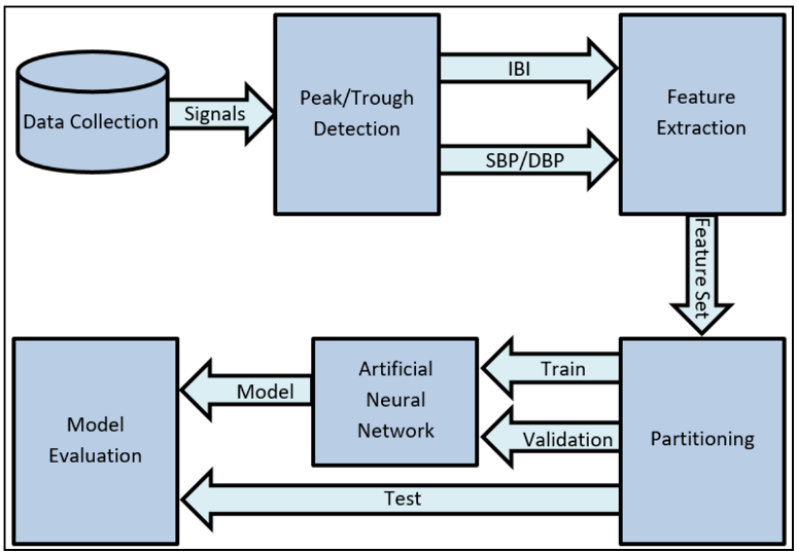

Figure 3-1. Block diagram of the proposed method for cuffless blood pressure estimation.

3.2.1 Data Collection

The pulse waveform may be recorded noninvasively and without a cuff using methods such as tonometry (Abreu et al., 2020). However, since we know that pulsation of blood pressure causes the pulsating of blood volume that generates the PPG signal and due to the fact that previous research has indicated high correlation between spectral components of the PPG and arterial pulse waveforms (Xing and Sun, 2016), we explored whether a PPG signal may also serve as a surrogate for the pulse waveform in terms of using signal dynamics to estimate BP.

In this study, the bio-signal data set from the University of California Irvine (UCI) Machine Learning Repository (Kachuee et al., 2015; UCI machine learning repository, 2015) is used. This collection is a subset of the Multiparameter Intelligent Monitoring in Intensive Care (MIMIC II) data, that is an open-source database. MIMIC II is provided by the PhysioNet organization and is a collection of multiparameter recordings gathered by patient monitors at various hospitals from more than 15000 intensive care unit (ICU) patients. The waveforms are sampled at 125Hz with at least 8-bit resolution. The UCI dataset is a selection from MIMIC II data obtained after the following processing steps. The original data is first divided into fixed size signal blocks. Then a simple averaging filter is applied to each part. Any block with irregular blood pressure or heartbeat is removed. Autocorrelation is then calculated for PPG signal to find the degree of similarity between successive pulses in a block, and any block that contains high variation between successive pulses is removed (Kachuee et al., 2015). For this work, PPG (from fingertip) and invasive arterial blood pressure (ABP) pulse waveforms are extracted from 590 patients with signal duration between 8 to 10 minutes. We have chosen our dataset by visually inspecting the signals with desirable duration and selecting the ones that provide minimal or no interruptions.

The ABP waveforms were transformed to uncalibrated arterial pulse waveforms through normalization. This was done by considering each set of data (data collected from one person)

and scaling it to fit within the range of 0 and 1. As a result of this process, information from blood pressure level that existed in the amplitude of the peaks and troughs of the arterial pulse waveform, corresponding to SBP and DBP respectively was eliminated.

3.2.2 Peak/Trough Detection

For both arterial pulse waveform and PPG peak/trough detections, we used an algorithm that is a modified version of the one developed by Pan and Tompkins for QRS detection (Pan and Tompkins, 1985). In this modified algorithm, the arterial pulse waveform or the PPG goes through a low pass, a high pass and moving average filter to clean the signal. The peaks for the signals are found based on the local maximum within a predefined time interval and through a set threshold for the output of the moving average filter. The same procedure is repeated on the inverted signals to find the troughs of the original signal.

3.2.3 Correlation between PPG and Invasive Intra-arterial Blood Pressure

Reference (Xing and Sun, 2016) reported that the amplitudes and phases of the alternating current components of a PPG signal are well correlated to invasive intra-arterial blood pressure values (Xing and Sun, 2016). However, another study by (Martinez et al., 2018), found that the relationship between the PPG and intra-arterial blood pressure is more complex. That study investigated three hypotheses on the correlation between PPG signals and corresponding ABP waveforms. The hypotheses were: amplitude of PPG and ABP is correlated, morphology of PPG and ABP is correlated, and there is mutual information between the two signals. Their conclusion for out-of-phase analysis (for the first and the third hypotheses) and through in-phase analysis (for the second hypothesis) was that there is poor correlation between ABP and PPG in terms of beat-by-beat amplitude. On the other hand, the morphology of the two signals is highly correlated in the time domain, although, as the ABP increases in amplitude, different phase shifts between the two signals appear. The results also

indicated that there is mutual information between the two signals in both time domain and frequency domain and increase in ABP amplitude results in increase of the coupling of the signals (Martinez et al., 2018).

Considering the above findings, we investigated the correlation between the inter-beat intervals (IBIs) for the PPG and the normalized intra-arterial blood pressure pulse waveforms to determine if the PPG could act as a surrogate waveform for the arterial pulse waveform for our proposed method. Evidence of a high correlation between IBIs of PPG and ABP would allow us to directly use the IBIs obtained from PPG signal for BP estimation. For this comparison we considered PPG and ABP signals from 390 patients. IBIs were measured for both signals (Figure 3-2) and the Pearson correlation coefficient was calculated between the two IBI sets using:

$$\rho_{X,Y} = \frac{\mathrm{cov}(X,Y)}{\sigma_X \sigma_Y} \qquad \textbf{Equation 3-1}$$

where cov is covariance, σ_X is the standard deviation of X (the IBI values for PPG), and σ_Y is the standard deviation of Y (the IBI values for ABP).

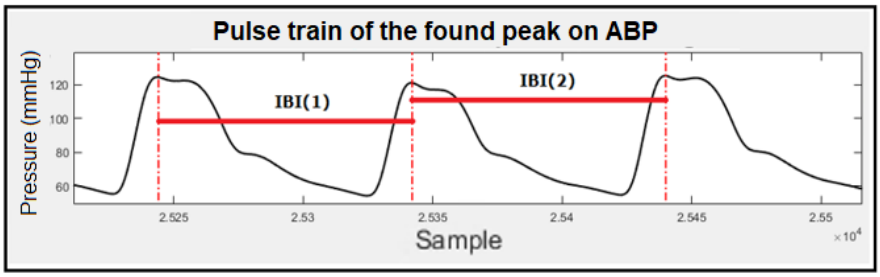

Figure 3-2. Determination of IBI using signal peaks. In this illustration, two time intervals associated with the IBI are indicated by IBI(1) and IBI(2).

3.2.4 Feature Extraction

We considered IBIs from the PPG signals as well as the normalized blood pressure waveform to extract features related to cardiovascular dynamics for estimation of blood pressure. Using IBI time series, we collected features through time domain, frequency domain, and nonlinear

analysis. The combination of IBI and blood pressure parameters also provided features based on baroreflex sensitivity (BRS), as discussed below.

For IBI analysis we used an open-source heart rate variability analysis software (Ramshur, 2010). Inputs to the analyzer are the time series containing IBI. For time domain analysis, statistical and geometric measurements are considered. Statistical features in this study include: mean IBI, standard deviation of IBI series (SDANN), root mean square of successive differences of the IBI series, number of successive differences that are greater than a user defined threshold (NNx) in milliseconds (threshold of 10 ms for this study), and percentage of NNx over the duration of the signal. As for geometric features, they are calculated based on IBI histogram and include: pulse rate variability triangular index (PRVti), and triangular interpolation of IBI histogram (TINN) (Malik et al., 1993).

For frequency domain analysis, power spectral density of IBI signals is calculated in the following three bands: very low frequency (VLF, 0.098-0.05Hz), low frequency (LF, 0.05-0.15Hz) and high frequency (HF, 0.15-0.5Hz). To obtain the power spectral density, we used the Lomb-Scargle periodogram (LSP) (Thong et al, 2004).

For the nonlinear analysis of the IBI series, we used Poincaré plot (Kamen and Tonkin, 1995), sample entropy (Richman and Moorman, 2000), and detrended fluctuation analysis (Peng et al., 1994). Self-similarity is the basis for Poincaré plot or return map and is quantified by mapping an IBI interval versus a previous IBI interval (Kamen and Tonkin, 1995). Sample entropy (SampleEn) is a method used to quantify signal complexity and can be defined as the negative natural logarithm of the conditional probability that if two sets of simultaneous m-length sequence have distance less than r and their length is increased to m+1, the new sets also have distance less than r (Richman and Moorman, 2000). Detrended fluctuation analysis (DFA) quantifies the self-similar properties of nonstationary time series (Peng et al., 1994).

Frequency domain analysis is performed on the pulse pressure, systolic, and diastolic waveforms to generate desired features that can be used for regression. The pulse pressure

is defined as the difference between each systolic peak and the corresponding diastolic trough in the blood pressure signal (Shao et al., 2020). Normalized blood pressure is used in pulse pressure waveform analysis as well as the systolic and diastolic waveform analysis. The pulse pressure waveform is generated by interpolating the collected data (the difference between each systolic peak and diastolic trough), then using spline interpolation and resampling at the rate of 1 kHz. The resulting signal then is down sampled to 5 Hz. The same principle is used to generate systolic and diastolic waveforms. All systolic blood pressure points in the arterial pulse waveform are connected together (through interpolation and resampling) to generate a systolic waveform while the same procedure on diastolic points results in a diastolic waveform.

Following the method in (Ando et al., 1997), each signal is subdivided into segments of 512 points with 50% overlap. Linear trend of the data is subtracted from the signals and a Blackman-Harris window is applied to reduce spectral leakage. The power spectrum is obtained from each segment and averaged over all the segments to minimize spectral variance for the desired frequency bands, namely very low frequency 0.098-0.05Hz, low frequency 0.05-0.15Hz, and high frequency 0.15-0.5Hz.

Another parameter that is considered in this study is the baroreflex, which is a basic mechanism that regulates blood pressure in the short term. Baroreflex sensitivity (BRS) is defined as the change in inter-beat intervals per unit change of blood pressure (Swenne et al., 2013). We obtained spectral BRS based on the method used by (Frattola et al., 1997). In this method both the original blood pressure waveform and the IBIs from normalized blood pressure waveform are used to generate two time-series: the IBI values and the systolic peaks. First, both time series are interpolated and resampled at 5 Hz to provide the IBI and the systolic peak waveforms. Both waveforms are then passed through a high pass filter with cut off frequency of 0.025 Hz, and the filtered signals are subdivided to segments of 256 points. The reverse arrangement test is performed on the data to detect segments that include

nonstationary data and exclude them from the time series. Each segment is further multiplied by a 10% cosine tapering window. In the last step of the process, power spectral density for each segment is calculated using FFT. To obtain BRS value, the square ratio between systolic blood pressure and IBI powers is calculated in the frequency range of 0.07Hz to 0.14Hz in any segment in which the coherence between the two signals is over 0.5. The same procedure is repeated to obtain BRS values for diastolic blood pressure. Table 3-1 summarizes all the computed parameters related to cardiovascular dynamics used as features in our study.

After collecting all the features as described above, we used wrapper subset evaluation with forward greedy stepwise search method to select features to be used in the estimation model (Hameed et al., 2018). This method resulted in 5 features for estimation of systolic blood pressure (mean IBI, NNx, pNNx, SD2 and α1) and 6 features for estimation of diastolic blood pressure (mean IBI, NNx, pNNx, PRVTi, SampleEn and the IBI ratio of LF/HF).

Table 3-1. List of considered parameters related to cardiovascular dynamics used in this study.

Type of Signal Used	Measure	Description
IBI Time-Domain	Mean IBI	Mean of IBI
	SDNN	Standard deviation of IBI
	RMSSD	Root mean square of successive differences of the IBI series
	NNx	Number of successive IBIs that are larger than a user define threshold in milliseconds
	pNNx	Percentage of NNx over duration of the signal
	PRVti	Pulse rate variability triangular index
	TINN	Triangular interpolation of IBI histogram
IBI Frequency-Domain	VLF	Power of very low frequency band
	LF	Power of low frequency band
	HF	Power of high frequency band
	LF/HF	Ratio between low and high frequency band posers
IBI Nonlinear-Domain	SD1	Standard deviation of instantaneous beat to beat variability (Poincaré plot)
	SD2	Standard deviation of continuous beat to beat variability (Poincaré plot)
	SampEn	Sample entropy
	$\propto_1$	Short term fluctuation slope in Detrended Fluctuation Analysis
	$\propto_2$	Long term fluctuation slope in Detrended Fluctuation Analysis
Pulse Pressure, Systolic, and Diastolic Waveforms	VLF	Power of very low frequency band
	LF	Power of low frequency band
	HF	Power of high frequency band
IBI and BP Waveforms	BRS	Baroreflex sensitivity - Spectral

3.2.5 Partitioning

The leave-one-out method was used to partition data for evaluating the performance of the estimator. Collected data was from 590 subjects (390 with normalized intra-arterial waveform and a separate set of 200 with PPG). We set aside all the features (5 features for systolic and 6 features for diastolic blood pressure) mentioned above from one subject to be used as the test data and the remaining features were divided into 85% training and 15% validation. This procedure was repeated 390 times for the normalized arterial waveform and 200 times for the PPG to test over the entire dataset. The validation data was used to avoid overfitting using the early stopping technique (Yao et al., 2007).

3.2.6 Artificial Neural Network

Initially, a number of different regression algorithms such as Linear Regression, Decision Tree, KNN Model and Artificial Neural Network (ANN) were considered to be used for estimation. However, due to the higher estimation accuracy obtained by the ANN, the Neural Network Toolbox in Matlab was adopted to be used in this work. The structure of the ANN was based on a two-layer feed-forward network with sigmoid hidden and output neurons. Different numbers of neurons (from 1 to 30) were examined to determine the best structure. The best performing structure consisted of 10 neurons in the hidden layer. The network was trained with Bayesian Regularization backpropagation algorithm and the structure of the ANN was fixed prior to evaluating with the test data. The extracted features (input) and the corresponding average SBP or DBP over the signal interval (target) were standardized to provide a mean of zero and standard deviation of one for both input and target. Two different networks were trained for each of ABP and PPG data.

3.2.7 Model Evaluation

The model was evaluated based on the mean error, mean absolute error, and the standard deviation of the error obtained with the test data. The equations below show the calculation

procedure for mean error (ME) and mean absolute error (MAE) where x_i is the prediction and y_i is the true value, which is obtained as the average SBP or DBP over the interval obtained from the original nonnormalized ABP waveform.

$$\mathbf{ME} = \frac{\sum_{i=1}^{n} y_i - x_i}{n} \qquad \textbf{Equation 3-2}$$

$$\mathbf{MAE} = \frac{\sum_{i=1}^{n} |y_i - x_i|}{n} \qquad \textbf{Equation 3-3}$$

Standard deviation of the error is calculated based on Equation 3-4 where e_i is the calculated error between the prediction and the true value ($e_i = y_i - x_i$) for each estimation and $\bar{e}$ is the average of e_i.

$$\mathbf{SDE} = \sqrt{\frac{\sum_{i=1}^{n} |e_i - \bar{e}|^2}{n}} \qquad \textbf{Equation 3-4}$$

3.3 Results

The work in this paper is divided into three main sections: blood pressure estimation based on normalized intra-arterial waveform, correlation between IBIs in PPG and intra-arterial waveform, and estimation of blood pressure based on PPG signals.

Blood pressure estimation results based on normalized arterial pulse waveform are shown in Table 3-2. This table displays the errors for SBP and DBP obtained through an ANN model and based on the extracted IBI features from 390 patients. Details of the feature selection and the model are described earlier in methodology section.

Table 3-2. Blood pressure estimation performance using IBI features from 390 normalized arterial pulse waveforms. 5 features are used for systolic BP and 6 features for diastolic BP. The results are averaged over the 390 patients.

	ME (mmHg)	**SDE (mmHg)**	**MAE (mmHg)**
Diastolic BP	-0.7	7.16	5.85
Systolic BP	-1.17	16.86	13.97

Table 3-3 shows the blood pressure estimation results obtained from intra-arterial pulse waveform along with the proposed method in this paper and compares them to the standard from the Association for Advancement of Medical Instrumentation/European Society of Hypertension/International Organization for Standardization (AAMI/ESH/ISO) (Stergiou et at., 2018). This standard requires a number of characteristics to be followed along with accuracy level of BP estimations. Solely base on the accuracy pass/fail criteria of the standard, our proposed method achieves a pass for DBP.

Table 3-3. Comparison between the proposed method and the AAMI/ESH/ISO standard using normalized arterial pulse waveforms from 390 patients.

		ME (mmHg)	**SDE (mmHg)**	**Subjects**
AAMI/ESH/ISO	SBP and DBP	≤ 5	≤ 8	≥ 85
Our Results	DBP	-0.7	7.16	390
	SBP	-1.17	16.86	390

The accuracy result from the above-mentioned model is also compared to the British Hypertension Society (BHS) standard. BHS requires a minimum sample size of 85 subjects and categorizes the performance into four grades based on the percentage of measurements differing from the reference measurement obtained by two trained observers. The difference between the test result and reference is calculated for each observer for both systolic and diastolic pressures separately (O'Brien et al., 1993). As shown in Table 3-4, the performance of the normalized arterial pulse waveform with the proposed method is consistent with grade B for DBP.

Table 3-4. Comparison between the proposed method and the BHS standard using normalized arterial pulse waveforms from 390 patients.

		Cumulative Error Percentage		
		≤ 5 mmHg	**≤ 10 mmHg**	**≤ 15 mmHg**
BHS	Grade A	60%	85%	95%
	Grade B	50%	75%	90%
	Grade C	40%	65%	85%
	Grade D	Worse than C		
Our Results	DBP	50.21%	81.03%	97.18%
	SBP	21.28%	40.26%	56.41%

In order to study the feasibility of replacing IBI features from the normalized arterial waveform with the ones from PPG signal, the correlation between IBIs obtained from these two signals was examined. The correlation coefficient was calculated by comparing the two sets of IBI values where each set contained all IBIs from 390 patients. As shown in Figure 3-3 the two sets of data (IBIs of ABP and IBIs of PPG) are strongly correlated (correlation coefficient equal to 0.994). This result indicated that the normalized arterial pulse waveform can be replaced with the PPG signal for estimating BP using IBI dynamics.

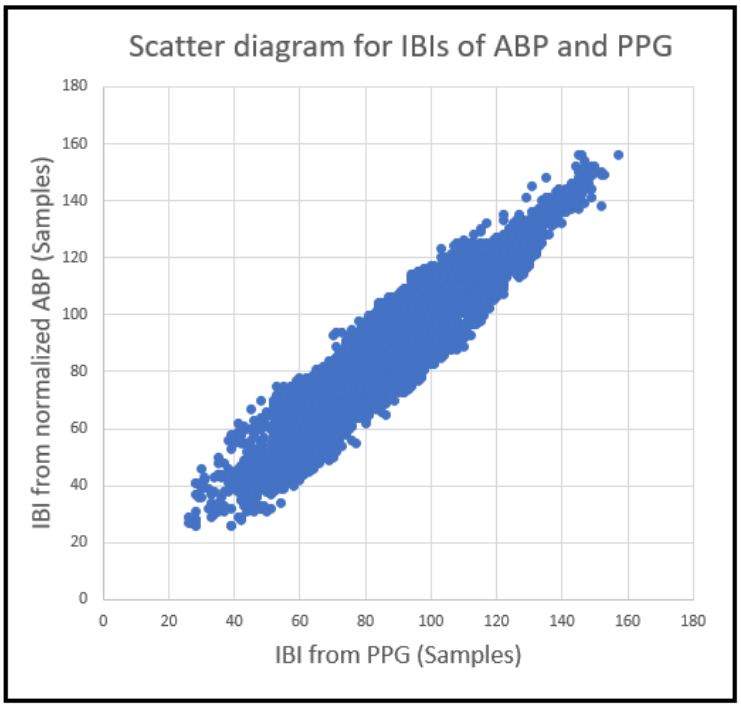

Figure 3-3. Scatter diagram for IBIs of ABP and PPG collected from 390 patients.

Having established that IBIs from the ABP and PPG signals are highly correlated, we then estimated BP based on IBI dynamics obtained from PPG signals in 200 new patients different from the 390 patients who were used for estimating BP from the normalized ABP signals. The same 8 IBI features were used (but this time from PPG instead of the normalized ABP) and the same ANN model as the one that was used earlier. Table 3-5, Table 3-6 and Table 3-7 show the blood pressure estimation results obtained using the IBI dynamics in the PPG signals based on AAMI/ESH/ISO and BHS standards respectively. The results show that our proposed method passes the accuracy requirement of the AAMI/ESH/ISO standard and a grade B of the BHS standard for DBP estimation.

Table 3-5. Blood pressure estimation performance using IBI features from 200 PPG waveforms. 5 and 6 features are used for systolic BP and diastolic BP respectively. Results are averaged over the 200 patients.

	ME (mmHg)	**SDE (mmHg)**	**MAE (mmHg)**
Diastolic BP	0.03	7.91	5.75
Systolic BP	0.09	18.81	14.49

Table 3-6. Comparison between the proposed method and the AAMI/ESH/ISO standard using PPG signals from 200 patients.

		ME (mmHg)	**SDE (mmHg)**	**Subjects**
AAMI/ESH/ISO	SBP and DBP	≤ 5	≤ 8	≥ 85
Our Results	DBP	0.03	7.91	200
	SBP	0.09	18.81	200

Table 3-7. Comparison between the proposed method and the BHS standard using PPG signals from 200 patients.

		Cumulative Error Percentage		
		≤ 5 mmHg	**≤ 10 mmHg**	**≤ 15 mmHg**
BHS	Grade A	60%	85%	95%
	Grade B	50%	75%	90%
	Grade C	40%	65%	85%
	Grade D	Worse than C		
Our Results	DBP	56%	83%	95%
	SBP	24%	46.5%	57%

3.4 Discussion

The findings of this work suggest that the proposed approach to cuffless blood pressure monitoring system based on analysis of the IBI dynamics over brief intervals, and using only the photoplethysmogram signal, could be useful on its own or as a complement to other cuffless BP estimation methods. One potential advantage of using IBI dynamics over pulse morphology is that it is likely less susceptible to changes in sensor position, differences in skin color, etc. because they depend only on the timings of peaks or troughs in the signal.

In this study we considered 23 features for our initial analysis prior to feature selection for ANN. Out of these features, 16 were related to IBI variability (seven in time domain, four in frequency domain and five from nonlinear analysis). The remaining 7 features were from BRS and frequency domain analysis of systolic, diastolic and pulse pressure waveforms. We then used wrapper subset evaluation with forward greedy stepwise search method for feature selection. Five features for SBP and 6 features for DBP estimation (all related to IBI variability) were selected to be used in the ANN. In the first part of the analysis, we used normalized ABP waveforms from 390 patients to estimate blood pressure. The DBP estimation using this method, meets the expected accuracy of the AAMI/ESH/ISO standard and a grade B based on the BHS standard. For SBP, although the result from mean error was well below the

acceptable threshold in the AAMI/ESH/ISO standard, the standard deviation was too high compared to the acceptable value.

In the second part of the analysis, we used the normalized ABP signals along with the PPG signals from 390 patients to examine whether the IBIs from both are sufficiently similar to allow the PPG to be used as a surrogate for the arterial pulse waveform in the estimation of BP based on IBI dynamics. Our analysis revealed a high correlation coefficient of 99.4% between the IBIs obtained from the ABP and PPG.

Having established that the PPG may be usable as a surrogate for the ABP, in the last part of the analysis we used IBIs obtained from PPG signals of 200 patients. The performance obtained using PPG signals is similar to what we obtained with the normalized ABP. This further supports the use of PPG as a substitute for the intra-arterial pulse waveform when estimating blood pressure based on IBI dynamics. Our analysis in this part showed that the accuracy for DBP estimation meets both the threshold for grade B of the BHS standard and the one for the AAMI/ESH/ISO standard. Similar to our results with normalized ABP, the estimates of SBP did not receive a passing grade.

Previous work has shown that PPG peaks can be used to measure HRV (Alqaraawi et al., 2016), and the finding by (Mori et al., 2014) on the association between HRV indices and BP could help explain the difference between estimation performance for SBP and DBP. A significant association between HRV indices and both SBP and DBP was found in females, whereas for males there was no association between these indices and SBP. Although information about the gender composition of the datasets that we analyzed is not available, it is likely that there is a relatively equal mix of males and females. As a result, BP estimation based on IBI dynamics would be expected to be less accurate for SBP than for DBP.

This study also had some limitations. Firstly, the MIMIC dataset that was used is based on signals collected from the intensive care unit (ICU). This means that almost all signals in our dataset were potentially collected while the patient was under influence of medications or

other interventions which could cause abnormal blood pressure dynamics. Secondly, people who are admitted to the ICU may have some type of heart condition, and hence BP estimation based on their cardiovascular signals may not be reflective of what could be obtained with the general population. Thirdly, some useful information such as age, height, weight, and gender of participants that can offer valuable data in the estimation process was not available.

Despite these limitations we show that using IBI dynamic changes in the photoplethysmogram (PPG) may be used to estimate DBP. As for SBP, greater improvement is needed to comply with the measurement standards.

3.5 Conclusion and Feature Work

In this work we investigated an approach for cuffless estimation of blood pressure that is based on the relationship between cardiovascular oscillatory dynamics and the blood pressure level. This approach is different from current popular approaches that are based on the pulse transit time or pulse morphology within individual beats. Our proposed method was to study dynamic changes over relatively short intervals and use the derived information to estimate blood pressure level.

The results confirmed our hypothesis that the cardiovascular oscillatory dynamics contain information useful for calibration-free estimation of blood pressure level. However, to be able to use the information from cardiovascular dynamics as a basis for accurate cuffless blood pressure monitoring system, further work should focus on developing a suitable calibration procedure to improve the estimation result for both SBP and DBP. This approach may also be combined with popular approaches based on the pulse transit time or pulse morphology within individual beats to improve cuffless BP estimation accuracy.

3.6 References

Abreu, P., Carneiro, F., & Restivo, M.T. (2020). Screening system for cardiac problems through non-invasive identification of blood pressure waveform. *Information*, *11*(150), 1-7.

Alqaraawi, A. Alwosheel, A. Alasaad, A. (2016). Heart rate variability estimation in photoplethysmography signals using Bayesian learning approach. *Healthcare Technology Letter*, 3(2), 136-142.

Ando, S., Dajani, H.R., & Floras, J.S. (1997). Frequency domain characteristics of muscle sympathetic nerve activity in heart failure and healthy humans. *American Journal of Physiology - Regulatory Integrative and Comparative Physiology, 273*, R205-R212.

Chen, Y., Shi, S., Liu, Y., Huang, S., & Ma, T. (2018). Cuffless blood pressure estimation method using a heart rate variability derived parameter. *Physiological Measurement*, 39(9).

Cifu, A.S., & Davis, A.M. (2017). Prevention, detection, evaluation, and management of high blood pressure in adults. *JAMA, 318*(21), 2132-2134.

Esmaelpoor, J., Moradi, M.H., & Kadkhodamohammadi, A. (2020). A multistage deep neural network model for blood pressure estimation using photoplethysmogram signals. *Computers in Biology and Medicine*, *120*, 103719.

Fong, M.W.K., Ng, E.Y.K., Jian, K.E.Z., & Hong, T.J. (2019). SVR ensemble-based continuous blood pressure prediction using multi-channel photoplethysmogram. *Computers in Biology and Medicine, 113*, 103392.

Frattola, A., Parati, G., Gamba, P., Paleari, F., Mauri, G., Di Rienzo, M., Castiglioni, P., Manica, G. (1997). Time and frequency domain estimates of spontaneous baroreflex sensitivity provide early detection of automatic dysfunction in diabetes mellitus. *Diabetologia*, *40*(12), 1470-1475.

Goldoozian, L., Zahedi, E., & Zarzoso, V. (2017). Time-varying assessment of heart rate variability parameters using respiratory information. *Computers in Biology and Medicine*, *89*, 355-367.

Guyenet, P.G. (2006). The sympathetic control of blood pressure. *Neuroscience*, *7*(5), 335-346.

Hameed, S.S., Petinrin, O.O., Hashi, A.O., & Saeed, F. (2018). Filter-wrapper combination and embedded feature selection for gene expression data. *International Journal of Advances in Soft Computing and its Applications*, *10*(1), 90-105.

Hosanee, M., Chan, G., Welykholowa, K., Cooper, R., Kyriacou, P.A., Zheng, D., Allen, J., Abbott, D., Menon, C., Lovell, N.H., Howard, N., Chan, W.S., Lim, K., Fletcher, R., Ward, R., & Elgendi, M. (2020). Cuffless single-site photoplethysmography for blood pressure monitoring. *Journal of Clinical Medicine*, *9*(723), 1-14.

Kachuee, M., Kiani, M.M., Mohammadzade, H., & Shabany, M. (2015). Cuff-less high-accuracy calibration-free blood pressure estimation using pulse transit time. *2015 IEEE International Symposium on Circuit and* Systems (ISCAS), Lisbon, Portugal.

Kachuee, M., Kiani, M.M., Mohammadzade, H., & Shabany, M. (2017). Cuffless blood pressure estimation algorithms for continuous health-care monitoring. *IEEE Transactions on Biomedical Engineering*, *64*(4), 859-869.

Kamen, P.W., & Tonkin, A.M. (1995). Application of the Poincaré plot to heart rate variability: a new measure of functional status in heart failure. *Internal Medicine Journal*, *25*(1), 18-26.

Malik, M., Xia, R., Odemuyiwa, O., Staunton, A., Poloniecki, J., & Camm, A.J. (1993). Influence of the recognition artefact in the automatic analysis of long-term electrocardiograms on time domain measurement of heart rate variability. *Medical and Biological Engineering and Computing*, *31*(5), 539-544.

Martinez, G., Howard, N., Abbott, D., Lim, K., Ward, R., & Elgendi, M. (2018). Can photoplethysmography replace arterial blood pressure in the assessment of blood pressure? *Journal of Clinical Medicine, 7*(10), 316.

Mori, H., Saito, I., Eguchi, E., Maruyama, K., kato, T., & Tanigawa, T. (2014). Heart rate variability and blood pressure among Japanese men and women: a community-based cross-sectional study. *Hypertension Research*, 37(8), 779-784.

Mukkamala, R., Hahn, J.O., Inan, O.T., Mestha, L.K., Kim, C.S., Toreyin, H., & Kyal, S. (2015). Toward ubiquitous blood pressure monitoring via pulse transit time: theory and practice. *IEEE Transactions on Biomedical Engineering, 62*(8), 1879-1901.

O'Brien, E., Petrie, J., Littler, W., de Swiet, M., Padfield, P.L., Altman, D.G., Bland, M., Coats, A., & Atkins, N. (1993). The British Hypertension Society protocol for the evaluation of blood pressure measuring devices. *Journal of Hypertension*, *11*(2), S43-S62.

Pan, J., & Tompkins, W.J. (1985). A real-time QRS detection algorithm. *IEEE Transactions on Biomedical Engineering*, *BME-32*(3), 230-236.

Peng, C.K., Buldyrev, S.V., Havlin, S., Simons, M., Stanley, H.E., & Goldberger, A.L. (1994). Mosaic organization of DNA nucleotides. *Physical Review E*, 49(2), 1685-1689.

Ramshur, J.T. (2010). *Design, evaluation, and application of heart rate variability analysis software* [M.S. thesis, University of Memphis].

Richman, J., & Moorman, J.R. (2000). Physiological time-series analysis using approximate entropy and sample entropy. *American Journal of Physiology*, *278*(6), H2039-H2049.

Sannino, G., Melillo, P., Stranges, S., De Pietro, G., & Pecchia, L. (2015). Short term heart rate variability to predict blood pressure drops due to standing: a pilot study. *BMC Medical Informatics and Decision Making*, 15(3), 1-9.

Shao, J., Shi, P., Hu, S., & Yu, H. (2020). A revised point to point calibration approach with adaptive errors correction to weaken initial sensitivity of cuff-less blood pressure estimation. *Sensors*, *20*(2205), 1-15.

Sharma, M., Barbosa, K., Ho, V., Griggs, D., Ghirmai, T., Krishnan, S., Hsiai, T.K., Chiao, J.C., & Cao, H. (2017). Cuff-less and continuous blood pressure monitoring: a methodological review. *Technologies,* 5(2), 21.

Soltan-Zadi, A., Alex, R., Zhang, R., Watenpaugh, D.E., & Behbehani, K. (2018). Arterial blood pressure feature estimation using photoplethysmography. *Computers in Biology and Medicine*, *102*, 104-111.

Stergiou, G.S., Alpert, B., Mieke, S., Asmar, R., Atkins, N., Eckert, S., Frick, G., Friedman, B., Grabl, T., Ichikawa, T., Ioannidis, J.P., Lacy, G., McManus, R., Murray, A., Myers, M., Palatini, P., Parati, G., Quinn, D., Sarkis, J., Shennan, A., Usuda, T., Wang, J., Wu, C.O., & O'Brien, E. (2018). A universal standard for the validation of blood pressure measuring devices: Association for the Advancement of Medical Instrumentation/European Society of

Hypertension/International Organization for Standardization (AAMI/ESH/ISO) Collaboration Statement. *Hypertension*, *71*(3), 368-374.

Swenne, C.A. (2013). Baroreflex sensitivity: mechanisms and measurement. *Netherlands heart journal: monthly journal of the Netherlands Society of Cardiology and the Netherlands Heart Foundation*, *21*(2), 58-60

Thong, T., McNames, J., & Aboy, M. (2004). Lomb-Welch periodogram for non-uniform sampling. *Proceedings of the 26th Annual International Conference of the IEEE EMBS*, San Francisco, CA, USA, 271-274.

Tobaldini, E., Nobili, L., Strada, S., Casali, K.R., Braghiroli, A., & Montano, N. (2013). Heart rate variability in normal and pathological sleep. *Frontiers in Physiology*, *4*(294).

UCI machine learning repository. (2015). *Cuffless blood pressure estimation data set*. https://www.archive.ics.uci.edu/ml/datasets/Cuff- Less+Blood+Pressure+Estimation.

World Health Organization. (2021, June 11). *Cardiovascual Diseases (CVD)*. https://www.who.int/news-room/fact-sheets/detail/cardiovascular-diseases-(cvds).

Xing, X., & Sun, M. (2016). Optical blood pressure estimation with photoplethysmography and FFT-based neural networks. *Biomedical Optics Express, 7*(8), 3007-3020.

Yan, W., Peng, R., Zhang, Y., & Ho, D. (2019). Cuffless continuous blood pressure estimation from pulse morphology of photoplethysmograms. IEEE Access, *7*, 141970-141977.

Yao, Y., Rosasco, L., & Caponnetto, A. (2007). On early stopping in gradient descent learning. *Constructive Approximation*, *26*(2), 289–315.

Zambrana-Vinaroz, D., Vicente-Samper, J.M., Juan, C.G., Esteve-Sala, V., & Sabater-Navarro, J.M. (2019). Non-invasive device for blood pressure wave acquisition by means of mechanical transducer. *Sensors*, *19*(19), 4311-4323.

Chapter 4: Cuffless Blood Pressure Estimation Using Calibrated Cardiovascular Dynamics in the Photoplethysmogram

---

Samimi, H., Dajani, H.R. (2022). Cuffless blood pressure estimation using calibrated cardiovascular dynamics in the photoplethysmogram. *Bioengineering*, *Special Issue on Machine Learning for Biomedical Applications*, *9*(446).

Abstract: An important means for preventing and managing cardiovascular disease is the non-invasive estimation of blood pressure. There is particular interest in developing approaches that provide accurate cuffless and continuous estimation of this important vital sign. This paper proposes a method that uses dynamic changes of the pulse waveform over short time intervals and calibrates the system based on a mathematical model that relates reflective PTT (R-PTT) to blood pressure. An advantage of the method is that it only requires collecting the photoplethysmogram (PPG) using one optical sensor, in addition to initial non-invasive measurements of blood pressure that are used for calibration. This method was applied to data from 30 patients, resulting in a mean error (ME) of 0.59 mmHg, a standard deviation of error (SDE) of 7.07 mmHg, and a mean absolute error (MAE) of 4.92 mmHg for diastolic blood pressure (DBP) and an ME of 2.52 mmHg, an SDE of 12.15 mmHg, and an MAE of 8.89 mmHg for systolic blood pressure (SBP). These results demonstrate the possibility of using the PPG signal for the cuffless continuous estimation of blood pressure based on the analysis of calibrated changes in cardiovascular dynamics, possibly in conjunction with other methods that are currently being researched.

4.1 Introduction

Cardiovascular disease (CVD) is one of the major contributors to human mortality worldwide (Barquera et al., 2015). A primary risk factor for CVD is high blood pressure (BP) or hypertension, which is also called the silent killer (Kachuee et al., 2017) because, in preliminary stages, it mostly develops with patients unaware of their condition (Hinton et al., 2020). Hypertension is not limited only to the older age group; 1 in 8 adults aged between 20 and 40 years suffers from high blood pressure (Hinton et al., 2020). The number of people affected by hypertension is expected to increase based on trends in lifestyle and behavior (such as low physical activity, poor eating habits, the high consumption of animal fat) and the lowering of the threshold for the diagnosis of hypertension (Hinton et al., 2020). In 2017, the American College of Cardiology and the American Heart Association introduced new definitions of hypertension, considering it present if the systolic blood pressure (SBP) or diastolic blood pressure (DBP) exceeds 130 mmHg or 80 mmHg, respectively. At the same time, an SBP between 120 and 129 mmHg is considered elevated (Tamura, 2021).

People who are diagnosed with hypertension take medication in an effort to keep their BP under control. Any undiagnosed or untreated hypertension in early stages can potentially result in myocardial infarction, ischemic and hemorrhagic stroke, heart failure, chronic kidney disease, cognitive decline, and early death (Bayrak and Tosun, 2018). Blood pressure is a dynamic vital sign that varies over time due to age, physical activity, mental stress, etc. Therefore, the continuous monitoring of blood pressure could reveal information on these dynamic characteristics (Le et al., 2020) and thus plays an important role in the diagnosis and effective management of hypertension (Kachuee et al., 2017). Despite the importance of continuous blood pressure monitoring, at the present time, there are no consumer devices on the market that are medically approved for measuring blood pressure non-invasively and continuously (Baker et al., 2021). Currently, the gold standard method for continuous BP monitoring is the direct (intra-arterial) method. This technique is mostly used in a clinical

setting for patients with an unstable condition or patients who are under vasoactive treatments. While it allows for continuous BP measurement with a high accuracy, this method requires the invasive insertion of an arterial line into the patient's artery (Esmaelpoor et al., 2020). Due to the setting limitation and the risk of severe bleeding upon accidental disconnection as well as infection for patients, this technique is not suitable for long-term BP monitoring (Esmaelpoor et al., 2020). Therefore, blood pressure is typically measured using non-invasive cuff-based methods which rely on the inflation and deflation of a cuff either manually or automatically. However, these methods cannot provide continuous monitoring, and applying pressure through a cuff wrapped around a limb can cause discomfort and potentially disturb sleep during nocturnal measurements (Tamura, 2021). Furthermore, the cuff-based method cannot be used on people with several pre-existing conditions such as lymphedema (Cemal et al., 2011). As a result, the development of cuffless BP measurement methods is in demand.

The most common physiological signals used in cuffless BP measurements are the electrocardiogram (ECG) and the photoplethysmogram (PPG). The ECG reflects the electrical excitation of the heart, while the PPG indicates blood volume changes in peripheral circulation (Esmaelpoor et al., 2021). These two signals are used in several of the major methods that are currently being researched for cuffless continuous blood pressure estimation, which are based on pulse transit time (PTT), pulse arrival time (PAT), pulse wave velocity (PWV), and pulse wave analysis (El-Hajj et al., 2020).

PTT is defined as the time that the pressure wave takes to travel between two arterial sites (Esmaelpoor et al., 2021), and it can be measured using photoplethysmogram (PPG) sensors placed at two sites on the body (Le et al., 2020). It can be calculated in different ways, such as the time delay between the proximal and distal PPG waveforms (Le et al., 2020), the time difference from the mid-point of the falling edge of the proximal PPG to the

peak of the peripheral PPG (Chen et al., 2012), or the time difference from the dicrotic notch of the proximal PPG to the peak of the peripheral PPG (Kao et al., 2019).

PAT is defined as the time interval between electrical activation of the heart and the arrival of the blood to the periphery from the aorta (Thambiraj et al., 2020) and it is usually measured as the time interval between the R-peak in the ECG and the pulse waveform in the PPG recorded at a peripheral site (El-Hajj et al., 2020). Both PTT and PAT vary inversely with BP due to the physical properties of arteries (El-Hajj et al., 2020). It is also worth mentioning that many studies incorrectly refer to PAT as PTT, and the use of the true PTT is not greatly researched (Le et al., 2020).

PWV is the speed of the pulse wave moving along the arterial vessels, and it is inversely related to PTT and PAT but is directly related to BP (Turgutkaya et al., 2021). PWV is often used as the basis for cuffless methods to estimate blood pressure and is founded on the theory of fluid wave propagation through elastic pipes (Blancher et al., 1999). PWV can be measured using a few different methods such as high-fidelity pulse pressure measuring devices, Doppler, and phase contrast magnetic resonance imaging (MRI) (Parikh et al., 2016). However, the main concept behind this measurement is to calculate the velocity as the distance the pulse wave travels divided by the time of travel (El-Hajj et al., 2020).

In addition to methods based on PAT, PTT, and PWV, there has been some work on BP estimation based on pulse wave analysis. In these methods, features are extracted from the pulse waveform, typically obtained with a single PPG sensor, which are then used in various machine learning estimation models. Most such features are generated from pulse morphology within individual beats (El-Hajj et al., 2020). In particular, data from a single PPG sensor have been used in some studies within a deep learning framework (Chen et al., 2022; Panwar et al., 2020). A detailed review of different PPG-based methods can be found in (Sulochana, 2021).

Some of the methods for the cuffless estimation of BP rely on mathematical models, which are usually established through the use of a transfer function (Zahedi et al., 2015), Windkessel models (Jana et al., 2020), the application of the Moens–Korteweg (M-K) equation, heuristic modeling with regression techniques, or predictive modeling with data-driven methods (Ding et al., 2017).

In previous work, we used a calibration-free method to estimate blood pressure using information from dynamic changes of the pulse waveform over brief time intervals (Samimi and Dajani, 2022). In this work, we added a model-based calibration stage. To implement this process, we used data from a single PPG sensor to calculate reflective PTT (R-PTT) and calibrate a mathematical model derived from the Moens–Korteweg and Bramwell–Hill equations to estimate blood pressure values. The estimated values, along with some characteristics of cardiovascular dynamics expressed in the arterial pulse waveform oscillation, were then used to improve the cuffless blood pressure estimates. The latter was done because PTT by itself or features derived from the morphology of individual pulses have not yet been shown to be sufficient for accurate blood pressure estimation, and there is likely important information related to BP contained in the dynamics of the human cardiovascular system (Chao et al, 2021). In this work, we use mean point-to-point pairing calibration (mPTP) to develop our model. This is a novel approach in model-based BP estimation based on reflective PTT. Furthermore, to the best of our knowledge, there has been no work done previously on combining R-PTT-based modeling and information from cardiovascular dynamics for the cuffless estimation of blood pressure.

4.2 Methods

Figure 4-1 shows a high-level block diagram of the proposed methodology for cuffless blood pressure estimation, which uses information related to cardiovascular dynamics extracted

from PPG signals along with a mathematical model based on Bramwell–Hill (Bramwell and Hill, 1922) and Moens–Korteweg equations (Brennan et al., 1998).

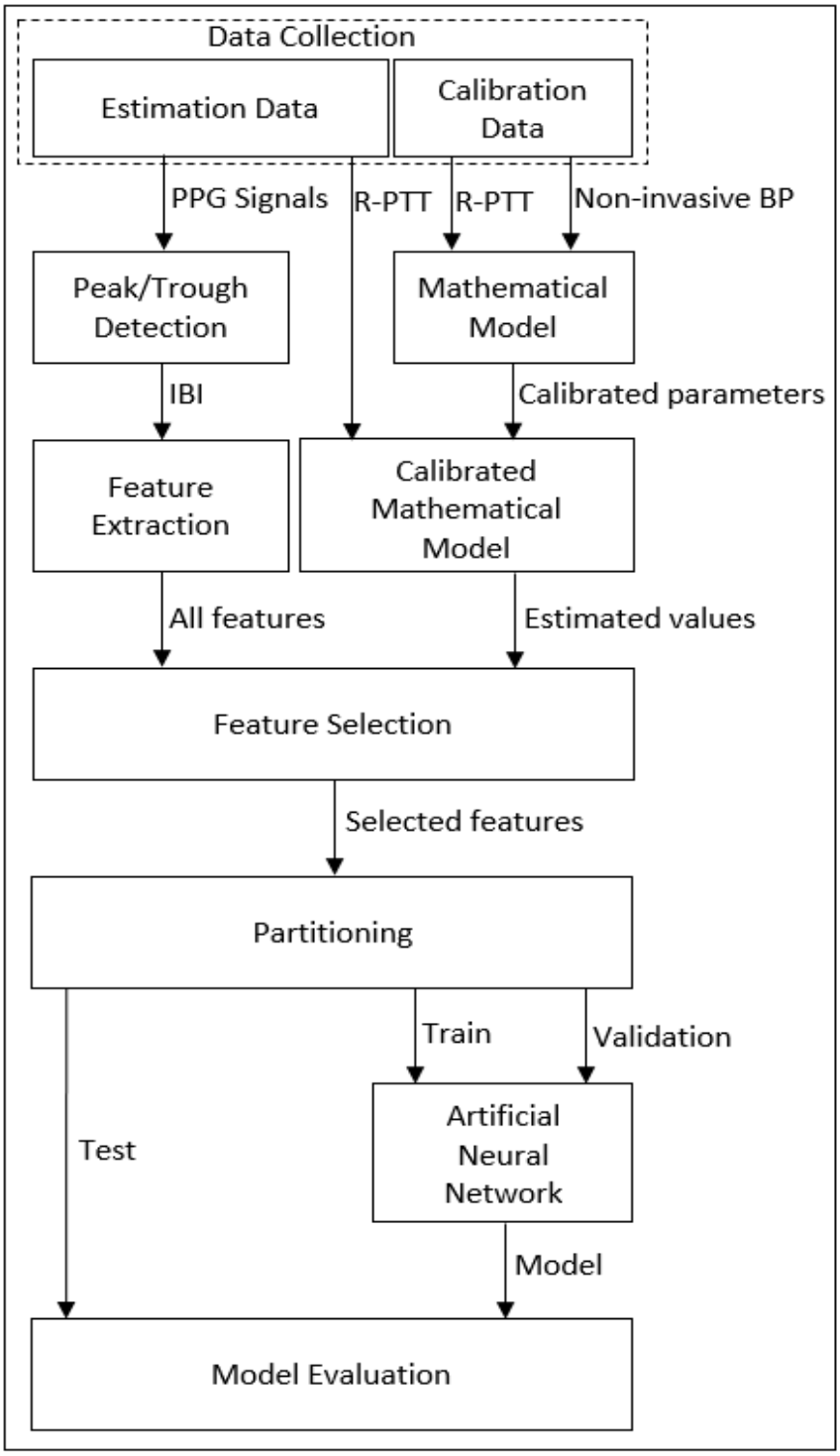

Figure 4-1. Block diagram of the method proposed in this paper for cuffless blood pressure estimation.

4.2.1 Data Collection

In this study, the bio-signal data from the University of Queensland Vital Signs Dataset (Liu et al., 2012) is used. This dataset is the result of recording in four operating rooms from 32 patients, with a duration ranging from 13 min to 5 h and a median of 105 min. The 32 recorded cases consist of 25 under general anesthetics, 3 under spinal anesthetics, and 4 sedation cases. The unique characteristic of this dataset, which does not exist in data collected from intensive care units, is that it includes entire cases of patients undergoing anesthesia for surgery, which results in rapid and dynamic vital sign changes during the induction and emergence phases of anesthesia and surgery (Liu et al., 2012). For all patients, ECG, PPG, and noninvasive arterial BP waveforms are recorded, while signals such as capnographs, airway flows, and others are collected on a case-by-case basis under the discretion of the anesthesiologist. The waveforms are sampled at 100 Hz.

In our work, we used only the PPG and noninvasive arterial BP signals from the dataset. Reference (Liu et al., 2012) does not specify the method used to collect the noninvasive arterial BP, but this signal is calibrated in mmHg. Of note, our method can make use of any calibrated BP measurements during an initial interval as inputs to the mathematical model (described below), including those obtained using a cuff-based method. We visually inspected all data and chose our dataset by selecting the ones with minimal or no interruption. As a result, our final selection consisted of data from 30 patients.

4.2.2 Peak/Trough Detection

To detect peaks and troughs of the PPG signals, we used a modified version of Pan and Tompkins' QRS detection algorithm (Pan and Tompkins, 1985). In this process, first, the PPG is filtered in two stages: a low-pass filter and a high-pass filter. The combination of these two filters forms a band-pass filter which reduces the effect of muscle noise, 60 Hz interference, and baseline wander. The filters used in this work are fourth-order low-pass with a cut-off

frequency of 10 Hz and third-order Butterworth high-pass with a cut-off frequency of 0.05 Hz.

After filtering, the signal goes through a moving average filter of length 38. A threshold is then set for the output of the moving average filter to determine the peaks of the signal based on the local maxima within a preset time interval. These maxima mark the locations of the arterial pulse waveform peaks or the PPG peaks. The troughs of the arterial pulse waveform or the PPG are detected by inverting the original signal and finding the peaks for the inverted waveform. Figure 4-2 shows the different stages of this process, and Figure 4-3 illustrates a sample of peak and trough detection for a typical PPG signal using the proposed algorithm.

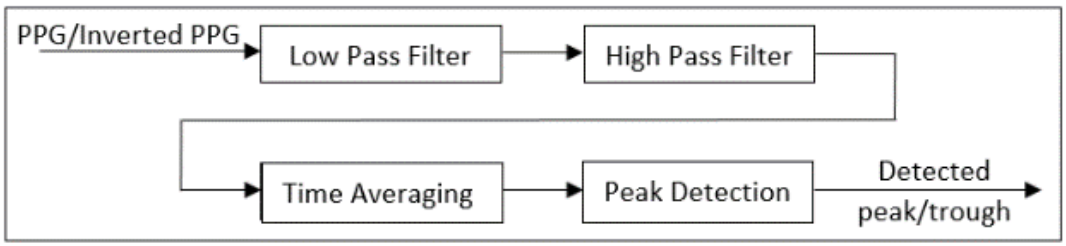

Figure 4-2. High-level block diagram of the peak/trough detection algorithm.

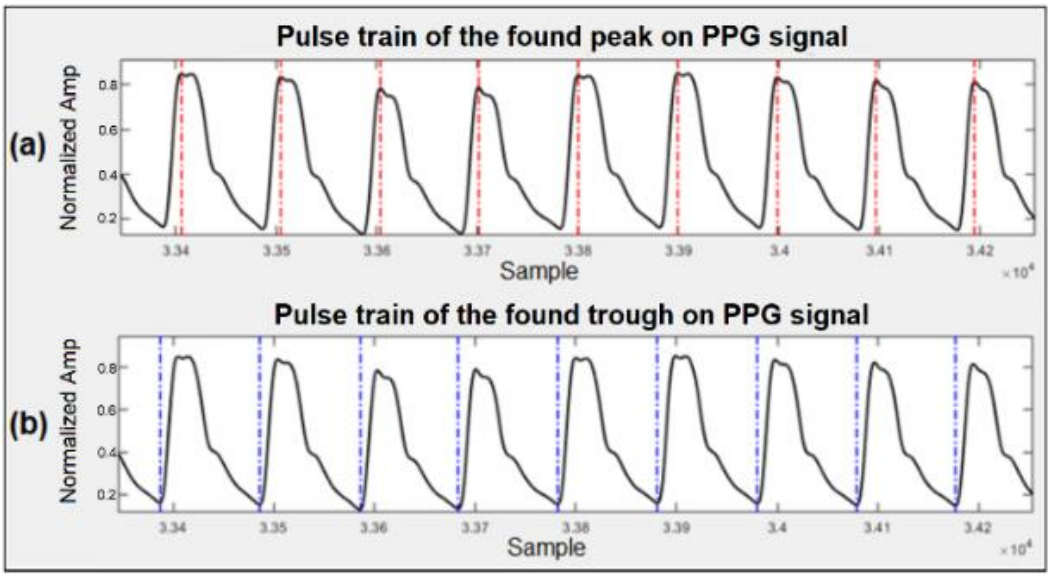

Figure 4-3. Detection of peaks and troughs in the PPG signal. (a) Detected peaks marked with dotted red lines. (b) Detected troughs marked with dotted blue lines.

4.2.3 Feature Extraction

We extracted features linked to cardiovascular dynamics from inter-beat intervals (IBIs) of the PPG signals through time domain, frequency domain, and nonlinear analysis. The analysis was performed on the last ten minutes of each of the thirty signals. For collecting IBI features, we used the open-source heart rate variability analysis software (HRVAS) (Ramshur, 2010). The time series containing IBI are the inputs to the analyzer, and the extracted features are the outputs.

For the IBI time domain analysis, both statistical and geometric measurements are considered. Statistical measurements are calculated directly from the IBI series and include: the mean IBI, the standard deviation for the IBI series (SDANN), the pulse rate variability triangular index (PRVti), the triangular interpolation of IBI (TINN), the root mean square of successive differences of the IBI series, the number of successive differences that are greater than a user-defined threshold (NNx) in milliseconds (for our analysis, the threshold was set to 10 ms), and the percentage of NNx over the duration of the signal.

To compute SDANN, first, the IBI series is divided into an equal number of segments with no overlaps; then, the mean IBI for each segment is calculated, and the standard deviation of all the means is determined. The following equation represents the above steps for calculating SDANN (Shaffer and Ginsberg, 2017).

$$\mathbf{SDANN} = \sqrt{\frac{\mathbf{1}}{\mathbf{M-1}}\sum_{\mathbf{i=1}}^{\mathbf{M}}[\mathbf{mean\ IBI(i)} - \overline{\mathbf{mean\ IBI}}]^{\mathbf{2}}} \qquad \textbf{Equation 4-1}$$

In this equation, $\mathrm{mean\ IBI(i)}$ represents the mean IBI value of the ith IBI segment, and M is the total number of segments.

Geometrical measurements are calculated based on the IBI histogram (Ramshur, 2010). The measured parameters are the pulse rate variability triangular index and the triangular interpolation of the IBI histogram. Figure 4-4 shows the histogram for a typical IBI time series

with a density distribution of D(t). Y on the graph represents the maximum value for D(t) at t = x. The pulse rate variability triangular index is calculated by dividing the area integral of D(t) by the value of Y. If distribution D(t) is based on a discrete horizontal scale, the area integral is then the total number of IBIs, and the pulse rate variability triangular index (PRVti) can be calculated as:

$$\mathbf{PRVti} = \frac{\mathbf{N_{IBI}}}{\mathbf{Y}} \qquad \textbf{Equation 4-2}$$

where N_{IBI} is the total number of IBIs and Y is the maximum value for D(t).

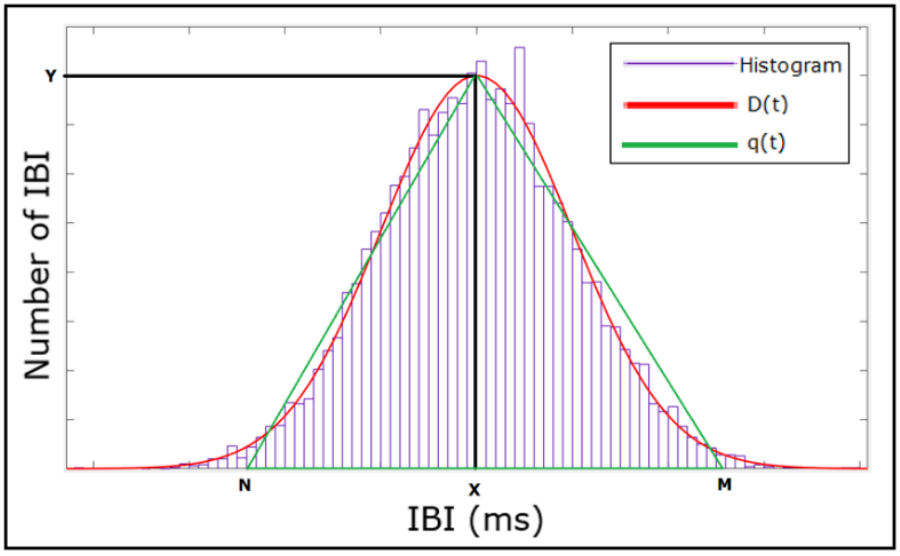

Figure 4-4. Histogram of a typical IBI time series. D(t) is a density distribution of IBI and q(t) is the triangular function fitted to D(t). Y is the maximum value of D(t), where t = x, and M and N are the other two vertices of the triangular function.

To obtain triangular interpolation of the IBI histogram, a triangular function q(t) is established in a way that the vertices of the triangle are Y, M, and N, where M and N are selected such that q(t) = 0 for $M \leq t \leq N$ and by minimizing:

$$\int_0^{+\infty} (\mathbf{D(t) - q(t)})^2 \mathbf{dt} \qquad \textbf{Equation 4-3}$$

The triangular interpolation of the IBI histogram (TINN) is then calculated as:

$$\mathbf{Triangular\ interpolation\ of\ IBI} = \mathbf{M} - \mathbf{N} \qquad \textbf{Equation 4-4}$$

The IBI frequency domain analysis is performed by using the Lomb–Scargle periodogram (LSP) (Thong et al., 2004). In the LSP method, the frequency spectrum is estimated by performing a least squares fitting of data by sinusoids. The LSP of non-uniformly sampled data is defined as:

$$\mathbf{P_{LS}(f)} = \frac{\mathbf{1}}{\mathbf{2\sigma^2}}\left(\frac{\left[\sum_{n=1}^{N}(X(t_n)-\bar{X})\ \cos(2\pi f(t_n-\tau))\right]^2}{\sum_{n=1}^{N}\cos^2(2\pi f(t_n-\tau))} + \frac{\left[\sum_{n=1}^{N}(X(t_n)-\bar{X})\ \sin(2\pi f(t_n-\tau))\right]^2}{\sum_{n=1}^{N}\sin^2(2\pi f(t_n-\tau))}\right) \qquad \textbf{Equation 4-5}$$

where X is a real valued data sequence of length N for arbitrary times t_n, $\bar{X}$ is the mean and σ is the variance of the time series, and τ is the frequency-dependent time delay defined as:

$$\tau = \frac{\tan^{-1}\left(\left(\sum_{n=1}^{N}\sin(4\pi f t_n)\right)/\left(\sum_{n=1}^{N}\cos(4\pi f t_n)\right)\right)}{4\pi f} \qquad \textbf{Equation 4-6}$$

to make the periodogram insensitive to the time shift.

In this method, the power spectral density of an IBI signal is calculated and divided into three sections labeled as very low frequency (VLF, 0.098–0.05 Hz), low frequency (LF, 0.05–0.15 Hz), and high frequency (HF, 0.15–0.5 Hz). The resistance to errors from data removal and resampling makes LSP a preferred method for power spectrum calculation for IBI signals (Clifford and Tarassenko, 2005).

A Poincaré plot, sample entropy, and detrended fluctuation analysis are used to analyze the nonlinear behavior of IBI signals. The Poincaré plot or return map is used to quantify self-similarity by mapping two consecutive IBIs in relation to each other (Kamen and Tonkin, 1995). An ellipse is fitted to this map, with the major and minor semi-axes of the ellipse referred to as SD2 and SD1, respectively. SD1 represents the standard deviation of instantaneous beat-to-beat variability, and SD2 characterizes the standard deviation of continuous beat-to-beat variability. These two axes are defined as

$$\mathbf{SD1} = \frac{\sqrt{2}}{2}\,\mathbf{SD}(x_n - x_{n-1}) \qquad \textbf{Equation 4-7}$$

$$\mathbf{SD2} = \sqrt{\mathbf{2SD(x_n)^2} - \frac{\mathbf{1}}{\mathbf{2}}\mathbf{SD(x_n - x_{n-1})^2}} \qquad \textbf{Equation 4-8}$$

where x_n and x_{n-1} are two consecutive data points, and SD represents the standard deviation of the time series.

Sample entropy is a measure used to quantify signal complexity (Richman and Moorman, 2000). It is represented by $\mathrm{SampEn(m.r,N)}$ and is defined as the negative logarithm of the conditional probability that, for a dataset with N number of data points, if two sets of simultaneous data points of length equal to embedding dimension m have a distance smaller than tolerance r, then two sets of simultaneous data points of length $m+1$ also have a distance smaller than r. A value of zero for the sample entropy indicates that the two consecutive sequences are identical, while a larger value represents higher complexity.

Detrended fluctuation analysis (DFA) (Peng et al., 1994) is another method that is used for the nonlinear analysis of IBI. DFA is a method to determine the statistical self-similarity of a signal and is based on the idea of the signal being similar to part of itself. For DFA processing, a bounded time series of IBIs is converted to an unbounded process through:

$$\mathbf{y(k)} = \sum_{\mathbf{i=1}}^{\mathbf{k}}[\mathbf{IBI(i)} - \overline{\mathbf{IBI}}] \qquad \textbf{Equation 4-9}$$

where $y(k)$ is cumulative sum or profile, $IBI(i)$ is the ith inter-beat interval, and $\overline{IBI}$ is the average inter-beat interval over the entire time series. The cumulative sum then is divided into segments of length N, and the square error for each part is minimized to fit a local least square straight-line to the data and define the local trend $y_n(k)$. The fluctuation is then considered as the root mean square deviation from the trend:

$$\mathbf{SF(n)} = \sqrt{\frac{\mathbf{1}}{\mathbf{N}}\sum_{\mathbf{k=1}}^{\mathbf{N}}\mathbf{(y(k) - y_n(k))^2}} \qquad \textbf{Equation 4-10}$$

where N represents the window size.

The above-mentioned process is repeated over different ranges of window sizes; then, the linear relationship between $F(n)$ and n is plotted to obtain the scaling exponents α_1 (short term scaling) and α_2 (long term scaling) for the inter-beat interval time series. Table 4-1 summarizes extracted IBI features for our analysis.

Table 4-1. List of considered features related to the cardiovascular dynamics used in this study.

Type of Signal Used	Measure	Description
IBI Time-Domain	Mean IBI	Mean of IBI
	SDNN	Standard deviation of IBI
	RMSSD	Root mean square of successive differences of the IBI series
	NNx	Number of successive IBIs that are larger than a user define threshold in milliseconds
	pNNx	Percentage of NNx over duration of the signal
	PRVti	Pulse rate variability triangular index
	TINN	Triangular interpolation of IBI histogram
IBI Frequency-Domain	VLF	Power of very low frequency band
	LF	Power of low frequency band
	HF	Power of high frequency band
	LF/HF	Ratio between low and high frequency band posers
IBI Nonlinear-Domain	SD1	Standard deviation of instantaneous beat to beat variability (Poincaré plot)
	SD2	Standard deviation of continuous beat to beat variability (Poincaré plot)
	SampEn	Sample entropy
	$\propto_1$	Short term fluctuation slope in Detrended Fluctuation Analysis
	$\propto_2$	Long term fluctuation slope in Detrended Fluctuation Analysis

4.2.4 Mathematical Model

To create a mathematical model for the estimation of blood pressure, we used the Bramwell–Hill and Moens–Korteweg equations. The blood pressure can be calculated based on the theory of pulse wave velocity using the following equation:

$$\mathbf{PWV} = \sqrt{\frac{\mathbf{V}}{\boldsymbol{\rho}}\frac{\boldsymbol{\Delta}\mathbf{P}}{\boldsymbol{\Delta}\mathbf{V}}} \qquad \textbf{Equation 4-11}$$

where V is the volume of blood in the artery, ρ is the blood density, ΔP is the difference between SBP and DBP, and ΔV is the corresponding blood volume change (Bramwell and Hill, 1922). Since, for each individual, the blood density, the blood volume in the artery, and the change in the blood volume are near constant, Equation 4-11 can be simplified as:

$$\mathbf{SBP} - \mathbf{DBP} = \frac{\boldsymbol{\rho}\boldsymbol{\Delta}\mathbf{V}}{\mathbf{V}}(\mathbf{PWV})^{\mathbf{2}} = \frac{\boldsymbol{\rho}\boldsymbol{\Delta}\mathbf{V}}{\mathbf{V}}(\frac{\mathbf{L}}{\mathbf{PTT}})^{\mathbf{2}} = \mathbf{K_a}\frac{\mathbf{1}}{\mathbf{PTT^2}} \qquad \textbf{Equation 4-12}$$

where PTT is the pulse transit time it takes the pressure wave to travel between two arterial sites separated by a distance L, and K_a is a parameter that needs to be calibrated for an individual by experiment (Kao et al., 2019).

In this study, we used a particular type of PTT called reflective PTT (R-PTT), whose main advantage is that it can be determined from the PPG signal obtained with a single optical sensor placed on the skin at a peripheral site, such as at the wrist. R-PTT is the duration that the pulse wave takes to travel from the radial artery to the end of the limb and reflect back to the radial artery again (Kao et al., 2019), and it can be measured by calculating the duration between the first and the second peaks of a single PPG pulse (McDuf et al., 2014). Substituting R-PTT in Equation 4-12, we can obtain the SBP value using:

$$\mathbf{SBP} = \mathbf{DBP} + \mathbf{K_a}\frac{\mathbf{1}}{\mathbf{R{-}PTT^2}} \qquad \textbf{Equation 4-13}$$

PWV can also be measured using the Moens–Korteweg equation (Brennan et al., 1998):

$$\mathbf{PWV} = \sqrt{\frac{\mathbf{E_{in}h}}{\mathbf{2\rho r}}} \qquad \textbf{Equation 4-14}$$

where E_{in} is the incremental elastic modulus of the artery, h is the thickness of the artery, r is the radius of the artery, and ρ is the density of the blood. Based on the experimental results obtained by (Bank et al., 1995), the elastic modulus of an artery can be represented as (Kao et al., 2019):

$$\mathbf{E_{in}} = \mathbf{E_0 e^{\gamma \times MBP}} \qquad \textbf{Equation 4-15}$$

where E_0 is the elastic modulus at zero pressure and γ is the coefficient depending on the particular vessel. The values of these two parameters are taken as 1428.7 and 0.031, respectively, which are the average values obtained in the study carried out by (Bank et al., 1995) for the brachial artery and have been used in a number of studies (Kao et al., 2019; Tseng and Tseng, 2020; Wang et al, 2020). MBP is the mean blood pressure and can be derived by:

$$\mathbf{MBP} \equiv \frac{\mathbf{1}}{\mathbf{3}}\mathbf{SBP} + \frac{\mathbf{2}}{\mathbf{3}}\mathbf{DBP} = \mathbf{K_b} + \frac{\mathbf{2}}{\mathbf{0.031}}\mathbf{ln}\left(\frac{\mathbf{K_c}}{\mathbf{R-PTT}}\right) \qquad \textbf{Equation 4-16}$$

while K_b and K_c are parameters that need to be calibrated for an individual by experiment (Kao et al., 2019)

By substituting Equation 4-13 into Equation 4-16, the DBP value can be calculated using:

$$\mathbf{DBP} = \mathbf{K_b} + \frac{\mathbf{2}}{\mathbf{0.031}}\mathbf{ln}\left(\frac{\mathbf{K_c}}{\mathbf{R-PTT}}\right) - \frac{\mathbf{K_a}}{\mathbf{3(R-PTT)^2}} \qquad \textbf{Equation 4-17}$$

The peak of the reflected wave can be located using the second derivative of the PPG signal (diastolic peak) (Elgendi et al., 2018). The separation between the systolic and diastolic peaks on the time axis marks the reflective PTT (Wang et al, 2020). Figure 4-5 shows the PPG waveform, its first and second derivatives, and the R-PTT.

An open-source software, PulseAnalyse (Charlton et al., 2019), was used in this work to compute the R-PTT values. In previous works, where the reflective pulse transit time was used to estimate blood pressure (Kao et al., 2019; Tseng and Tseng, 2020; Wang et al, 2020), the R-PTT was utilized in the context of one point-to-point (oPTP) calibration. However, studies that were conducted on PTT-based BP estimation have shown that the oPTP method is not robust (Shao et al., 2020). One way to make it more robust is to use mean point-to-point pairing calibration (mPTP) (Shao et al., 2020), which is what we did in this work. We calculated the average R-PTT over the first 30 s of the waveform pulse (i.e., mPTP) instead of in a single pulse, in addition to the average values of non-invasive SBP and DBP during this interval, and used this information to calibrate the K_a, K_b, and K_c parameters in our model for each individual using Equation 4-13 and Equation 4-17.

We then considered the last ten minutes of the dataset for each of the 30 patients to estimate the blood pressure using the developed mathematical model. Using this segment of the signals for estimation gave us the most separation from the calibration interval and thus provided a more realistic performance result of the model for real applications. For the estimation segment (last ten minutes of the waveform), we substituted the earlier calculated and calibrated parameters (K_a, K_b, and K_c from the first 30 s of the waveforms) and R-PTT values using the mPTP method (from the last 10 min of the waveforms) into Equation 4-13 and Equation 4-17 and calculated the SBP and DBP values for this segment. These model-based values of SBP and DBP obtained based on the initial calibration are in turn fed as features into the machine learning model, as described below.

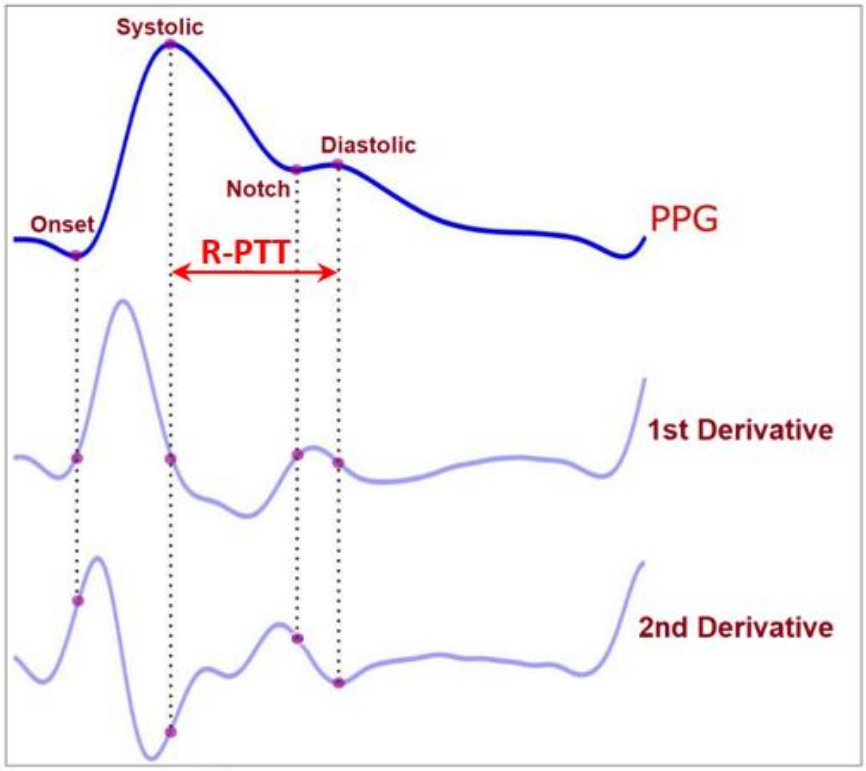

Figure 4-5. Illustration of the PPG signal and its first and second derivatives. The second derivative can locate the peak of the reflected wave (diastolic peak). The difference between the systolic peak and diastolic peak, in time, represents the reflective PTT (R-PTT) indicated by the horizontal line in the figure. (Adapted with modification from (Elgendi et al., 2018).)

4.2.5 Feature Selection

We used wrapper subset evaluation with the forward greedy stepwise search method (Hameed et al., 2018) to determine two separate feature sets. For the first set, we only used features from cardiovascular dynamics that were generated using the IBI series. This provided us with four features for the estimation of systolic blood pressure (NNx, α1, LF, and HF) and five features for the estimation of diastolic blood pressure (SDNN, RMSSD, SD1, LF, and α1). These are the feature sets that were used with the Artificial Neural Network model to generate an estimation baseline. The estimation result from this baseline (cardiovascular dynamics features) is compared with the result obtained from the second set of the features to investigate the effect of incorporating the mathematical model on the estimation accuracy. For the second set, we used the estimated blood pressure values from the mathematical model in addition to the features from cardiovascular dynamics. This provided us with three

features for the estimation of systolic blood pressure (SampleEn, α1, and systolic estimation from the mathematical model) and also three features for the estimation of diastolic blood pressure (SampleEn, HF, and diastolic estimation from the mathematical model).

4.2.6 Partitioning

In order to partition data to obtain the baseline estimation, we used the leave-one-out method. The same method was also considered to evaluate the performance of the new estimator that incorporates the mathematical model. The collected data were from 30 patients. For both feature sets, all of the above-mentioned features from one patient were set aside to be used as the test data, while the remaining features were split into 85% training and 15% validation. This process was repeated 30 times to cover the entire dataset. To avoid overfitting, validation data with the early stopping technique were used (Yao et al., 2007).

4.2.7 Artificial Neural Network

An Artificial Neural Network (ANN) from the Deep Learning Toolbox version 13.0 in Matlab R2019b was used for regression. An ANN with a two-layer feed-forward network structure, a sigmoid layer followed by a linear output layer, was used. We tested different numbers of neurons to find the best structure for the network and chose a hidden layer with ten neurons based on the performance. To train the network, we used a Bayesian Regularization backpropagation algorithm and fixed the structure of the network prior to applying it to the test data. A separate network was trained for each of the two feature sets for SBP and DBP.

4.2.8 Model Evaluation

The estimation performance was evaluated based on the mean error (ME), the mean absolute error (MAE), and the standard deviation of error (SDE) obtained with the test data. The ME and MAE are calculated using the following equations:

$$\mathbf{ME} = \frac{\sum_{i=1}^{n} y_i - x_i}{n} \qquad \textbf{Equation 4-18}$$

$$\mathbf{MAE} = \frac{\sum_{i=1}^{n} |y_i - x_i|}{n}$$ **Equation 4-19**

where y_i is the prediction and x_i is the true value for the SBP or DBP from the dataset. The true values are determined by averaging the SBP or DBP values that were measured non-invasively over the whole 10 min test interval.

The SDE was calculated based on the following equation:

$$\mathbf{SDE} = \sqrt{\frac{\sum_{i=1}^{n} |e_i - \bar{e}|^2}{n}}$$ **Equation 4-20**

where e_i is the error between the prediction and the true value ($e_i = y_i - x_i$) for each estimation, and $\bar{e}$ is the average of e_i.

4.2.9 Sensitivity Analysis of the Mathematical Model

Sensitivity analysis (SA) predicts the level of sensitivity of a model output to changes in parameter values (Song et al., 2012). Models with a high uncertainty and high sensitivity may experience a large variation in the output with a small change in the inputs (Song et al., 2012). SA is used to evaluate the relative importance of each input parameter and rank the model parameters from most to least influential (Song et al., 2012). In general, SA methods can be divided into local and global methods. Local SA is usually derivative-based and works by changing one variable at a time while keeping all the other variables constant and measuring changes in the output. This method is relatively simple to use; however, it provides information only at the central point and not the whole parameter space (Song et al., 2012). On the other hand, global SA covers the whole input parameter space, since all the input parameters are changed together, but at the expense of a higher computational cost (Saltelli et al., 2010).

In this work, we used an open-source toolbox in Matlab called Sensitivity Analysis For Everyone (SAFE) (Pianosi et al., 2015) to analyze the sensitivity of the calibration parameters

in our mathematical model. This toolbox takes advantage of variance-based sensitivity analysis in order to determine the global SA.

For a generic model, $Y = f(X_1, X_2, X_3, \dots, X_k)$, where Y is a scalar, a variance-based first-order effect for a generic factor X_i can be shown as:

$$\mathbf{Var_{X_i}}\left(\mathbf{E_{X_{\sim i}}(Y|X_i)}\right) \qquad \textbf{Equation 4-21}$$

where Var_{X_i} is the variance taken over all possible values of X_i, X_i is the i-th factor, $X_{\sim i}$ is the matrix of all factors except X_i, and $E_{X_{\sim i}}$is the expected value of Y over all possible values of $X_{\sim i}$. The first-order sensitivity that estimates the single contribution of each input parameter on the output variance and sensitivity can be measured as:

$$\mathbf{S_i} = \frac{\mathbf{Var_{X_i}}\left(\mathbf{E_{X_{\sim i}}(Y|X_i)}\right)}{\mathbf{Var(Y)}} \qquad \textbf{Equation 4-22}$$

where S_i is a normalized index, as $\mathrm{Var}_{X_i}\left(E_{X_{\sim i}}(Y|X_i)\right)$ varies between zero and $\mathrm{Var}(Y)$. The total sensitivity index that measures the total contribution of each input parameter to the output variance and sensitivity can be calculated as:

$$\mathbf{S_{Ti}} = \frac{\mathbf{E_{X_{\sim i}}}\left(\mathbf{Var_{X_i}(Y|X_{\sim i})}\right)}{\mathbf{Var(Y)}} = \mathbf{1} - \frac{\mathbf{Var_{X_{\sim i}}}\left(\mathbf{E_{X_i}(Y|X_{\sim i})}\right)}{\mathbf{Var(Y)}} \qquad \textbf{Equation 4-23}$$

where S_{Ti} is the total sensitivity index and $\mathrm{Var}_{X_{\sim i}}$ is the variance taken over all possible values of $X_{\sim i}$ (Saltelli et al., 2010).

4.2.10 Computational Complexity

Table 4-2 summarizes the computational complexity analysis that was performed on every step of this work using the Matlab profiling capability. The computational complexity was determined based on the execution time and the amount of allocated memory for each part.

It is to be noted that, although training the model can be somewhat time-consuming, testing is not, especially because, in a real-world application, testing would be done on a single set of measurements and not 30, as was done here (i.e., the execution time would be divided by 30).

Table 4-2. Computational complexity based on execution time and memory allocation. The CPU clock speed during this process was 2.501 GHz. The execution time was measured with a precision of $1.00*10^{-7}$ sec. The data for the peak/trough detection, feature extraction, and mathematical model are from a single sample file. These values are the same for both the training and test data. For ANN, the numbers correspond to a set of 30 measurements (our complete dataset).

	Total Execution Time (sec)	**Total Allocated Memory (Mbytes)**
Peak/trough detection	183.72	941.66
Feature extraction	59.80	261.33
Mathematical model	218.30	2051.61
ANN training	509.31	8.48
ANN testing	11.65	4.63

4.3 Results

In this work, we proposed a model-based approach to calibrate estimates of blood pressure using PPG signals. In this process, we estimated both systolic and diastolic blood pressure with the 30 patients using the following three methods:

- Information from cardiovascular dynamics was used to estimate blood pressure. This is a calibration-free method that we developed in our previous work (Samimi and Dajani, 2022). The blood pressure estimation results based on this method are shown in Table 4-3. This table shows the error for the SBP and DBP attained using an ANN model on five extracted IBI features for DBP and four extracted IBI features for SBP:
- Calibrated mathematical model to estimate blood pressure, as was described in the methodology section. The blood pressure estimation based on this method is presented in Table 4-4. This table shows the error for the SBP and DBP obtained using this methodology;

- Information from cardiovascular dynamics, in addition to the calibrated mathematical model, is used for blood pressure estimation. The estimation results using this method are shown in Table 4-5. This table shows the error for the SBP and DBP obtained through an ANN model and based on three extracted IBI features for both SBP and DBP. This result can also be evaluated in reference to the IEEE 1708-2014 Standard for Wearable Cuffless Blood Pressure Measuring Devices (IEEE Standard Association, 2014). This standard requires a number of conditions to be met and includes grading of the devices based on the obtained MAE. Solely based on the MAE criteria of the standard, our proposed method achieves a passing grade of A for DBP.

Table 4-3. Blood pressure estimation performance using IBI features from 30 PPG waveforms. Five features are used for DBP and four are used for SBP. Estimation is carried out using the ANN described in the text, and the results are averaged over the 30 patients.

Dynamics			
	ME (mmHg)	**SDE (mmHg)**	**MAE (mmHg)**
Diastolic BP	0.14	10.97	7.54
Systolic BP	-0.39	22.16	15.26

Table 4-4. Blood pressure estimation performance using reflective PTT in a calibrated mathematical model with 30 PPG waveforms. The results are averaged over the 30 patients.

Modeling			
	ME (mmHg)	**SDE (mmHg)**	**MAE (mmHg)**
Diastolic BP	0.45	8.36	5.47
Systolic BP	3.18	12.49	9.11

Table 4-5. Blood pressure estimation performance using IBI features and estimation from a calibrated mathematical model from 30 PPG waveforms. Three features are used for SBP and DBP. Estimation is carried out using the ANN described in the text, and the results are averaged over the 30 patients.

Dynamics + Modeling			
	ME (mmHg)	**SDE (mmHg)**	**MAE (mmHg)**
Diastolic BP	0.59	7.07	4.92
Systolic BP	2.52	12.15	8.89

We also performed sensitivity analysis for the proposed mathematical model to determine the stability of the model and evaluate the relative importance of each of the calibration parameters in the system. This analysis provided a ranking for the model parameters based on their influence on the system. Figure 6 shows the ranking result from the sensitivity analysis for the SBP model, and Figure 7 presents the ones for the DBP model. Rankings are based on first-order sensitivity indices, S_i (contribution of each individual input to changes in the model output), and total effect sensitivity indices, S_{Ti} (the first-order sensitivity plus all the interactions involving that parameter). For both the systolic and diastolic models, K_a and K_c were the most and the least influential parameters, respectively. Therefore, according to the results from the sensitivity analysis, the K_a parameter is mainly responsible for the variation in model predictions. Since the mathematical model was found to be sensitive to this parameter, effort should be made in carefully choosing its value during experimentation.

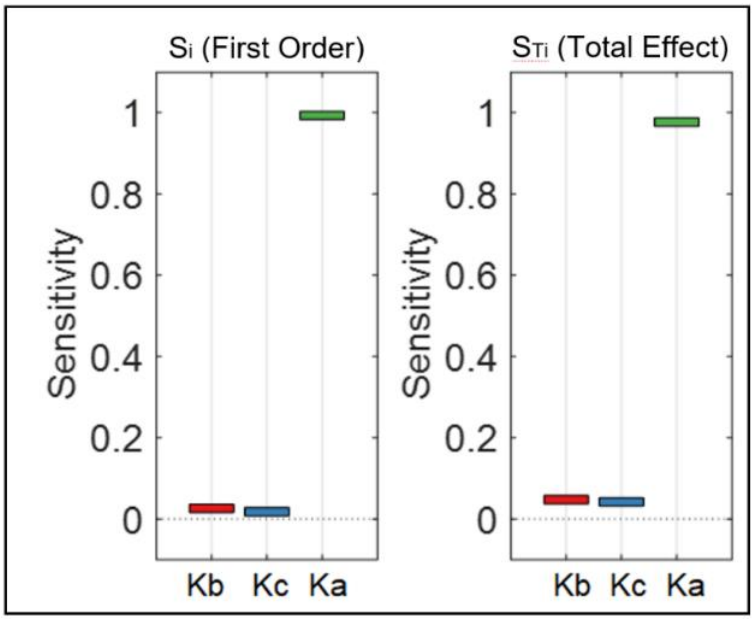

Figure 4-6. Sensitivity ranking for the SBP model. $\mathbf{S_i}$ and $\mathbf{S_{Ti}}$ show the results for first-order sensitivity and total effect sensitivity, respectively. Red, blue and green bars correspond to $\mathbf{K_b}$, $\mathbf{K_c}$ and $\mathbf{K_a}$ parameters respectively.

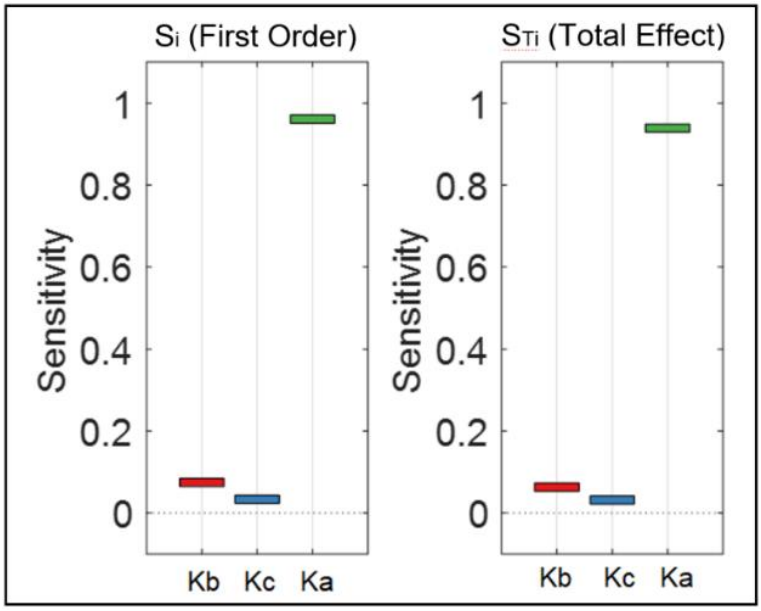

Figure 4-7. Sensitivity ranking for the DBP model. $\mathbf{S_i}$ and $\mathbf{S_{Ti}}$ show the results for first order sensitivity and total effect sensitivity, respectively. Red, blue and green bars correspond to $\mathbf{K_b}$, $\mathbf{K_c}$ and $\mathbf{K_a}$ parameters respectively.

4.4 Discussion

The results of this research indicate that the proposed approach based on IBI dynamics over short intervals in conjunction with a mathematical calibration model using only a single photoplethysmogram signal could be used for cuffless blood pressure estimation. This approach may be used on its own or as a complement to other cuffless BP estimation methods. The advantage of this method is that, since the IBI dynamics of PPG signals rely only on the timing variation between the peaks or troughs of the signals, it is likely less sensitive to changes in sensor placement or to different skin colors. This may make blood pressure estimation using this method more favorable compared to methods, including those based on deep learning, that rely on within-beat PPG pulse morphology.

In this work, we looked into both a calibrated model as well as a calibration-free model for the cuffless estimation of BP. We collected 16 features from PPG IBI variability which were examined in our previous work (Samimi and Dajani, 2022). We used wrapper subset evaluation with the forward greedy stepwise search technique to select a subset of these

features as inputs to the ANN. For the calibration-free approach, five features for DBP estimation and four for SBP estimation were selected.

We also used a mathematical model for calibration based on the reflective PTT and initial non-invasive blood pressure measurements. Sensitivity analysis and parameter ranking showed that one of the parameters was dominant in terms of the sensitivity of the model to it. Considering this model, we selected three features to be used with the ANN for both SBP and DBP estimation using the wrapper subset evaluation with the forward greedy stepwise search method. It is seen that adding the mathematical calibration model led to a substantial reduction in most of the error measures, particularly the critical measures of SDE and MAE. These measures were reduced by 45% and 42% for SBP and 36% and by 35% for DBP, respectively.

The lower errors found for DBP vs. SBP may be partly explained by the strong relation that has been found between HRV indices and both SBP and DBP in females, while for males, there was no relation between these indices and SBP (Mori et al., 2014). For the dataset that we used, there was no information provided regarding the gender composition; however, it is safe to assume that the number of male and female participants is likely to be close. Therefore, this could result in BP estimation based on IBI dynamics that is less accurate for SBP than for DBP. In addition, (Takalo et al., 1994) found that changes in IBI are more clearly present in DBP compared to SBP. Therefore, the closer relationship between IBI dynamics and DBP could have contributed to the higher estimation accuracy of DBP.

In our previous work, we estimated blood pressure based on features from cardiovascular dynamics without calibration (Samimi and Dajani, 2022). In the current study, features from cardiovascular dynamics were also considered for BP estimation; however, a mathematical calibration model was also added to investigate if it provided an improvement in performance. The selected features related to IBI dynamics in the two studies were different for both SBP and DBP estimation. In the previous study, five IBI-related features for the estimation of SBP

(mean IBI, NNx, pNNx, SD2, and α1) and six features for the estimation of DBP (mean IBI, NNx, pNNx, PRVTi, SampleEn, and the IBI ratio of LF/HF) were selected, while in this work, we ended up using four features for the estimation of SBP (NNx, α1, LF, and HF) and five features for the estimation of DBP (SDNN, RMSSD, SD1, LF, and α1). The discrepancy in IBI-related feature selection may be due to the different target data in the two studies. In our previous work, the target for the estimation model was the invasive arterial blood pressure, whereas, in this study it was noninvasive arterial blood pressure. As noted in the literature, not only are there differences in BP readings between invasive and noninvasive methods, but substantial differences in BP measurements are also observed when different devices are used (Ribezzo et al., 2014). Another reason for the divergence in feature selection could be due to the choice of datasets. In our previous study, the dataset was collected in the intensive care unit (ICU), where the patient was possibly under the influence of medications or other interventions that could cause abnormal blood pressure dynamics. Additionally, some medications such as inotropes could result in BP measurement differences between invasive and noninvasive methods, and the difference increases with the amount of medication used (Kaur et al., 2019). We used signals from patients undergoing anesthesia for surgery, which results in rapid and dynamic vital sign changes during the induction and emergence phases of anesthesia. This study also had some limitations. First, some useful information such as the age, height, weight, and gender of the participants was missing from the dataset. These basic variables could provide valuable information for the estimation process. Second, the quality of the PPG signals was inspected manually, which is not an ideal practice in real-life scenarios. An automated replacement for this step that evaluates the quality of signals in a preprocessing stage would be useful. Third, the loss of blood volume during surgical procedures was not recorded. This would be of interest to us since our mathematical model assumes a near constant blood volume in arteries, and this could be affected by blood loss. Fourth, the size of the dataset imposed a limitation on providing a separate and independent test dataset to validate the accuracy of the model. A larger database would provide the

flexibility to set aside a portion of the data solely for testing purposes and offer a larger training set for the network that can ultimately increase the accuracy of the estimation, as was found in some previous studies such as the ones in (Chen et al., 2022) and (Panwar et al., 2020), where a larger dataset was used. However, there could be other reasons behind their reported better performance, such as:

- Reference blood pressure values were taken invasively, whereas, in our study, these values are collected through noninvasive methods.
- In (Chen et al., 2022), because of the large dataset, the authors could afford to apply a BP range constraint, meaning that, whenever the output was beyond a certain threshold, it was eliminated and not considered for performance evaluation.
- The input in those studies was based on segmented windows of the collected data with overlaps. This could cause the network to be exposed to the test data during training and result in a higher reported accuracy.

Regardless of these limitations, we showed that changes in IBI dynamics extracted from the photoplethysmogram (PPG) can be used to estimate BP. The estimation accuracy was further improved with the use of a mathematical calibration model. Even greater improvement might be achieved by combining the method proposed in this study with other approaches for cuffless BP estimation.

4.5 Conclusions and Future Work

The concept of blood pressure estimation based solely on cardiovascular dynamics is different from current prevalent approaches that use pulse transit time or pulse morphology within individual beats. It is understood that the cardiovascular dynamics carry useful information that can help to recognize conditions such as hypertension (Malpas, 2002). This was demonstrated in the study by (Takalo et al., 1994), where it was concluded that there are differences in the short-term oscillation in blood pressure (BP) between normotensive,

borderline hypertensive and hypertensive individuals (Takalo et al., 1994). Inspired by the above findings, our proposed method to estimate blood pressure is to use information from dynamic changes (that are collected over short intervals of a few minutes) and incorporate a mathematical calibration model based on the initial measured values of blood pressure.

In this paper, we compared the estimated values for both SBP and DBP using a calibration-free model and the proposed calibrated model. The overall estimation results were in line with the expectation that the cardiovascular dynamics contain valuable information for the estimation of blood pressure. In addition, the result also showed that the calibration stage improved the accuracy in both SBP and DBP estimation. However, to further improve cuffless BP accuracy measurement, in future work, this approach may be combined with widely used methods based on the pulse morphology within beats or the pulse transit time.

4.6 References

IEEE Standard Association. (2014). *IEEE Standard for Wearable Cuffless Blood Pressure Measuring Devices* (1708-2014), 1-38.

Baker, S., Xiang, W., & Atkinson, I. (2021). A hybrid neural network for continuous and non-invasive estimation of blood pressure from raw electrocardiogram and photoplethysmogram waveforms. *Comput. Methods Programs Biomed.*, *207*, 106191.

Bank, A.J., Wilson, R.F., Kubo, S.H., Holte, J.E., Dresing, T.J., & Wang, H. (1995). Direct effects of smooth muscle relaxation and contraction on in vivo human brachial artery elastic properties. *Circulation Research*, *77*(5), 1008–1016

Barquera, S., Pedroza-Tobias, A., Medina, C., Hernandez-Barrera, L., Bibbins-Domingo, K., Lozano, R., & Moran, A.E. (2015). Global overview of the epidemiology of atherosclerotic cardiovascular disease. *Arch. Medical Research*, *46*(5), 328–338.

Bayrak, D., & Tosun, N. (2018). Determination of nursing activities for prevention of heart attack and stroke in hypertension patients. *Int. J. Caring Sci., 11*(2), 1073–1082.

Blancher, J., Asmar, R., Djane, S., London, G.M., & Safar, M.E. (1999). Aortic pulse wave velocity as a marker of cardiovascular risk in hypertensive patients. *Hypertension*, *33*(5), 1111–1117.

Bramwell, J.C., & Hill, A.V. (1922). The velocity of the pulse wave in man. *Proceedings of the Royal Society B: Biological Sciences*, *93*(652), 298–306.

Brennan, E.G., O'Hare, N.J., & Walsh, M.J. (1998). Transventicular pressure-velocity wave propagation in diastole: Adherence to the Moens-Korteweg equation. *Physiological Measurement, 19*(1), 117–123

Cemal, Y., Pusic, A., & Mehrara, B.J. (2011). Preventative measures for lymphedema: Separating fact from fiction. *J. Am. Coll. Surg.*, *213*(4), 543–551.

Chao, P.C.P., Wu, C.C., Nguyen, D.H., Nguyen, B.S., Huang, P.C., & Le, V.H. (2021). The machine learnings leading the cuffless PPG blood pressure sensors into the next stage. *IEEE Sensors Journal, 21*(11), 12498-12510.

Charlton, P.H., Harana, J.M., Vennin, S., Li, Y., Chowienczyk, P., & Alastruey, J. (2019). Modeling arterial pulse waves in healthy aging: A database for in silico evaluation of hemodynamics and pulse wave indexes. *American Journal of Physiology-Heart and Circulatory Physiology*, *317*(5), H1062–H1085

Chen, Y., Zhang, D., Karimi, H.R., Deng, C., & Yin, W. (2022). A new deep learning framework based on blood pressure range constraint for continuous cuffless BP estimation. *Neural Networks*, *152*, 181–190.

Chen, Y., Wen, C., Tao, G., & Bi, M. (2012). Continuous and noninvasive measurement of systolic and diastolic blood pressure by one mathematical model with the same model parameters and two separate pulse wave velocities. *Annals of Biomedical Engineering*, *40*(4), 871-882.

Clifford, G.D., & Tarassenko, L. (2005). Quantifying errors in spectral estimates of HRV due to beat replacement and resampling. *IEEE Transactions on Biomedical Engineering*, *52*(4), 630–638.

Ding, X., Yan, B.P., Zhang, Y.T., Liu, J., Zhao, N., & Tsang, H.K. (2017). Pulse transit time based continuous cuffless blood pressure estimation: A new extension and a comprehensive evaluation. Scientific Reports, *7*(1), 11554.

Elgendi, M., Liang, Y., & Ward, R. (2018). Toward generating more diagnostic features from photoplethysmogram waveforms. *Disease*, *6*(1), 20

El-Hajj, C., Kyriacou, P.A. (2020). A review of machine learning techniques in photoplethysmography for non-invasive cuff-less measurement of blood pressure. *Biomed. Signal Processing Control.*, *58*, 101870

Esmaelpoor, J., Moradi, M.H., & Kadkhodamohammadi, A. (2020). A multistage deep neural network model for blood pressure estimation using photoplethysmogram signals. *Computers in Biology and Medicine*, *120*, 103719.

Esmaelpoor, J., Moradi, M.H., & Kadkhodamohammadi, A. (2021). Cuffless blood pressure estimation methods: Physiological model parameters versus machine-learned features. Physiol. Meas., *42*(3), 035006.

Hameed, S.S., Petinrin, O.O., Hashi, A.O., & Saeed, F. (2018). Filter-wrapper combination and embedded feature selection for gene expression data. *International Journal of Advances in Soft Computing and its Applications*, *10*(1), 90-105.

Hinton, T.C., Adams, Z.H., Baker, R.P., Hope, K., Paton, J., Hart, E., & Nightingale, A. (2020). Investigation and treatment of high blood pressure in young people. *Hypertension*, *75*(1), 16–22.

Jana, B., Oswal, K., Mitra, S., Saha, G., & Banerjee, S. (2020). Windkessel model-based cuffless blood pressure estimation using continuous wave doppler ultrasound system. *IEEE Sensors Journal*, *20*(17), 9989–9999.

Kachuee, M., Kiani, M.M., Mohammadzade, H., & Shabany, M. (2017). Cuffless blood pressure estimation algorithms for continuous health-care monitoring. *IEEE Transactions on Biomedical Engineering*, *64*(4), 859-869.

Kamen, P.W., & Tonkin, A.M. (1995). Application of the Poincaré plot to heart rate variability: a new measure of functional status in heart failure. *Internal Medicine Journal*, *25*(1), 18-26.

Kao, Y.H., Chao, P.C.P., & Wey, C.L. (2019). Design and validation of a new PPG module to acquire high-quality physiological signals for high-accuracy biomedical sensing. *IEEE Journal of Selected Topics in Quantum Electronics*, *25*(1), 69000210.

Kaur, B., Kaur, S., Yaddanapudi, L.N., & Singh, N.V. (2019). Comparison between invasive and noninvasive blood pressure measurements in critically ill patients receiving inotropes. *Blood Pressure Monitoring*, *24*(1), 24–29

Le, T., Ellington, F., Lee, T.Y., Vo, K., Khine, M., Krishnan, S.K., Dutt, N., & Cao, H. (2020). Continuous non-invasive blood pressure monitoring: a methodological review on measurement techniques. *IEEE Access*, *8*, 212478-212498.

Liu, D., Gorges, M., & Jenkins, S.A. (2012). University of Queensland vital signs dataset: Development of an accessible repository of anesthesia patient monitoring data for research. *Anesthesia and Analgesia, 114*(3), 584–589.

McDuf, D., Gontarek, S., & Picard, R.W. (2014). Remote detection of photoplethysmographic systolic and diastolic peaks using a digital camera. *IEEE Transactions on Biomedical Engineering*, *61*(12), 2948–2954.

Malpas, S.C. (2002). Neural influences on cardiovascular variability: possibilities and pitfalls. *American Journal of Physiology-Heart and Circulatory Physiology*, *282*(1), H6-H20.

Mori, H., Saito, I., Eguchi, E., Maruyama, K., kato, T., & Tanigawa, T. (2014). Heart rate variability and blood pressure among Japanese men and women: a community-based cross-sectional study. *Hypertension Research*, 37(8), 779-784.

Pan, J., & Tompkins, W.J. (1985). A real-time QRS detection algorithm. *IEEE Transactions on Biomedical Engineering*, *BME-32*(3), 230-236.

Panwar, M., Gautam, A., Biswas, D., & Acharrya, A. (2020). PP-Net: A deep learning framework for PPG based blood pressure and heart rate estimation. *IEEE Sens. Journal*, *20*(17), 10000–10011.

Parikh, J.D., Hollingsworth, K.G., Kunadian, V., Blamire, A., & MacGowan, G.A. (2016). Measurement of pulse wave velocity in normal aging: Comparison of vicorder and magnetic resonance phase contrast imaging. *BMC Cardiovasc. Disord., 16*(50).

Peng, C.K., Buldyrev, S.V., Havlin, S., Simons, M., Stanley, H.E., & Goldberger, A.L. (1994). Mosaic organization of DNA nucleotides. *Physical Review E*, 49(2), 1685-1689.

Pianosi, F., Sarrazin, F., & Wagener, T. (2015). A Matlab toolbox for global sensitivity analysis. *Environmental Modelling & Software*, *70*, 80–85

Ramshur, J.T. (2010). *Design, evaluation, and application of heart rate variability analysis software* [M.S. thesis, University of Memphis].

Ribezzo, S., Spina, E., Di Bartolomeo, S., & Sanson, G. (2014). Noninvasive techniques for blood pressure measurement are not reliable alternative to direct measurement: A randomized crossover train in ICU. *Scientific World Journal*, *2014*, 353628.

Richman, J., & Moorman, J.R. (2000). Physiological time-series analysis using approximate entropy and sample entropy. *American Journal of Physiology*, *278*(6), H2039-H2049.

Samimi, H., & Dajani, H.R. (2022). Cuffless blood pressure estimation using cardiovascular dynamics. *In Proceedings of the International Conference on Electrical, Computer and Energy Technologies (ICECET)*, Prague, Czech Republic. Available from: https://ieeexplore.ieee.org/document/9872800.

Saltelli, A., Annoni, P., Azzini, I., Campolongo, F., Ratto, M., & Tarantola, S. (2010). Variance based sensitivity analysis of model output. Design and estimator for the total sensitivity index. *Computer Physics Communications*, *181*(2), 259–270.

Shaffer, F., & Ginsberg, J.P. (2017). An overview of heart rate variability metrics and norms. *Frontiers in Public Health*, *5*, 258.

Shao, J., Shi, P., Hu, S., & Yu, H. (2020). A revised point-to-point calibration approach with adaptive errors correction to weaken initial sensitivity of cuff-less blood pressure estimation. *Sensors*, *20*(8), 2205.

Song, X., Bryan, B.A., Paul, K.I., & Zhao, G. (2012). Variance-based sensitivity analysis of a forest growth model. *Ecological Modeling*, *247*, 135–143.

Sulochana, C.H. (2021). A review of photoplethysmography based measurement of blood pressure and heart rate variability. *Journal of Bioengineering & Biomedical Science*, *11*(1), 862-866.

Takalo, R., Korhonen, I., Turjanmaa, V., Majahalme, S., Tuomisto, M., & Uusitalo, A. (1994). Short-term variability of blood pressure and heart rate in borderline and mildly hypertensive subjects. *Hypertension*, *23*(1), 18-24.

Tamura, T. (2021). Cuffless blood pressure monitors: principles, standards and approval for medical use. *IEICE Transactions on Communications, E104B*(6).

Thambiraj, G., Gandhi, U., Mangalanathan, U., Jose, V.J.M., & Anand, M. (2020). Investigation on the effect of Womersley number, ECG and PPG features for cuff less blood pressure estimation using machine learning. *Biomedical Signal Processing and Control*, *60*, 101942.

Thong, T., McNames, J., & Aboy, M. (2004). Lomb-Wech periodogram for non-uniform sampling. *In Proceedings of the 26th Annual International Conference of the IEEE EMBS*, San Francisco, CA, USA, 271–274.

Tseng, T.J., & Tseng, C.H. (2020). Cuffless blood pressure measurement using a microwave near-field self-injection-locked wrist pulse sensor. *IEEE Transactions on Microwave Theory and Techniques*, *68*(11), 4865–4874.

Turgutkaya, A., & Asci, G. (2021). The association between Hba1c and arterial stiffness among non-diabetic patients with chronic kidney disease. *J. Vasc. Bras.*, *20*, e20200245.

Wang, H.S.J., Yeh, M.H., Chao, P.C.P., Tu, T.Y., Kao, Y.H., & Pandey, R. (2020). A fast chip implementing a real-time noise resistant algorithm for estimating blood pressure using a non-invasive, cuffless PPG sensor. *Microsystem Technologies*, *26*(11), 3501–3516.

Yao, Y., Rosasco, L., & Caponnetto, A. (2007). On early stopping in gradient descent learning. *Constructive Approximation*, *26*(2), 289–315.

Zahedi, E., Sohani, V., Ali, M.A.M., Chellappan, K., & Beng, G.K. (2015). Experimental feasibility study of estimation of the normalized central blood pressure waveform from radial photoplethysmogram. *Journal of Healthcare Engineering*, *6*(1), 121–144.

Chapter 5: A PPG-Based Calibration-Free Cuffless Blood Pressure Estimation Method Using Cardiovascular Dynamics

---

Samimi, H., Dajani, H.R. (2023). A PPG-Based Calibration-Free Cuffless Blood Pressure Estimation Method Using Cardiovascular Dynamics. *Sensors, Special Issue on Recent Advancements in Sensor Technologies for Healthcare and Biomedical Applications (Volume II), 23*(4145).

Abstract: Traditional cuff-based sphygmomanometers for measuring blood pressure can be uncomfortable and particularly unsuitable to use during sleep. A proposed alternative method uses dynamic changes in the pulse waveform over short intervals and replaces calibration with information from photoplethysmogram (PPG) morphology to provide a calibration-free approach using a single sensor. Results from 30 patients show a high correlation of 73.64% for systolic blood pressure (SBP) and 77.72% for diastolic blood pressure (DBP) between blood pressure estimated with the PPG morphology features and the calibration method. This suggests that the PPG morphology features could replace the calibration stage for a calibration-free method with similar accuracy. Applying the proposed methodology on 200 patients and testing on 25 new patients resulted in a mean error (ME) of −0.31 mmHg, a standard deviation of error (SDE) of 4.89 mmHg, a mean absolute error (MAE) of 3.32 mmHg for DBP and an ME of −4.02 mmHg, an SDE of 10.40 mmHg, and an MAE of 7.41 mmHg for SBP. These results support the potential for using a PPG signal for calibration-free cuffless blood pressure estimation and improving accuracy by adding information from cardiovascular dynamics to different methods in the cuffless blood pressure monitoring field.

5.1 Introduction

Blood pressure is the main driver of blood flow through vessels, which leads to blood circulation in the body. It also marks the health of the human cardiovascular system (Wang et al., 2018). Hypertension, which is elevated blood pressure (BP) that results in higher force exerted on blood vessels (Agham and Chaskar, 2021), is the main risk factor for cardiovascular diseases, which, according to the World Health Organization, can often result in death and disability (World Health Organization, 2023). If untreated, hypertension may increase the risk of severe health conditions, such as myocardial infarction, stroke, atherosclerosis, blood clots, kidney failure and dementia (Agham and Chaskar, 2021). To detect hypertension, measurement of blood pressure is necessary. In addition, because blood pressure fluctuates, it is important to perform the measurement frequently to detect any variation (Yamokoshi et al., 2021). This variation could be caused by many factors, such as stress, food, exercise, emotion, use of medication, etc., and is usually hard to detect through infrequent clinical measurement (Xing et al., 2019). Therefore, it is important for the general population, and especially for people with hypertension, to have regular blood pressure monitoring outside of clinical settings (Slapnicar et al., 2019).

The measurement of blood pressure can be divided into two major methods: invasive and noninvasive. In the invasive method, a catheter is inserted into the artery to measure the blood pressure accurately. However, this method has a high risk of causing complications such as blood clotting, bleeding (Hassani and Foruzan, 2019), distal ischemia, thrombosis and infection (Ruiz-Rodriguez et al., 2013). Due to the risks involved and the difficulty of the process, this method is not widely used outside of specific hospital settings (Wang et al., 2018). On the other hand, the noninvasive methods are safe, straightforward and inexpensive, and that makes them more favorable for use both at home and in a clinic; however, this comes at the cost of lower accuracy (Hassani and Foruzan, 2019).

There are different techniques for measuring blood pressure noninvasively. The gold standard for over 100 years has been the mercury sphygmomanometer. In this method a cuff placed around the upper arm is inflated to control the blood flow in the brachial artery. A trained listener is required to recognize the Korotkoff sounds through a stethoscope that is placed above the brachial artery while the cuff is deflated, easing the blood flow in the artery (Mohebbian et al., 2020). Another popular method that is used in home healthcare devices is ocsillometry. Oscillometry uses a cuff around the arm or the wrist and a transducer to record the pressure oscillation during the cuff deflation (Mohebbian et al., 2020). From the measured oscillation in blood pressure, systolic blood pressure and diastolic blood pressure are approximated based on the oscillation pattern (Mohebbian et al., 2020).

Volume clamping and tonometry are two other noninvasive blood pressure measurement techniques. Although these methods provide continuous blood pressure values, they are mainly used in research (El-Hajj and Kyriacou, 2021). Volume clamping uses a small cuff, that is placed on a finger, and a photoplethysmography (PPG) sensor. This method provides instantaneous blood pressure readings but is expensive, and the fact that a cuff is used in the process can make this method uncomfortable. Tonometry does not require a cuff; however, since it uses a manometer-tipped probe pressed on an artery, it is very sensitive to arm or probe movement, and therefore, requires constant calibration using a cuff-based device (El-Hajj and Kyriacou, 2021).

In recent years, cuffless blood pressure measurement methods, a generic term for blood pressure monitoring techniques that do not use a cuff, have seen increased interest due to limitations that other methods impose such as discomfort, inconvenience, high cost, complexity and lack of ability to provide continuous measurement (Samimi and Dajani, 2022a). One of the approaches that is used by many for this purpose is based on the pulse transit time (PTT), which corresponds to the time delay for a pulse wave to travel from one arterial site to another. Variations in the PTT are well-correlated with SBP and DBP (Wang and

Zhang, 2017); however, this method requires data to be collected from two different sensors (Fukushima et al., 2013) which means two signals have to be monitored, pre-processed and analyzed. In addition, the two signals need to be synchronized precisely, which requires effort and has its own complications. These limitations along with the increase in use of wearable devices have given rise to research on BP monitoring methods using a single PPG signal; however, these methods are less understood in comparison to the well-established PTT-based methods (Slapnicar et al., 2019).

The PPG signal measure changes in blood volume in capillaries by monitoring the variation in light absorption on the skin (Fati et al., 2021). With the help of developments in PPG acquisition technology, this signal can be used to estimate BP noninvasively and continuously (Pan and Zhang, 2017). In this method, blood pressure is not measured, but rather it is predicted based on analysis of the waveform (Xing et al., 2019). Studies have shown that there are similarities between PPG and the arterial blood pressure (ABP) waveform in terms of morphology (Li and Laleg-Kirati, 2021) and dynamics (Samimi and Dajani, 2022b), and therefore, extracted features from PPG will carry valuable information regarding the BP (Li and Laleg-Kirati, 2021). Features that are mostly generated from pulse morphology within individual beats are most commonly used in various machine learning models to estimate blood pressure (Samimi and Dajani, 2022a). Sulochana (Sulochana, 2021) provides a recent review of PPG-based methods that have been used in different studies. The methods can be a variation of linear regression models, such as the work by (Sagirova et al., 2021) and (Li and Laleg-Kirati, 2021), or based on different approaches of artificial neural networks (ANN) (Kurylyak et al., 2013; Malayeri and Khodabakhshi, 2022; Soh et al., 2020). One of the derivatives of the ANN that has gained popularity in recent years is deep learning (Paviglianiti et al., 2022). Different approaches within this method could include recurrent neural network (RNN), long short-term memory (LSTM) and the gated recurrent unit (GRU) that was used by (El-Hajj and Kyriacou, 2021), convolutional neural network (CNN), or the combination of CNN

and LSTM that was used by (Paviglianiti et al., 2022), or some new approaches with modified versions of deep learning such as deeply supervised net (DSN) used by (Lee et al., 2015) and U-NET that was the basis for the research conducted in (Ibtehaz et al., 2022). These methods have gained attention due to their often superior performance compared to traditional ANN.

In previous work, we investigated BP estimation based on information from dynamic changes in PPG signal while a mathematical model was used for calibration stage (Samimi and Dajani, 2022a). In this work, we investigated the possibility of replacing the calibration stage with information from PPG morphology in order to provide a calibration-free method for BP estimation. To implement this process, we estimated BP by using both a mathematical model and PPG morphology, then along with features of cardiovascular dynamics expressed in the PPG oscillation, BP values were estimated and compared to reference measurements. In addition to the possibility of achieving a calibration-free estimate, this approach was taken because there is a high possibility that the dynamics of human cardiovascular system carry important information related to BP, while features derived solely from the morphology of individual pulses have not provided a sufficient level of accuracy in BP estimation (Chao et al., 2021).

In this work, we used mean point-to-point (mPTP) features derived from the morphology of the PPG pulses and averaged over all the pulses for the duration of the signal to develop our estimation model. This is a novel approach in BP estimation based on PPG morphological characteristics. Another innovation in this work is the use of PPG morphology features along with the information from the dynamics of these signals. Furthermore, to the best of our knowledge, there has been no previous research conducted on replacing the calibration stage in the BP estimation process with the PPG morphology features.

5.2 Materials and Methods

Figure 5-1 shows a high-level flowchart for the proposed methodology for cuffless blood pressure estimation, which uses information related to cardiovascular dynamics and morphology, both derived from a PPG signal recorded with a single sensor. Information related to cardiovascular dynamics is extracted based on our previous work (Samimi and Dajani, 2022a), and the ones related to PPG morphology are inspired by the proposed methodologies in two previous studies (El-Hajj and Kyriacou, 2021; Kurylyak et al., 2013). This figure shows a general design that is used during the design development and evaluation, as well as the testing phase with new data. During the development of the ANN and evaluation process, the leave-one-out method (LOO) is used, where each iteration of LOO takes one patient with all associated signals out for testing, while it trains on the remaining signals. In the testing phase, the ANN is trained on a complete dataset and tested on signals from 25 new patients that have never been seen by the structure.

We can divide our work into two major parts based on the PPG morphology feature extraction, where one uses a feedforward artificial neural network model and the other uses a deep learning model (Figure 5-1).

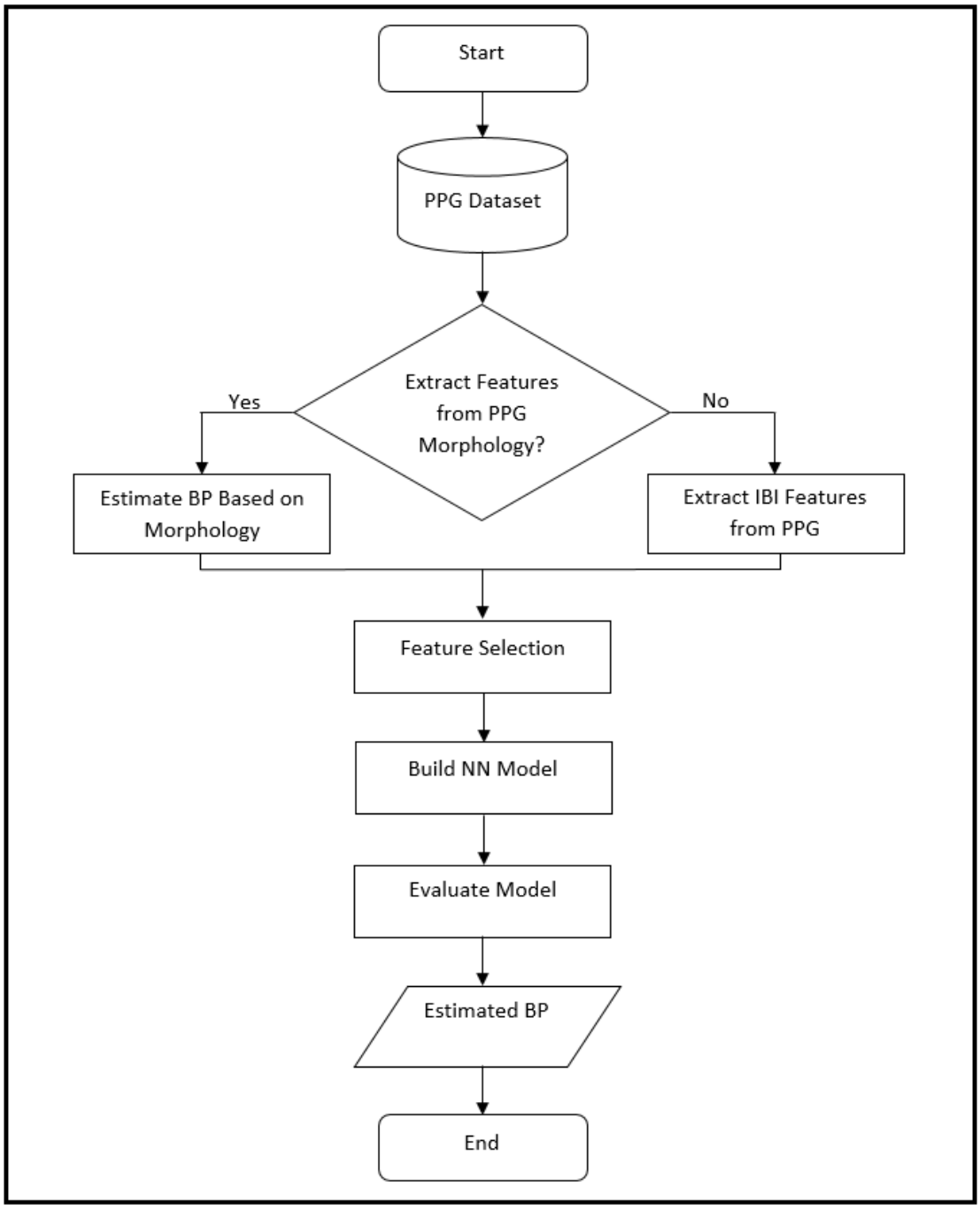

Figure 5-1. Flowchart of the proposed method in this paper for cuffless blood pressure estimation, which shows the process of BP estimation for design, evaluation and testing. During the design phase, the ANN model is based on leave-one-out (LOO) method, where it is evaluated on data from a single patient at a time and repeated over all patients. The same structure is used during the final testing phase where the ANN is trained on the complete dataset, and then, tested on a new set of data from 25 patients that have never been seen by the structure. In this process the choice of whether to use extracted features from PPG morphology depends on whether the analysis is based on morphology or interbeat interval (IBI) features (as explained in the text).

5.2.1 Bio-Signal Datasets

In this study, we used two separate bio-signal datasets, one from the University of Queensland Vital Signs Dataset (Liu et al., 2012) and another from the University of California Irvine (UCI) Machine Learning Repository (Kachuee et al., 2015).

Data from the University of Queensland includes ECG, PPG and noninvasive arterial BP waveforms recorded from 32 patients (25 under general anesthetics, 3 under spinal anesthetics, and 4 sedation cases) in four operating rooms, and sampled at the rate of 100 Hz. The recording ranged from 13 min to 5 h with a median of 105 min. These data cover the complete duration of the anesthesia that patients go through, which means there could be rapid variations in vital signs in the induction and emergence phases of anesthesia and surgery. This makes the dataset unique compared to others, such as data collected from intensive care units (Liu et al., 2012).

The second dataset, the one from UCI, is a subset of the Multiparameter Intelligent Monitoring in Intensive Care (MIMIC II) data. MIMIC II is an open source multiparameter recording provided by the PhysioNet organization that is collected from 15,000 intensive care units (ICU) in multiple hospitals. The collected signals are sampled at 125 Hz with at least 8-bit resolution. The following process was followed in order to generate the subset of the MIMIC II dataset that is provided by UCI:

- The original data are divided into fixed size signal blocks. Each block is processed through a simple averaging filter to smoothen the signal;
- Any block with irregular blood pressure value or heart rate is removed;
- Autocorrelation is calculated for PPG signal to indicate the degree of similarity between successive pulses in a block;
- Any block with high alteration between successive pulses, based on the calculated autocorrelation in the previous step, is removed (Kachuee et al., 2015).

In our work, we used PPG signals and noninvasive arterial BP signals from the University of Queensland data, and PPG signals and ABP signals from the UCI data. In the case of ABP, the reference values for systolic blood pressure (SBP) and diastolic blood pressure (DBP) were calculated by averaging the values of the peaks and troughs of the waveform (respectively) for each patient over the duration of the test signal. For the data from the University of Queensland, the reference values were obtained by averaging the provided beat-to-beat noninvasive SBP and DBP values over the duration of the signal for each patient. In both cases we visually inspected the waveforms and chose the ones with minimal or no interruption. In the case of data from UCI, since the dataset comprises some signals with short duration, we only selected the ones with 8 to 10 min in length and excluded the signals that were short in duration. The resulting datasets consisted of signals from 200 patients for the data from UCI and 30 patients for the data from the University of Queensland. In addition, we set aside an extra set of signals, 25 randomly selected patients from the UCI dataset with an SBP range of 105.40 mmHg to 151.70 mmHg and a DBP range of 53.85 mmHg to 72.93 mmHg, to be used as never-seen test data in the final step of our work.

5.2.2 Morphology-Based Estimation

For this part, we used both datasets mentioned earlier to estimate SBP and DBP. These are the same datasets that we used in our previous works (Samimi and Dajani, 2022a; Samimi and Dajani, 2022b), and by reusing them in this research (that proposes a different method), the estimation results and accuracy of the models can be compared. Our work has mainly focused on features related to human cardiovascular dynamics. In order to extract dynamics features, we used a modified version of Pan and Tompkins' QRS detection algorithm to detect the peaks and troughs of the PPG signals and ultimately calculate the interbeat intervals (IBI) in the signal under test. Figure 5-2 shows a sample of peak and trough detection for the PPG signal using the algorithm and the resulting IBIs. We used IBIs of the peaks for SBP

estimation, and IBIs of the troughs for DBP estimation. The details of this process are reported in our previous work (Samimi and Dajani, 2022a).

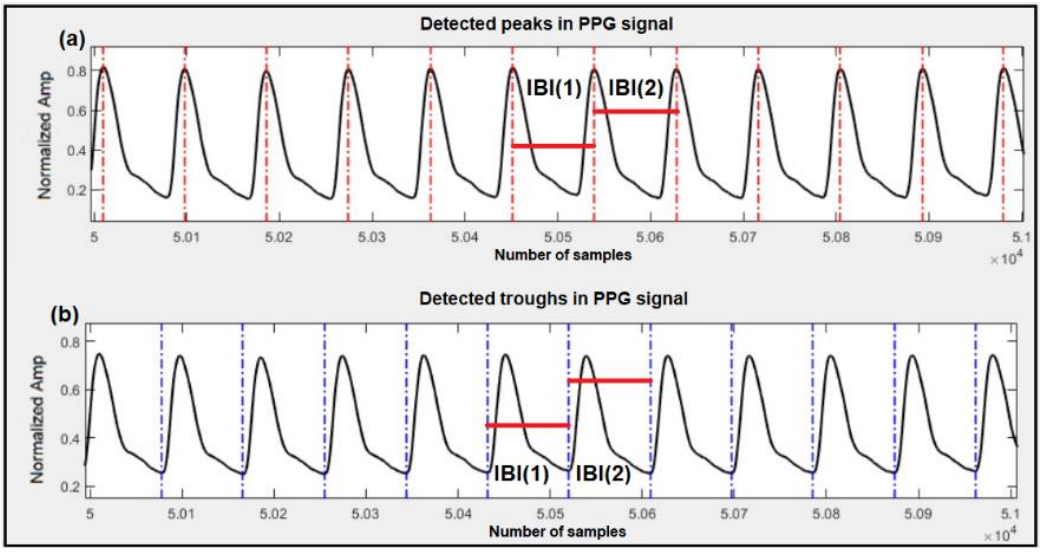

Figure 5-2. Detection of peaks, troughs and corresponding IBIs in the PPG signal. (a) Detected peaks are marked with vertical red lines and sample IBIs, used for SBP estimation, are marked with horizontal red lines; (b) Detected troughs are marked with vertical blue lines and sample IBIs, used for DBP estimation, are marked with horizontal red lines.

In (Samimi And Dajani, 2022b), we used the dataset from UCI and extracted features from the IBI series of the PPG signals through the time domain, frequency domain, and nonlinear analysis, as well as the features of pulse pressure, systolic and diastolic waveforms, and baroreflex sensitivity. After a feature selection process through wrapper subset evaluation with the forward greedy stepwise search (Hameed et al., 2018), we ended up using 5 features for SBP estimation (mean IBI, NNx, pNNx, SD2 and α1) and 6 features for DBP estimation (mean IBI, NNx, pNNx, PRVTi, SampleEn and IBI ratio of LF/HF). The details of the methodology and calculation of each of these features are reported in (Samimi and Dajani, 2022b).

In (Samimi and Dajani, 2022a), we used the dataset from the University of Queensland to extract cardiovascular dynamics features. In that work, we investigated the possibility of BP estimation using calibration-free and calibrated cardiovascular dynamics obtained with the PPG. The IBI features selected for the calibration-free method were NNx, α1, LF and HF for

the SBP estimation, and SDNN, RMSSD, SD1, LF and α1 for the DBP estimation. For the calibrated model, the selected IBI-related features were SampleEn and α1 for the SBP estimation and SampleEn and HF for the DBP estimation. To the features for the calibrated method, we also added the estimation from a calibrated mathematical model as an extra feature for both SBP and DBP.

In this work, blood pressure was estimated based on the same features, as mentioned above (for both datasets), when the same methodology was required for result comparison.

5.2.2.1 Feedforward Artificial Neural Network Model

In this work, BP estimation from the PPG morphology was used in addition to extracted features from the PPG dynamics. For this purpose, 21 features were extracted based on the research conducted in (Kurylyak et al., 2013). However unlike (Kurylyak et al., 2013), which collects the features in the context of one point-to-point (oPTP), we used the mPTP method, which takes an average of the feature over an interval of the signal. This modification was made because previous studies on BP estimation have shown that the oPTP method is not robust, and one way to overcome this shortcoming is to use the mPTP technique (Shao et al., 2020).

The extracted features for the estimation of SBP and DBP are listed below and shown in Figure 5-3.

- Cardiac period;
- Systolic upstroke time;
- Diastolic time;
- Diastolic width at 10%, 25%, 33%, 50%, 66% and 75% of the pulse height;

  For example, the diastolic width at 10% is calculated based on the time difference between the point at 10% of the peak amplitude that coincides in time with the peak

(point M in Figure 5-3) and the point at 10% of the peak amplitude located in the diastolic region of the pulse (point P in Figure 5-3).

- Sum of systolic width and diastolic width at 10%, 25%, 33%, 50%, 66% and 75% of the pulse height;
- Ratio of diastolic width to systolic width at 10%, 25%, 33%, 50%, 66% and 75% of the pulse height.

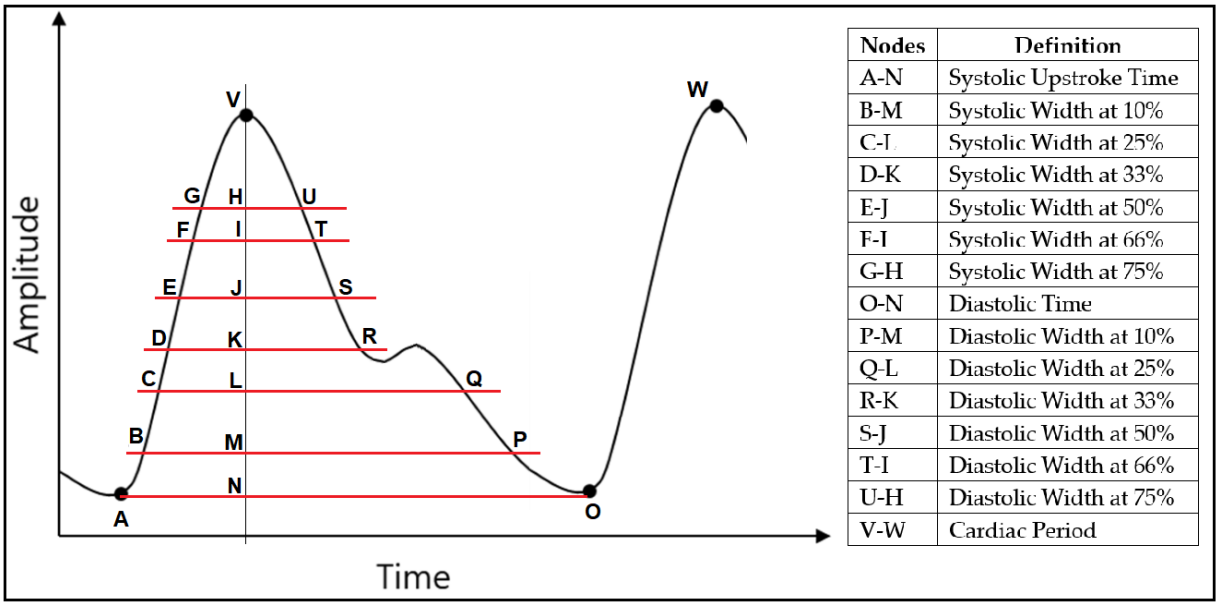

Nodes	Definition
A-N	Systolic Upstroke Time
B-M	Systolic Width at 10%
C-I	Systolic Width at 25%
D-K	Systolic Width at 33%
E-J	Systolic Width at 50%
F-I	Systolic Width at 66%
G-H	Systolic Width at 75%
O-N	Diastolic Time
P-M	Diastolic Width at 10%
Q-L	Diastolic Width at 25%
R-K	Diastolic Width at 33%
S-J	Diastolic Width at 50%
T-I	Diastolic Width at 66%
U-H	Diastolic Width at 75%
V-W	Cardiac Period

Figure 5-3. Extracted parameters from the PPG signal to generate the 21 features used in this study.

As for the structure of the artificial neural network, a multilayer feedforward back propagation ANN with 21 inputs and 2 output neurons was considered to simultaneously estimate SBP and DBP. In this architecture, 2 hidden layers were included with 35 neurons on the first hidden layer and 20 on the second one. The hidden layer neurons have sigmoid activation functions, while the output layer neurons for both SBP and DBP possess linear activation functions. This network structure was implemented based on (Kurylyak et al., 2013).

5.2.2.2 Deep Learning Model

In this part we looked into ANN deep learning for BP estimation based on the morphology features of the PPG. Seven parameters were selected based on the work in (El-Hajj and Kyriacou, 2021), and the mPTP method was used to generate each of the features that are listed below.

- Cardiac period;
- Diastolic time;
- Diastolic width at 25% and 75% of the pulse height;
- Sum of systolic width and diastolic width at 33% and 75% of the pulse height;
- Ratio of diastolic width to systolic width at 10% of the pulse height.

For the ANN model, we considered three different approaches: feedforward deep neural network, LSTM and GRU (El-Hajj and Kyriacou, 2021). The structure of each model is described below.

- Feedforward deep neural network: This model is similar to the one used in Section 5.2.2.1, which consisted of non-recurrent feedforward connections between the neurons, and it was constructed with three hidden layers containing 70, 100 and 150 neurons for Layers 1, 2 and 3 respectively (El-Hajj and Kyriacou, 2021);
- LSTM: Long short-term memory uses feedback connections to process sequential time domain data. It was originally developed to overcome the vanishing gradient problem during the training of the recurrent neural network due to long term prediction (El-Hajj and Kyriacou, 2021). The LSTM used in this work was constructed with two hidden layers of 64 and 512 neurons;
- GRU: The gated recurrent unit is similar to the LSTM but since it uses fewer parameters, it is somewhat less computationally expensive. It has also shown better performance on certain smaller datasets compared to LSTM (El-Hajj and Kyriacou,

2021). The network used here was constructed with three hidden layers of 128, 256 and 512 neurons in consecutive layers.

In the deep learning models, a sigmoid activation function is used for the feedforward deep neural network, while a rectified linear unit (ReLU) activation function is used for both LSTM and GRU approaches.

5.2.3 Blood Pressure Estimation Model

The blood pressure estimation result from the PPG morphology based on the above-mentioned methodologies was considered an extra feature to be added to the ones extracted from cardiovascular dynamics. The dataset was partitioned based on the leave-one-out method, where all features from one patient were set aside to be used as the test data, while the remaining features were split into 85% training and 15% validation. This process was repeated for all patients to cover the entire dataset. The purpose of setting aside 15% of the dataset for validation was to use the early stopping technique in order to avoid overfitting (Yao et al., 2007).

To estimate both systolic and diastolic blood pressure, an ANN with a two-layer feedforward network structure was used for regression. The two layers consisted of a sigmoid layer followed by a linear output layer. Based on our previous work with the same datasets (Samimi and Dajani, 2022a; Samimi and Dajani, 2022b) and the performance of the model with different numbers of neurons, a hidden layer with ten neurons was selected in this study. The Bayesian regularization backpropagation algorithm was used to train the network, and the structure was fixed prior to applying it to the test data.

The estimation performance was evaluated based on the mean error (ME), the mean absolute error (MAE), and the standard deviation of error (SDE) obtained with the test data. The ME and MAE are calculated using the following equations:

$$\mathbf{ME} = \frac{\sum_{i=1}^{n} y_i - x_i}{n}$$ **Equation 5-1**

$$\mathbf{MAE} = \frac{\sum_{i=1}^{n} |y_i - x_i|}{n}$$ **Equation 5-2**

where y_i is the prediction and x_i is the true value for the blood pressure from the dataset. The true values are determined by averaging either the noninvasive BP (for the data from the University of Queensland) or the invasive arterial BP (for the data from UCI) of each patient over the duration of the test signal.

The SDE was calculated using the following equation:

$$\mathbf{SDE} = \sqrt{\frac{\sum_{i=1}^{n} |e_i - \bar{e}|^2}{n}}$$ **Equation 5-3**

where e_i is the error between the prediction and the true value ($e_i = y_i - x_i$) for each estimation, and $\bar{e}$ is the average of e_i.

5.3 Results

The BP estimation results in this paper are based on three different datasets: PPG and noninvasive BP from 30 patients (University of Queensland dataset), the PPG and invasive arterial blood pressure waveform from 200 patients (UCI dataset) and the PPG and invasive arterial blood pressure waveform from 25 new patients (UCI dataset).

5.3.1 Estimation of BP with 30 patients from the University of Queensland Dataset

In this part, we estimated both systolic and diastolic blood pressure from 30 patients using the following three methods:

- Features from cardiovascular dynamics extracted from PPG signal. This is a calibration-free method that we developed in (Samimi and Dajani, 2022b);

- Information based on PPG morphology features. Estimation for both SBP and DBP was performed based on 21 extracted morphology features;
- A calibrated mathematical model. This is part of our previous work (Samimi and Dajani, 2022a), where we used a mathematical model to calibrate the blood pressure estimator.

Results from the proposed methods are shown in Table 5-1 and the corresponding Bland–Altman plots for these estimations are shown in Figure 5-4.

Table 5-1. Systolic and diastolic blood pressure estimation performance from 30 patients using: (1) PPG dynamics features, (2) PPG morphology features, and (3) Calibrated mathematical model, as explained in the text. Results are averaged over the 30 patients.

		Systolic BP (mmHg)			**Diastolic BP (mmHg)**		
		ME	**SDE**	**MAE**	**ME**	**SDE**	**MAE**
1	**PPG IBI**	-0.39	22.16	15.26	0.14	10.97	7.54
2	**PPG Morphology**	0.06	14.22	10.10	0.01	8.32	6.16
3	**Calibrated Mathematical Model**	3.18	12.49	9.11	0.45	8.36	5.47

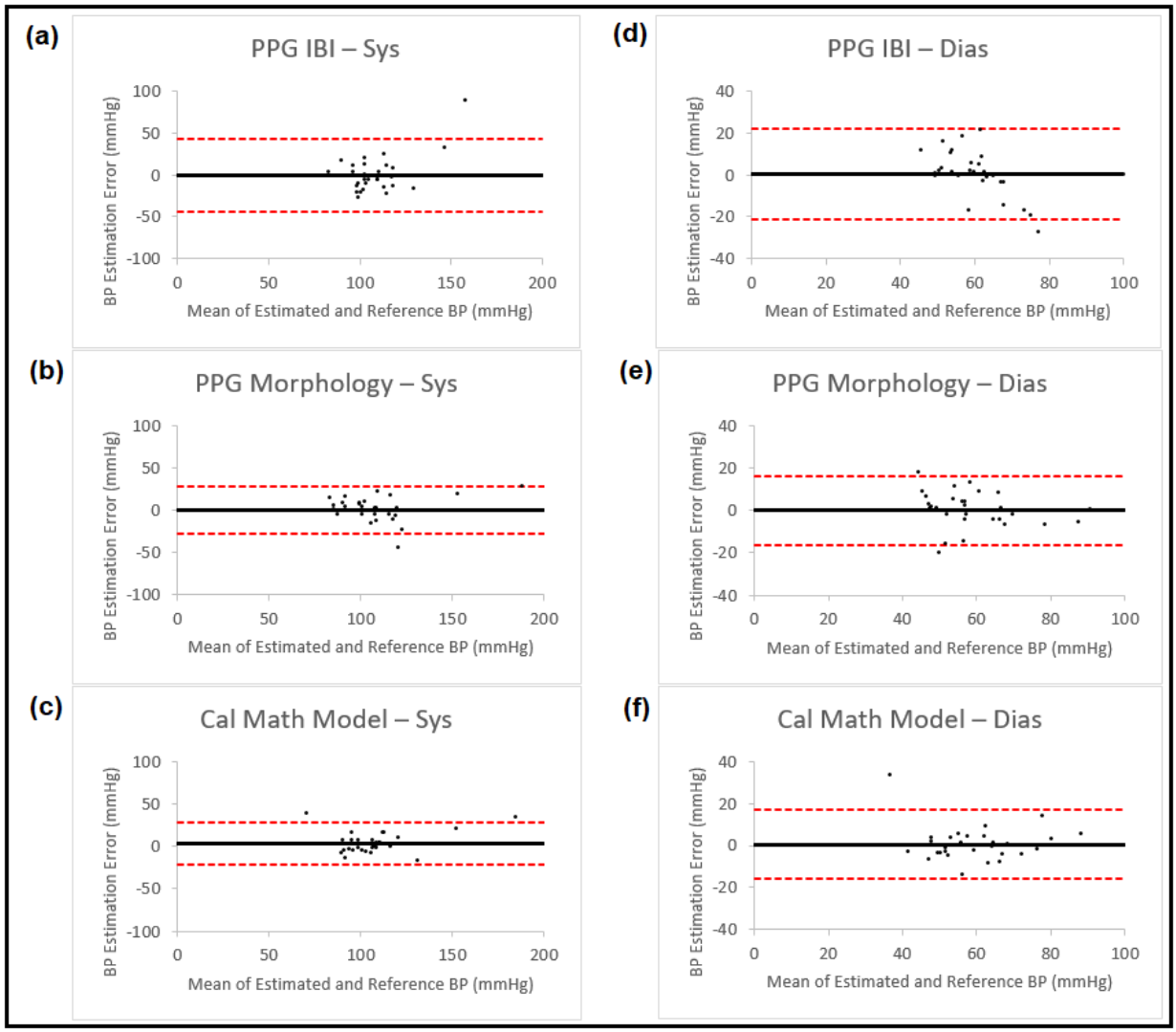

Figure 5-4. Bland–Altman plots presenting systolic and diastolic blood pressure estimation using three different methods (IBI features from PPG, PPG morphology features and calibrated mathematical model). The left column shows the results for systolic BP and the right column for diastolic BP. Each of the plots is named corresponding to the method that is used for estimation. In all the plots, the black horizontal line is the bias and the two dashed red lines are the 95% limits of agreement.

We also combined the estimation methodologies mentioned above to obtain higher accuracy. This was completed through two different approaches:

- Fusion technique;
- Feature combination.

In fusion technique, we used the sensor fusion method to combine different estimation results. Sensor fusion is a process used to combine data derived from different sources in

order to reduce uncertainty that would otherwise have come from each of the sources, and it is calculated using (Wang et al., 2019):

$$\mathbf{x_3} = \boldsymbol{\sigma_3^2}(\boldsymbol{\sigma_1^{-2}}\mathbf{x_1} + \boldsymbol{\sigma_2^{-2}}\mathbf{x_2}) \quad \textbf{Equation 5-4}$$

where x_3 is the resulting information and $x_1$and x_2 are the measurements obtained from two sources with noise variances σ_1^2 and σ_2^2 respectively. σ_3^2 is the variance of the combined estimate and can be calculated as:

$$\boldsymbol{\sigma_3^2} = (\boldsymbol{\sigma_1^{-2}} + \boldsymbol{\sigma_2^{-2}})^{-1} \quad \textbf{Equation 5-5}$$

Table 5-2 shows the estimation results for both SBP and DBP obtained using the sensor fusion process on the results achieved from earlier-mentioned methods, and Figure 5-5 presents the corresponding Bland–Altman plots for the estimation results.

Table 5-2. Blood pressure estimation performance using fusion process on the results obtained from: (1) IBI features of PPG signals and PPG morphology features; (2) IBI features of PPG signals and calibrated mathematical model; and (3) IBI features of PPG signals, PPG morphology features and calibrated mathematical model from 30 patients. Results are averaged over all the patients.

		Systolic BP (mmHg)			Diastolic BP (mmHg)		
		ME	**SDE**	**MAE**	**ME**	**SDE**	**MAE**
1	**Fusion of PPG IBI and PPG Morphology**	-0.25	17.54	11.16	0.11	9.42	6.60
2	**Fusion of PPG IBI and Calibrated Mathematical Model**	0.70	17.22	11.03	-0.03	9.60	6.76
3	**Fusion of PPG IBI, PPG Morphology and Calibrated Mathematical Model**	0.58	14.85	8.95	-0.03	8.52	6.09

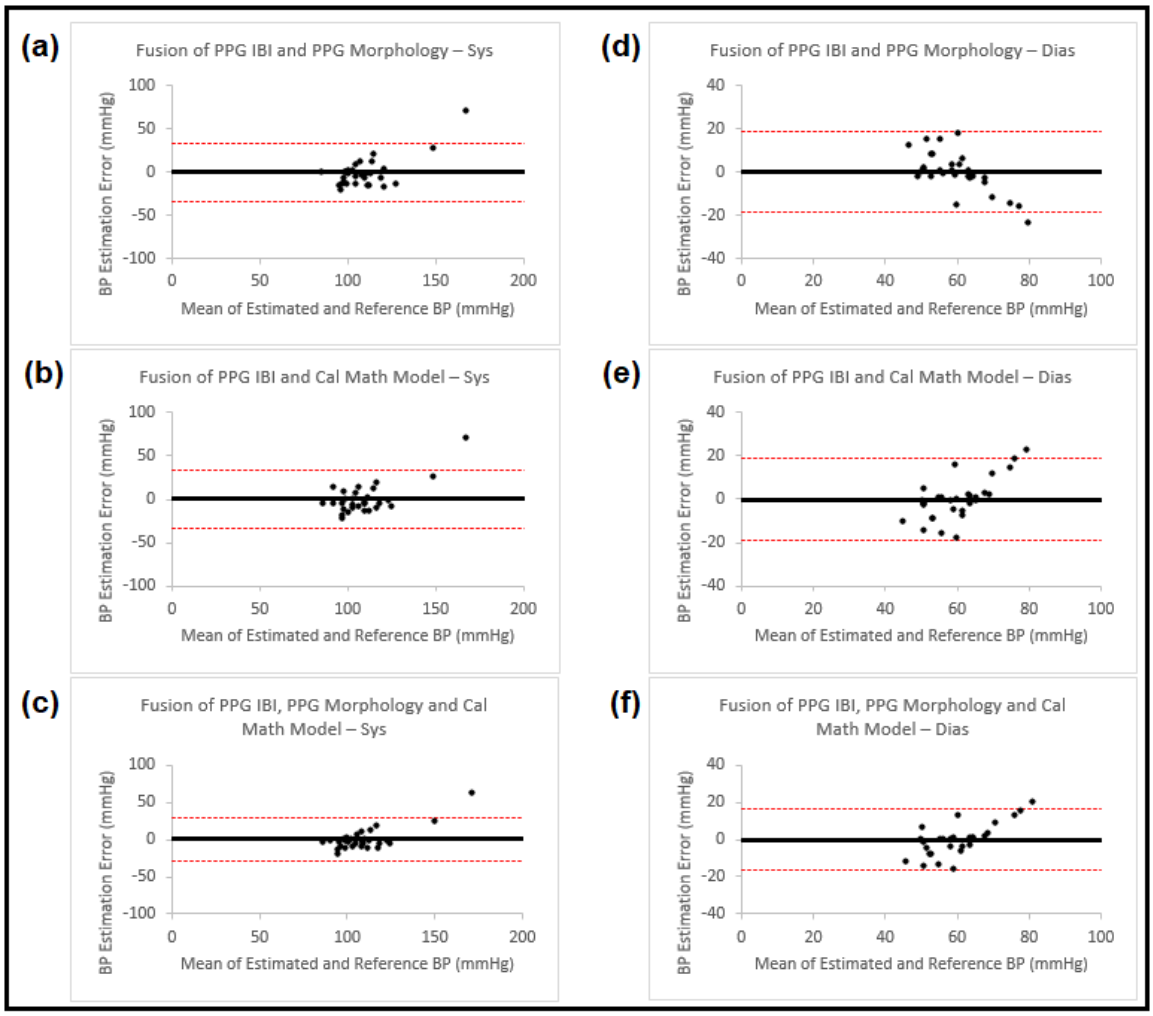

Figure 5-5. Bland–Altman plots presenting systolic and diastolic blood pressure estimation using fusion on three different methods (IBI features from PPG, PPG morphology features and calibrated mathematical model). The left column shows the results for systolic BP, and the right column for diastolic BP. Each of the plots is named accordingly. In all the plots the black horizontal line is the bias and the two dashed red lines are the 95% limits of agreement.

In the second method, we used blood pressure estimation from PPG morphology or the calibrated mathematical model as extra features and added them to the PPG IBIs, one at a time or both together (having three combinations that were the same as the ones in the fusion process). We then used wrapper subset evaluation with the forward greedy stepwise search method and determined the best features for the ANN estimator. The blood pressure estimation results for SBP and DBP obtained using this method are shown in Table 5-3 and the corresponding Bland–Altman plots for the estimation results are shown in Figure 5-6.

Table 5-3. Blood pressure estimation performance using IBI features in combination with: (1) Estimation from morphology features; (2) Estimation from calibrated mathematical model; and (3) Estimation from morphology features and estimation from calibrated mathematical model from 30 PPG waveforms. Results are averaged over all the patients.

		Systolic BP (mmHg)			Diastolic BP (mmHg)		
		ME	**SDE**	**MAE**	**ME**	**SDE**	**MAE**
1	**PPG IBI and PPG Morphology**	-1.51	11.23	7.50	-0.42	6.14	4.94
2	**PPG IBI and Calibrated Mathematical Model**	2.52	12.15	8.89	0.59	7.07	4.92
3	**PPG IBI, PPG Morphology and Calibrated Mathematical Model**	-1.15	10.69	7.41	-1.11	6.07	4.90

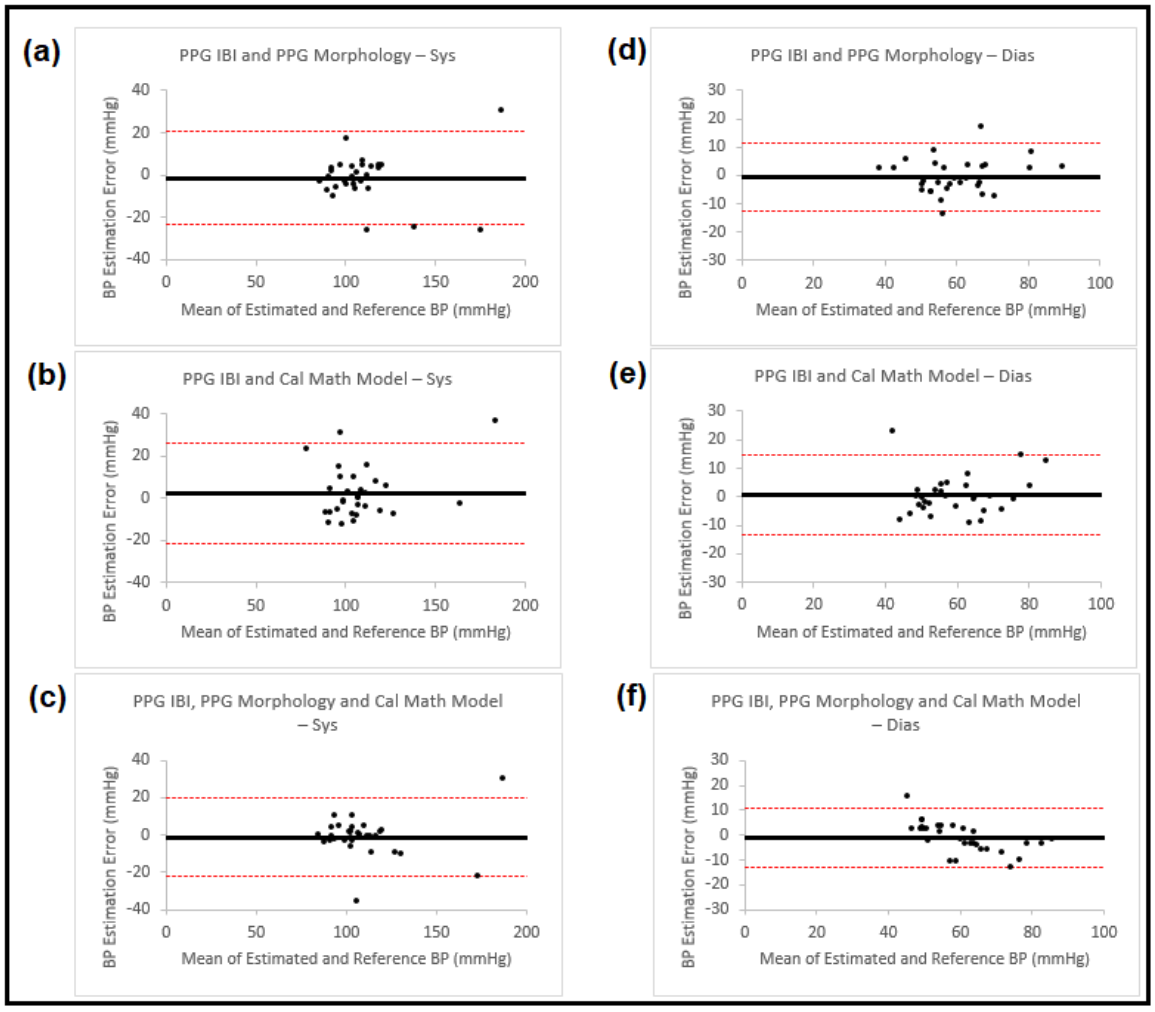

Figure 5-6. Bland–Altman plots presenting systolic and diastolic blood pressure estimation using three different sets of features from PPG waveforms (IBI and morphology, IBI and calibrated mathematical model and IBI, morphology and calibrated mathematical model). The left column shows the results for systolic BP and the right column for diastolic BP. Each of the plots is named accordingly. In all the plots, the black horizontal line is the bias and the two dashed red lines are the 95% limits of agreement.

Comparing the two previously mentioned methods (fusion process and feature combination) shows that the fusion process resulted in lower accuracy. As for the results obtained from combining PPG dynamics features and estimation from PPG morphology and the calibrated mathematical model, they showed that while adding either results from morphology or calibration to the PPG IBI features improved the estimation results, adding both at the same time did not have much of an improvement, especially for diastolic blood pressure. Considering this new finding, we decided to compare the correlations between the estimation results obtained using PPG dynamics, PPG morphology and the PPG mathematical calibration model by calculating the correlation coefficient:

$$\rho_{X,Y} = \frac{\mathrm{cov}(X,Y)}{\sigma_X \sigma_Y} \qquad \textbf{Equation 5-6}$$

where cov is covariance, σ_X is the standard deviation of X, and σ_Y is the standard deviation of Y.

The resulting correlation coefficients showed that while there is a low level of correlation between the estimation results from IBI and morphology or IBI and the calibration method, the blood pressure estimation values from morphology and calibration methods are highly correlated. Correlation results were similar for both SBP and DBP. These correlations are shown in Table 5-4 and the scatter diagrams are presented in Figure 5-7.

Table 5-4. Correlation between blood pressure estimation using three different methods. In the table, IBI refers to BP estimation using PPG dynamics, morphology refers to BP estimation using PPG morphology features and calibration refers to BP estimation using the calibrated mathematical model. All three methods are described in the text and the results are from 30 PPG waveforms.

Correlation between BP Estimation Using Different Methods for PPG Signals			
	IBI and Calibration	**IBI and Morphology**	**Morphology and Calibration**
Systolic BP	0.23	0.16	0.74
Diastolic BP	0.45	0.29	0.78

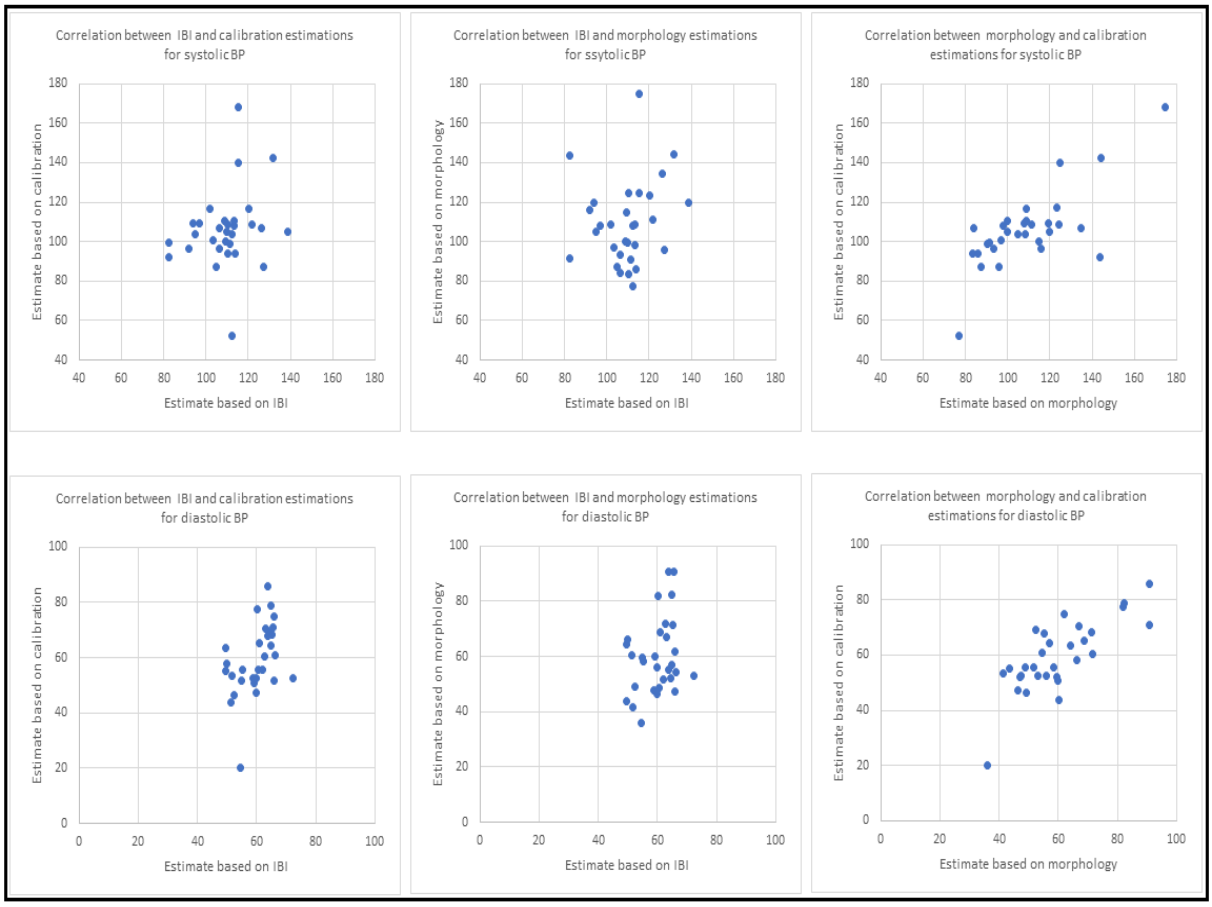

Figure 5-7. Scatter diagrams for blood pressure estimation using three different methods. The top row has the results for systolic BP and bottom row shows the results from diastolic BP. For both rows, the first plot from the left shows correlation between BP estimation using PPG dynamics and PPG morphology, the second plot displays BP estimation correlation between PPG dynamics and the calibration model and the third plot illustrates blood pressure estimation correlation using morphology and the calibration model. All the results are based on collected PPG waveforms from 30 patients. All estimates in this figure are in mmHg.

Given the finding of high correlation between BP estimation results obtained from PPG morphology features and the calibration model, we used the estimation from the PPG morphology features as a substitute for the calibration model in our remaining experiments.

5.3.2 Estimation of BP with 200 patients from the UCI Dataset

In this part, we estimated both the systolic and diastolic blood pressure of 200 patients using features from cardiovascular dynamics and PPG morphology. As was mentioned in Section 5.2.3 above, the blood pressure was estimated using features from the PPG morphology, and the estimated value was added to the collected features from cardiovascular dynamics to

replace the calibration step we had used in our previous study (Samimi and Dajani, 2022a). The BP estimation based on the PPG morphology features was carried out using the following four different ANN models: the feedforward back propagation neural network, the feedforward deep neural network, LSTM and GRU. The blood pressure estimation results using cardiovascular dynamics through PPG IBI, the different models for the PPG morphology, and the proposed method obtained by using estimation using the PPG morphology in addition to the PPG IBI, are shown in Table 5-5, the corresponding Bland–Altman plots for SBP are presented in Figure 5-8 and for DBP, in Figure 5-9.

Table 5-5. Blood pressure estimation performance using PPG signals from 200 patients. The estimation is based on: (1) IBI features; (2) Morphology features using feedforward artificial neural network; (3) Morphology features using feedforward deep artificial neural network; (4) Morphology features using LTSM; (5) Morphology features using GRU; (6) Combining IBI features and estimated BP values from feedforward artificial neural network using morphology features; (7) Combining IBI features and estimated BP values from feedforward deep neural network using morphology features; (8) Combining IBI features and estimated BP values from LSTM using morphology features; and (9) Combining IBI features and estimated BP values from GRU using morphology features.

		Systolic BP (mmHg)			**Diastolic BP (mmHg)**		
		ME	**SDE**	**MAE**	**ME**	**SDE**	**MAE**
1	**PPG IBI**	0.09	18.81	14.49	0.03	7.91	5.75
2	**PPG Morphology using Feedforward Neural Network Model**	-0.52	20.30	14.51	0.64	9.29	6.78
3	**PPG Morphology using Feedforward Deep Neural Network Model**	0.36	13.81	11.24	0.12	6.49	4.75
4	**PPG Morphology using LTSM Model**	-0.17	19.11	15.20	-0.05	7.35	5.59
5	**PPG Morphology using GRU Model**	0.07	19.22	15.30	0.10	7.29	5.59
6	**PPG Morphology using Feedforward NN Model and PPG IBI**	0.01	16.38	13.04	-0.30	6.67	5.31
7	**PPG Morphology using Feedforward Deep NN Model and PPG IBI**	0.15	12.40	9.74	-0.01	6.29	4.65
8	**PPG Morphology using LSTM Model and PPG IBI**	0.11	18.49	14.63	-0.04	7.77	6.05
9	**PPG Morphology using GRU Model and PPG IBI**	0.10	18.87	14.90	-0.04	7.78	6.07

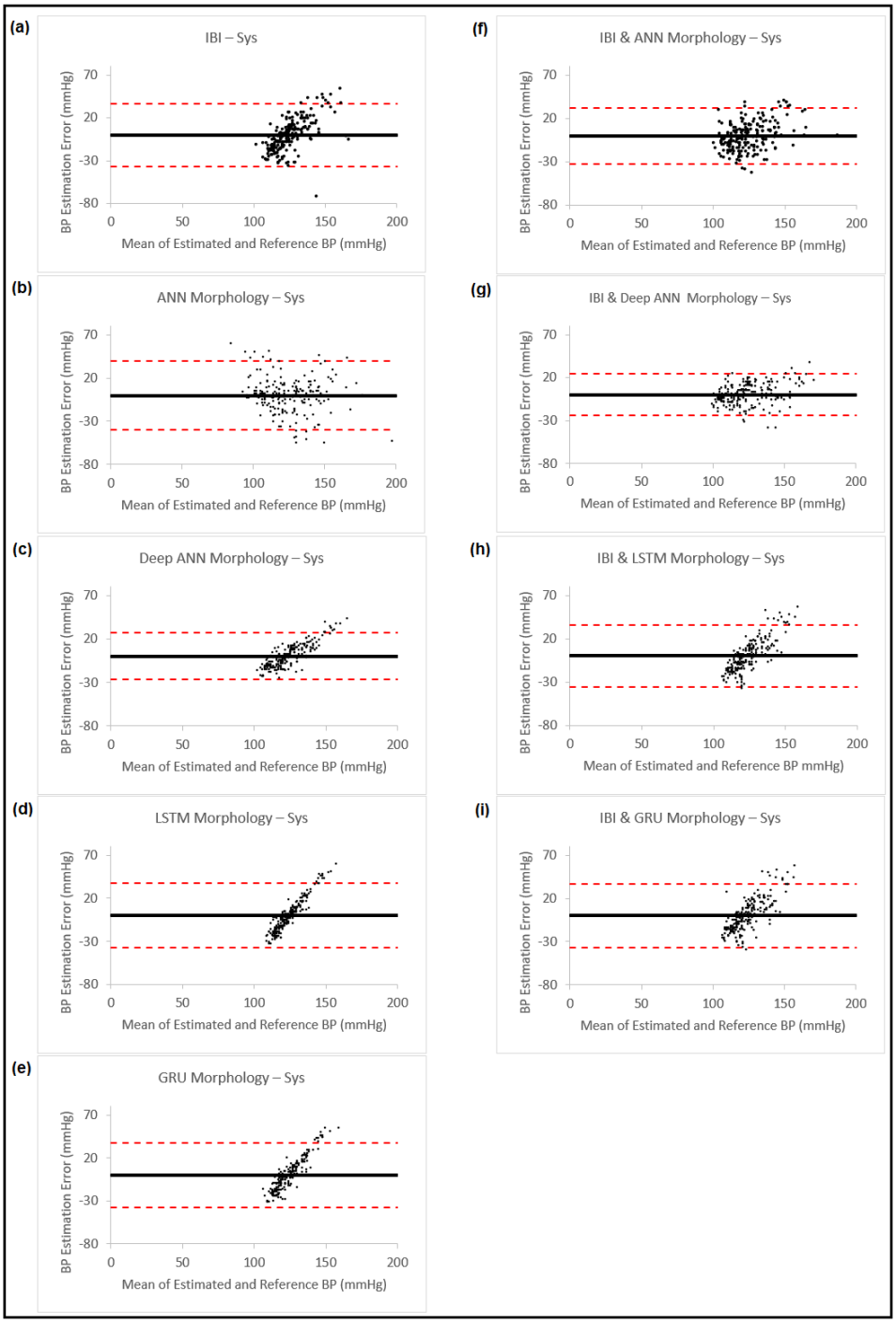

Figure 5-8. Bland–Altman plots presenting systolic blood pressure estimation using different methods: (a) Estimation using PPG dynamics features and ANN model; (b) Estimation using PPG morphology features and ANN model; (c) Estimation using PPG morphology features and feedforward deep NN model; (d) Estimation using PPG morphology features and LSTM model; (e) Estimation using PPG morphology features and GRU model; (f) Estimation combining the estimated BP result from (b) and PPG dynamics and use them in ANN model; (g) Estimation combining the estimated BP result from (c) and PPG dynamics and use them in ANN model; (h) Estimation combining the estimated BP result from (d) and PPG dynamics and use them in ANN model; (i) Estimation combining the estimated BP result from (e) and PPG dynamics and use them in ANN model. In all the plots, the black horizontal line is the bias and the two dashed red lines are the 95% limits of agreement.

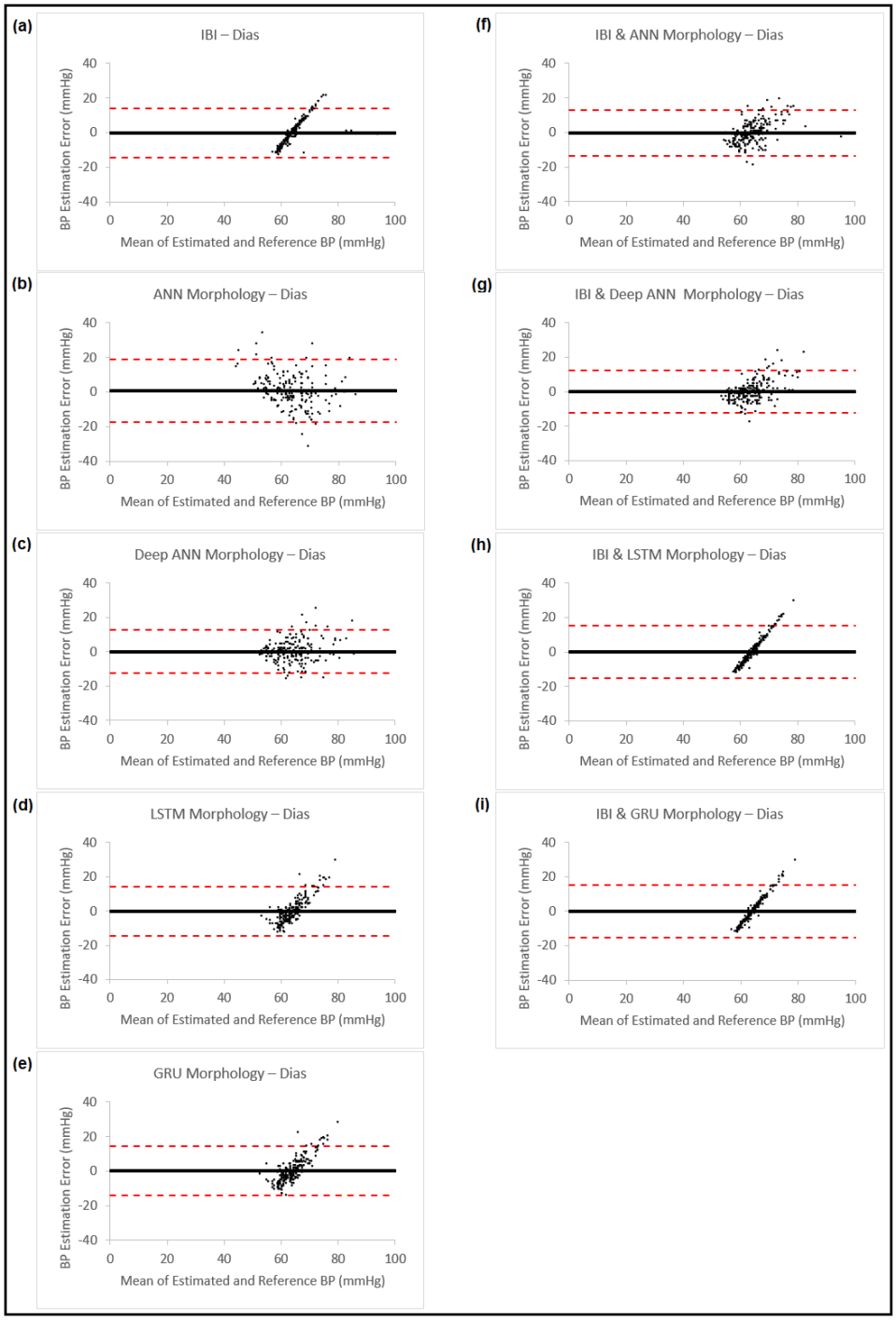

Figure 5-9. Bland–Altman plots presenting diastolic blood pressure estimation using different methods: (a) Estimation using PPG dynamics features and ANN model; (b) Estimation using PPG morphology features and ANN model; (c) Estimation using PPG morphology features and feedforward deep NN model; (d) Estimation using PPG morphology features and LSTM model; (e) Estimation using PPG morphology features and GRU model; (f) Estimation combining the estimated BP result from (b) and PPG dynamics and use them in ANN model; (g) Estimation combining the estimated BP result from (c) and PPG dynamics and use them in ANN model; (h) Estimation combining the estimated BP result from (d) and PPG dynamics and use them in ANN model; (i) Estimation combining the estimated BP result from (e) and PPG dynamics and use them in ANN model. In all the plots, the black horizontal line is the bias and the two dashed red lines are the 95% limits of agreement.

5.3.3 Estimation of BP with 25 New Patients from the UCI Dataset

In this part, we tested our proposed estimation model with the data from 25 patients that were not seen by the model before. Our feature set for the proposed ANN model consisted of the seven PPG dynamics features (SDNN, PRVTi, TINN, LF, HF, $\alpha 1$ and $\alpha 2$) and the BP estimation obtained by using the PPG morphology features with feedforward deep neural network. Figure 5-10 is a graphical representation of the structure of the proposed model.

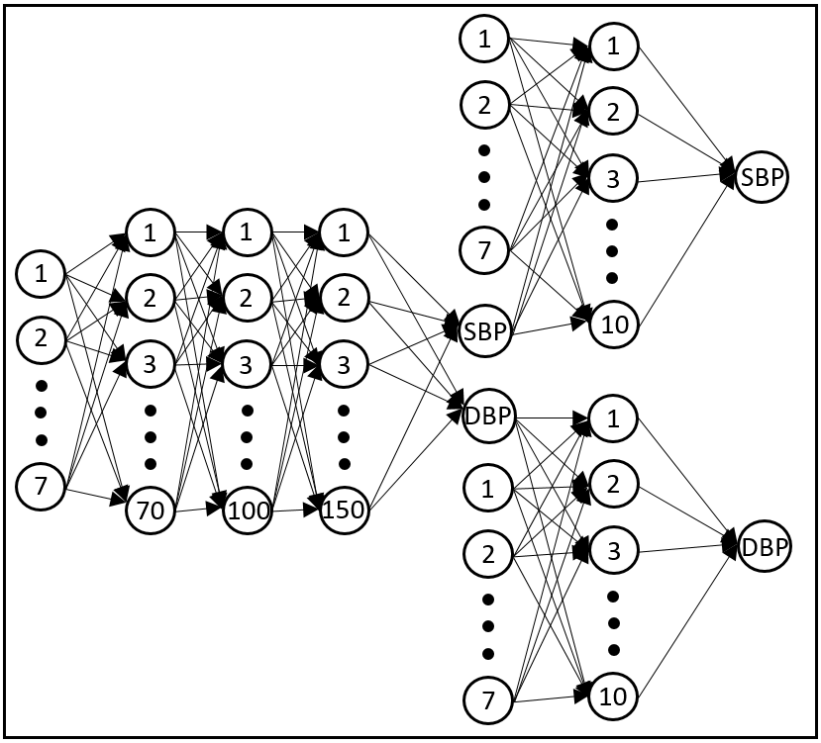

Figure 5-10. Structure of the proposed neural network model. This network consists of three subnetworks. The one on the left has seven inputs that are PPG morphology features, three hidden layers that use sigmoid activation functions and an output layer that uses a linear activation function. The outputs of this subnetwork are estimated SBP and DBP that are then used in the subsequent subnetworks to estimate the final BP values. Each of these two subnetworks (on the right) has eight inputs (seven features related to cardiovascular dynamics plus the estimated BP value from morphology features from the prior subnetwork). Furthermore, each of these two networks has a single hidden layer with a sigmoid activation function and an output layer with a linear activation function. The resulting SBP and DBP from this stage are the final BP estimation values.

This model was chosen based on the results achieved from earlier experiments in Section 5.3.2, which showed that the feedforward deep neural network model gave the best performance among the methods that were used. This allowed us to have a calibration-free model that can be used to estimate both SBP and DBP. We then trained the model on 200

signals that were used in Section 5.3.2. The trained model was used to estimate blood pressure values for the 25 new patients. The estimation results and the related errors are shown in Table 5-6, with the corresponding Bland–Altman plots shown in Figure 5-11.

Table 5-6. Blood pressure estimation performance using the proposed model on the test data from 25 never-seen-before patients.

IBI and Estimation from Feedforward Deep NN with ANN Model			
	ME (mmHg)	**SDE (mmHg)**	**MAE (mmHg)**
Systolic BP	-4.02	10.40	7.41
Diastolic BP	-0.31	4.89	3.32

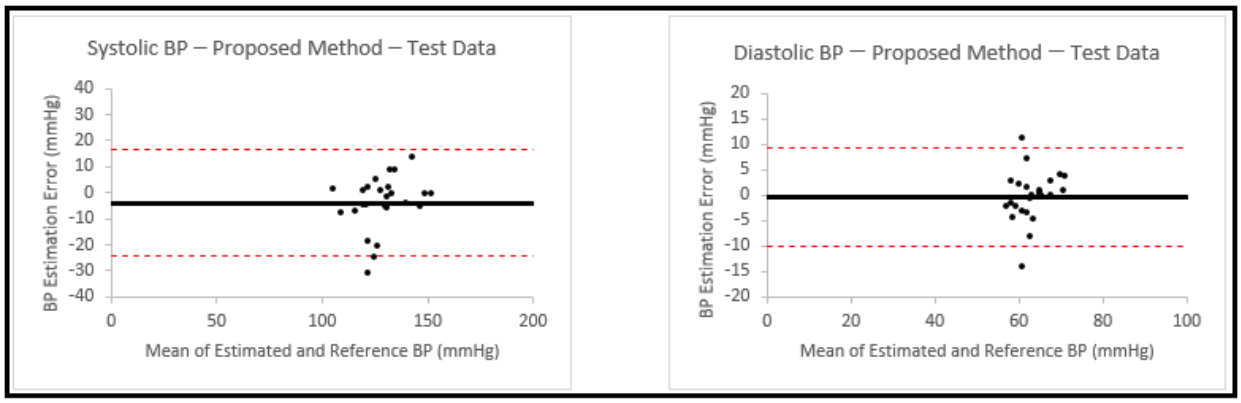

Figure 5-11. Bland–Altman plots presenting systolic and diastolic blood pressure estimations using the proposed model on the test data from 25 never-seen-before patients. In both plots, the black horizontal line is the bias and the two dashed red lines are the 95% limits of agreement.

5.4 Discussion

The results of this study indicate that the proposed method based on PPG dynamics over short intervals combined with the blood pressure estimation from the PPG morphology could be used as a calibration-free technique to obtain blood pressure estimation using only a single photoplethysmogram signal. Although reference BP values were used during the process of training the neural network, this method is considered calibration-free since no calibration is involved in the actual usage when testing on new subjects. One advantage of this method is that the PPG dynamics, which are obtained only from timing variation between the peaks and troughs of the signal and that are used as part of the model, would be expected to be less susceptible to poor sensor placement or different skin colors than the commonly used pure

morphology features. This may be one of the reasons why we see improvement in estimation when IBI features are added to the estimation from morphology.

In the first part of this study, we investigated a calibrated model and explored the possibility of replacing the calibration step with estimation from morphology features to obtain a calibration-free method. We started from our previous study (Samimi and Dajani, 2022a), where we extracted 16 features from PPG IBI, and through wrapper subset evaluation with a forward greedy stepwise search technique, we selected four features for SBP estimation and five features for DPB estimation. Using the same feature selection method for the calibrated model resulted in choosing two IBI-related features for both SBP and DBP estimations in addition to the calibration feature. To study the possibility of replacing the calibration step with information from the PPG morphology, we then replaced the calibration feature with an estimation obtained from the morphology. Our results showed that similar BP estimation accuracy was obtained from the following three different methods: a calibrated IBI model, replacing the calibration feature with a morphology estimation in the calibrated IBI model, or adding a PPG morphology estimation to the IBI calibrated model. While adding calibration or estimation from morphology led to substantial reduction in most of the error measures compared to the estimation from the IBI features, particularly the critical measures of SDE and MAE (by about 50% in both cases), when they were both added at the same time, the improvement in error measurement (compared to when only estimation from morphology was added to the IBI) were minimal (SDE and MAE were reduced by 5% and 1% for SBP and 1% and 1% for DBP, respectively). To further evaluate the possibility of replacing calibration with estimation from the PPG morphology, we looked at the correlation between blood pressure estimation when IBI features, PPG morphology features or mathematical estimation model were used. The results showed that while there were no strong correlations between the estimation results from IBI and the calibrated mathematical model or IBI and PPG morphology, the blood pressure estimation from the PPG morphology features and the

calibrated mathematical model were relatively strongly correlated (correlation coefficient equal to 0.74 for SBP and 0.78 for DBP). Therefore, this suggested that the calibration step may be replaced by estimation from the PPG morphology (when using our dataset and the proposed methodology), which results in a calibration-free estimation method. Our experimental results also showed that the PPG dynamics can be added to the estimation from the PPG morphology to increase the overall estimation accuracy.

In the second part of the work, we looked at improving the estimation accuracy of the proposed method and also confirming that the information from the PPG dynamics could improve the estimation results obtained from different methods. For this purpose, we based the work on our previous study of BP estimation using a calibration-free method (Samimi and Dajani, 2022b), where we extracted 16 IBI features from PPG signals and selected 5 features for SBP estimation and 6 features for DBP estimation, based on the same feature selection technique that was used in the first part. We obtained the estimation from the PPG morphology (21 features) with a feedforward back propagation artificial neural network. This was the same methodology that we used in the first part of this study. We also proceeded with implementing three different deep learning methods (feedforward deep NN, LSTM and GRU) to be used with seven features from the PPG morphology for the BP estimation to improve the accuracy of our proposed model. The estimation results, in particular the measures of SDE and MAE, were compared for the five different methods (IBI features with ANN, morphology features with ANN, morphology features with three deep learning models). We then added the obtained estimation from the PPG morphology (through different models) to the PPG IBI features (same as the proposed calibration-free method in part one) and selected eight features (seven IBI features and the PPG morphology estimate) for both SBP and DBP using the wrapper subset evaluation with a forward greedy stepwise search technique. The eight resulting features were used in an ANN model to estimate the finalized estimation for SBP and DBP. The results showed that for all four models, adding IBI features

improved the accuracy. This confirms that PPG dynamics contain useful information that can improve blood pressure estimation for different methods. We also found that using the proposed feedforward deep NN model consisting of more hidden layers and neurons instead of the shallow NN that was originally used in our proposed method, reduced the measured error; particularly, the critical measures of SDE and MAE by 24% and 25% for SBP and 6% and 13% for DBP.

In the last part of this work, we used the proposed model to estimate SBP and DBP with PPG signals from 25 new patients. This part was important in validating our method since the information from these patients was not previously seen by our model. The result showed a SDE and MAE of 10.4 mmHg and 7.41 mmHg for SBP, and 4.89 mmHg and 3.32 mmHg for DBP. This result presents an improvement in accuracy when compared to our previous studies.

In this work, we used two different datasets: one was the University of Queensland Vital Signs Dataset (Liu et al., 2012), from which we extracted PPG and noninvasive arterial BP waveforms, and the other dataset was derived from the University of California Irvine Machine Learning Repository (Kachuee et al., 2015), from which we used PPG signals and invasive arterial blood pressure signals. Except for the 25 new patients, who did not take part in any of our previous studies, these are the same datasets and signals that were used in our previous studies, (Samimi and Dajani, 2022a; Samimi and Dajani, 2022b), which resulted in different IBI-related features being selected for blood pressure estimations in these two studies. In our current work, with the new proposed method for BP estimation, we also observed similar discrepancy when it came to IBI feature selection. As was discussed in (Samimi and Dajani, 2022a), this difference could be the result of different target data for the two datasets (noninvasive BP for the University of Queensland data and invasive BP for UCI data), as there are differences in BP readings between invasive and noninvasive methods (Ribezzo et al., 2014). The population of the datasets could also have an impact on the feature

selection. The data provided by UCI were collected in intensive care units, where the patients were possibly under the influence of medications that could impact blood pressure dynamics or, in the case of inotropes, could result in a different BP measurement between invasive and noninvasive methods, with variations being directly related to the amount of medication that was used (Kaur et al., 2019). On the other hand, the data from the University of Queensland were collected from patients undergoing anesthesia for surgery, which could result in rapid and dynamic vital sign changes during induction and emergence phases of anesthesia.

Several of the Bland–Altman plots show an increasing (or in some cases a decreasing) trend in the error, with increase in the mean of the BP estimated using our models and the reference BP. A similar effect has been found in the past in Bland–Altman analyses of BP pressure estimated using other methods (Shimada et al., 2015; Verberk et al., 2005). The study by Shimada et al. (Shimada et al., 2015) carefully examined this effect and determined that it was likely due to differences in interindividual variability obtained with the two methods that were compared, which may also apply to our study. However, it should be noted that in our final structure, we used a model that did not show severe trends for SBP and DBP of this type (Figure 5-11).

The lower errors found for DBP vs. SBP also follow the same trend that we found with different methods, and it could be due to the strong relation between HRV indices and both SBP and DBP in females, while this relation is limited to DBP for males (Mori et al., 2014). The datasets that we used in this study did not include information regarding gender composition. If we assume that the male and female participants were close in number, then the BP estimation result based on IBI dynamics will show lower accuracy for SBP than DBP, and that is what we saw in this study. Additionally, since changes in IBI are more clearly present in DBP compared to SBP (Takalo et al., 1994), this could be a contributor to the higher estimation accuracy of DBP. Another possible reason behind the lower reported error for DBP

could be because the baseline DBP values are lower compared to the ones for SBP, which could also cause the errors to be lower.

This study also had some limitations. First, the datasets did not include some useful information regarding characteristics such as race, age, gender and weight that have an impact on blood pressure levels and that could provide valuable information contributing to the accuracy of the estimation results (Kan et al., 2015; Reckelhoff, 2001). Second, the sizes of the datasets could have impacted the deep learning algorithm results. Since the effectiveness of deep learning techniques is impacted by the size of the dataset (Barbedo, 2018), having a larger dataset ultimately could improve the blood pressure estimation results. Third, in this work, the quality of the PPG signals was inspected manually, and like any other non-automated process, they could introduce errors, especially with the sizes of the dataset that were analyzed. Implementing an automated approach for this process would be highly beneficial for real-life scenarios. Finally, our replacement of calibration with estimation based on morphology was evaluated on a relatively limited dataset (University of Queensland dataset from 30 patients) with short measurement intervals (less than 5 h). The ability to retain a calibration-free estimation needs to be confirmed by testing longer signal durations over more samples.

5.5 Conclusions and Future Work

In this paper, we focused on a cuffless blood pressure estimation based solely on information carried by PPG signals. We demonstrated that the cardiovascular dynamics carry useful information that can help to improve the accuracy of BP estimation when features based on pulse morphology are also used. Another finding of this work was that we were able to replace a calibration method (that was introduced in our previous work (Samimi and Dajani, 2022a)) with an estimation from the PPG morphology, and by doing so, we were able to provide a calibration-free method for blood pressure estimation, which provided similar accuracy as the

calibrated method. It is worth mentioning that the estimation made using PPG morphology was reliant on the same features used in previous studies (El-Hajj and Kyriacou, 2021; Kurylyak st al., 2013), and did not incorporate any new ones. However, if different or additional PPG morphology features are used, there is a possibility to further improve the overall estimation accuracy.

Since in this paper adding information from cardiovascular dynamics to a number of different BP estimation techniques based on pulse morphology showed considerable improvement in the estimation accuracy, this approach may also be useful for improving the BP estimation accuracy of other methods, such as the widely used ones that are based on the pulse transit time.

5.6 References

Agham, N., Chaskar, U. (2021). An advanced LAN model based on optimized feature algorithm: Towards hypertension interpretability. *Biomedical Signal Processing and Control*, *68*, 102760.

Barbedo, J.G.A. (2018). Impact of dataset size and variety on the effectiveness of deep learning and transfer learning for plant disease classification. *Computers and Electronics in Agriculture*, *153*, 46-53.

Chao, P.C.P., Wu, C.C., Nguyen, D.H., Nguyen, B.S., Huang, P.C., Le, V.H. (2021). The machine learnings leading the cuffless PPG blood pressure sensors into the next stage. *IEEE Sens. J., 21*, 12498–12510.

El-Hajj, C., Kyriacou, P.A. (2021). Deep learning models for cuffless blood pressure monitoring from PPG signals attention mechanism. *Biomedical Signal Processing and Control*, *65*, 102301.

Fati, S.M., Muneer, A., Akbar, N.A., Taib, S.M. (2021). A continuous cuffless blood pressure estimation using tree-based pipeline optimization tool. *Symmetry*, *13*(686).

Fukushima, H., Kawanaka, H., Bhuiyan, M.S., Oguri, K. (2013). Cuffless blood pressure estimation using only photoplethysmography based on cardiovascular parameters. Proceedings of the Annual International Conference of the IEEE Engineering in Medicine and Biology Society, EMBS, Osaka, Japan, 2132-2135.

Hameed, S. S., Petinrin, O. O., Hashi, A. O., Saeed, F. (2018). Filter-wrapper combination and embedded feature selection for gene expression data. *International Journal of Advances in Soft Computing and its Applications, 10*, 90-105.

Hassani, A., Foruzan, A.H. (2019). Improved PPG-based estimation of the blood pressure using latent space features. *Signal, Image and Video Processing*, *13*, 1141-1147.

Ibtehaz, N., Mahmud, S., Chowdhury, M.E.H., Khandakar, A., Salman Khan, M., Ayari, M.A., Tahir, A.M., Rahman, M.S. (2022). PPG2ABP: translating photoplethysmogram (PPG) signals to arterial blood pressure (ABP) waveforms. *Bioengineering, 9*(692).

Kachuee, M., Kiani, M.M., Mohammadzadeh, H., Shabany, M. (2015). Cuffless high-accuracy calibration-free blood pressure estimation using pulse transit time. IEEE International Symposium on Circuit and Systems (ISCAS"15), Lisbon, Portugal.

Kan, A.W., Hussain, T., Carson, K.A., Purnell, T.S., Yeh, H.C., Albert, M., Cooper, L.A. (2015). The contribution of age and weight to blood pressure levels among blacks and whites receiving care in community-based primary care practices. *Preventing Chronic Disease*, *12*, 150069.

Kaur, B., Kaur, S., Yaddanapudi, L.N., Singh, N.V. (2019). Comparison between invasive and noninvasive blood pressure measurements in critically ill patients receiving inotropes. *Blood Press. Monit., 24*, 24–29.

Kurylyak, Y., Lamonaca, F., Grimaldi, D. (2013). A neural network-based method for continuous blood pressure estimation from a PPG signal. 2013 IEEE International Instrumentation and Measurement Technology Conference (I2MTC), Minneapolis, MN, USA.

Lee, C.Y., Xie, S., Gallagher, P., Zhang, Z., Tu, Z. (2015). Deeply-supervised nets. In Proceedings of the Artificial Intelligence and Statistics, Valencia, Spain, 562–570.

Li, P., Laleg-Kirati, T.M. (2021). Central blood pressure estimation from distal PPG measurement using semiclassical signal analysis features. *IEEE Access*., *9*, 44963-44973, 9374974.

Liu, D., Gorges, M., Jenkins, S.A. (2012). University of Queensland vital signs dataset: Development of an accessible repository of anesthesia patient monitoring data for research. *Anesth. Analg., 114*, 584–589.

Malayeri, A.B., Khodabakhshi, M.B. (2022). Concatenated convolutional neural network model for cuffless blood pressure estimation using fuzzy recurrence properties of photoplethysmogram signals. *Scientific Reports*, *12*, 6633.

Mohebbian, M.R., Dinh, A., Wahid, K., Alam, M.S. (2020). Blind, cuff-less, calibration-free and continuous blood pressure estimation using optimized inductive group method of data handling. *Biomedical Signal Processing and Control*, *57*, 101682.

Mori, H., Saito, I., Eguchi, E., Maruyama, K., Kato, T., Tanigawa, T. (2014). Heart rate variability and blood pressure among Japanese men and women: A community-based cross-sectional study. *Hypertens. Res., 37*, 779–784.

Pan, J., Zhang, Y. (2017). Improved blood pressure estimation using photoplethysmography based on ensemble method. Proceedings - 14th International Symposium on Pervasive Systems, Algorithms and Networks, I-SPAN, 11th International Conference on Frontier of Computer Science and Technology, FCST and 3rd International Symposium of Creative Computing, ISCC, 105-111.

Paviglianiti, A., Randazzo, V., Villata, S., Cirrincione, G., Pasero, E. (2022). A comparison of deep learning techniques for arterial blood pressure prediction. *Cognitive Computation*, *14*, 1689-1710.

Reckelhoff, J.F. (2001). Gender differences in the regulation of blood pressure. *Hypertension*, *37*, 199-208.

Ribezzo, S., Spina, E., Di Bartolomeo, S., Sanson, G. (2014). Noninvasive techniques for blood pressure measurement are not reliable alternative to direct measurement: A randomized crossover train in ICU. *Sci. World J., 2014*, 353628.

Ruiz-Rodriguez, J.C., Ruiz-Sanmartin, A., Caballero, J., Garcia-Roche, A., Riera, J., Nuvials, X., de Nadal, M., de Sola-Morales, O., Serra, J., Rello, J. (2013). Innovative continuous non-invasive cuffless blood pressure monitoring based on photoplethysmography technology. *Intensive Care Med*., *39*, 1618-1625.

Sagirova, Z., Kuznetsova, N., Gogiberidze, N., Gognieva, D., Suvorov, A., Chomakhidze, P., Omboni, S., Saner, H., Kopylov, P. (2021). Cuffless blood pressure measurement using a smartphone-case based ECG monitor with photoplethysmography in hypertensive patients. *Sensors*, *21*, 3525.

Samimi, H., Dajani, H.R. (2022a). Cuffless blood pressure estimation using calibrated cardiovascular dynamics in the photoplethysmogram. *Bioengineering*, *Special Issue on Machine Learning for Biomedical Applications, 9*(446).

Samimi, H., Dajani, H.R. (2022b). Cuffless blood pressure estimation using cardiovascular dynamics. In Proceeding of the International Conference on Electrical, Computer and Energy Technologies (ICECET 2022), Prague, Czech Republic, available in IEEE Xplore: https://ieeexplore-ieee-org.proxy.bib.uottawa.ca/document/9872800.

Shao, J., Shi, P., Hu, S., Yu, H. (2020). A revised point-to-point calibration approach with adaptive errors correction to weaken initial sensitivity of cuff-less blood pressure estimation. *Sensors, 20*, 2205.

Shimada, K., Kario, K., Kushiro, T., Teramukai, S., Ishikawa, Y., Kobayashi, H., Saito, I. (2015). Differences between clinic blood pressure and morning home blood pressure, as shown by Bland-Altman plots, in a large observational study (HONEST study). *Hypertens. Res.*, *38*, 876–882.

Slapnicar, G., Mlakar, N., Lustrek, M. (2019). Blood pressure estimation from photoplethysmogram using a spectro-temporal deep neural network. *Sensors*, *19*, 3420.

Soh, D.C.K., Ng, E.Y.K., Jahmunah, V., Oh, S.L., Tan, R.S., Acharya, U.R. (2020). Automated diagnostic tool for hypertension using convolutional neural network, *Computers in Biology and Medicine*, *126*, 103999.

Sulochana, C.H. (2021). A review of photoplethysmography based measurement of blood pressure and heart rate variability. *J. Bioeng. Biomed. Sci., 11*(862).

Takalo, R., Korhonen, I., Turjanmaa, V., Majahalme, S., Tuomisto, M., Uusitalo, A. (1994). Short-term variability of blood pressure and heart rate in borderline and mildly hypertensive subjects. *Hypertension, 23*, 18–24.

Verberk, W.J., Kroon, A.A., Kessels, A.G.H., de Leeuw, P.W. (2005). Home blood pressure measurement: a systematic review. *J. Am. Coll. Cardiol.*, *46*, 743–751.

Wang, Q., Zeng, Q., Tao, J., Sun, L., Zhang, L., Gu, T., Wang, Z., Chen, L. (2019). Estimating $PM_{2.5}$ concentrations based on MODIS AOD and NAQPMS data over Beijing–Tianjin–Hebei. *Sensors*, *19*, 1207.

Wang, Z., Zhang, Y. (2017). A novel frequency domain method for estimating blood pressure from photoplethysmogram. Proceedings of the 9th International Conference on Signal Processing Systems, 201-206.

Wang, L., Zhou, W., Xing, Y., Zhou, X. (2018). A novel neural network model for blood pressure estimation using photoplethesmography without electrocardiogram. *Journal of Healthcare Engineering*, *2018*, 7804243.

World Health Organization. (2023, January 05). *WHO reveals leading causes of death and disability worldwide: 2000-2019*. https://www.who.int/news/item/09-12-2020-who-reveals-leading-causes-of-death-and-disability-worldwide-2000-2019.

Xing, X., Ma, Z., Zhang, M., Zhou, Y., Dong, W., Song, M. (2019). An unobtrusive and calibration-free blood pressure estimation method using photoplethysmography and biometrics. *Scientific Reports*, *9*, 8611.

Yamakoshi, T., Rolfe, P., Yamakoshi, K.I. (2021). Cuffless blood pressure estimation based on haemodynamic principles progress towards mobile healthcare. *Peer J.*, *9*(e11479).

Yao, Y., Rosasco, L., Caponnetto, A. (2007). On early stopping in gradient descent learning. *Constr. Approx., 26*, 289–315.

Chapter 6: Conclusions and Future Work

This work focused on using cardiovascular dynamics as a means for cuffless blood pressure monitoring. We investigated the feasibility of this idea by studying cardiovascular dynamics over short intervals of a few minutes. During this process, calibration-free and calibrated methods that use IBI information on its own or as a complement to other cuffless BP estimation techniques were developed and evaluated. We focused on using information solely from the photoplethysmogram signal as opposed to multiple signals that are generated from different sensors in order to simplify the approach. More sensors result in more complications during data collection as one needs to consider artifacts etc., while a single sensor simplifies the hardware and possibly makes it practical for in wearable devices such as health watches. Also, processing signals that come from different sources create its own difficulties like synchronization or denoising. In addition, when we use information from IBI dynamics, that relies on the timing variation between the peaks or troughs of the signals, it is expected to reduce sensitivity to changes in sensor placement or different skin colours. This advantage, however, needs to be verified in future studies.

We started this work by looking at the possibility of using cardiovascular dynamics as a stand-alone method for cuffless estimation of blood pressure. Initially, we used normalised ABP and after establishing the possibility of use of PPG as a surrogate for the arterial pulse waveform in estimation of BP, based on analysis of dynamic changes, we moved to perform the BP estimation using the PPG signal. We obtained promising results especially for DBP estimation.

We then added a calibration stage using a mathematical model based on reflective PTT. This new method improved our estimation accuracy measured by standard deviation of error and mean absolute error. MAE and SDE were reduced by 42% and 45% for SBP and by 35% and 36% for DBP, respectively. With the substantial improvement that we achieved by adding the calibration stage, we performed some additional experiments to determine the feasibility

of substituting the mathematical calibration with information from PPG morphology in order to achieve a calibration-free BP estimation method. The results from the new proposed process gave similar improvement as the calibrated method. Using features from PPG morphology to replace the calibration step increased the accuracy of the estimation. MAE and SDE were reduced by 51% and 49% for SBP and by 34% and 44% for DBP, when compared to the results solely from IBI dynamics. We then tested our new algorithm on never-seen data collected from 25 new patients and were able to estimate the blood pressure for this group with MAE/SDE of 7.41 mmHg/10.40 mmHg for SBP and 3.32 mmHg/4.89 mmHg for DBP.

In conclusion, this work has demonstrated that the information from cardiovascular dynamics can be used by itself or in conjunction with other known methodologies such as PPG morphology, for the purpose of cuffless blood pressure estimation. This research can be extended in the future to include combining IBI dynamics features with other BP estimation methodologies to improve the accuracy.

Overall, the contribution of this work can be summarized as:

- IBI dynamics of PPG signals over brief intervals may be used for cuffless BP estimation.
- The PPG can be used as a surrogate for the arterial pulse waveform in the estimation of BP, based on IBI dynamics.
- A mathematical model based on R-PTT can be used as a means for calibration of cuffless BP estimation.
- Calibration step could be replaced by an estimation from the PPG morphology to provide a calibration-free BP estimation method.
- Information from cardiovascular dynamics can be combined with other cuffless BP estimation methods to improve the accuracy.

This work faced number of limitations with the majority of them being closely tied to the nature of the dataset that was used. One of the constraints was unavailability of certain information such as the age, height, weight, and sex of the participants that could have provided valuable insights in the estimation process. Additionally, the size of dataset and signal duration were also limited, causing difficulty in proper evaluation and comparison of methods. A more extensive dataset would have enabled a more comprehensive assessment and generalization of the methods used. Similarly, longer signal duration would have helped in verification of the proposed methods under varying physical conditions. Furthermore, regarding the calibration method, it is noteworthy that the non-invasive blood pressure measurement used in this study was based on the average value obtained over multiple beats. It would be advantageous to have the dataset with a single reading from a cuff-based measurement, as this would better represent real life applications. While most of the limitations were due to factors beyond our control, others such as manually inspecting PPG signals instead of implementing an automated tool, may have been avoidable with further work.

In conclusion, it is important to note that the limitations mentioned above should not overshadow the findings of this research. Instead they should be used in helping to set a clear path for future research in the area of cuffless blood pressure estimation. To achieve this goal several areas of future research are proposed.

First, it would be beneficial to confirm whether the calibration-free status of the proposed methodology can be maintained over extended periods by using longer datasets. By doing so, researchers can determine if the proposed method is reliable for long term blood pressure monitoring without need of calibration. Second, the use of datasets collected from wearable devices such as healthwatches could be explored. These devices are readily available commercially and that makes collection of large dataset more convenience, and blood pressure estimation through healthwatches would make this application more accessible to a wider demographic. It is important to highlight that all the data used in our study was collected

in a hospital environment (either ICU or surgical unit), where patients were in a stationary position on a bed with almost no movement. This data would differ from that collected with healthwatches, as arm movement or wrist position not only interduce noise but they also have the potential to impact the morphology of the PPG. Third, the hypothesis that blood pressure estimation based on IBI dynamics is less susceptible to skin color can be explored by collecting datasets from individuals with different skin colors. Researchers could then evaluate the effectiveness of the proposed methodology and determine if it can overcome the limitation that other methods are facing when estimating blood pressure associated with different skin color. Fourth, it would be beneficial to evaluate the accuracy of the proposed method under different physical conditions. For this, datasets that are collected during daily activities that may affect the quality of the PPG signal used in blood pressure estimation could be considered. Also, additional information such as age, height, weight, and sex of participants can be added to the datasets. This information can positively contribute to the accuracy of the estimation and allow the method to be more effective. Last, combining IBI dynamics features with other blood pressure estimation methodologies could lead to more reliable blood pressure estimation. By using multiple estimation methods, the accuracy and robustness of the blood pressure estimation may be improved which in turn would make monitoring and management of blood pressure more effective.

Addendum

A: Data that is used in this research

In our work we used two main data directories with different number of signals used for each experiment. The table below presents the data that was used for each experiment.

Table A-1. List of datasets that were used for each experiment in a chapter along with number of patients that the signal was collected from.

Relevant chapter	Experiment	Dataset	Number of patients
Chapter 3	BP estimation based normalized on ABP	UCI	390
Chapter 3	Correlation between normalized ABP and PPG	UCI	390
Chapter 3	BP estimation based on PPG	UCI	200
Chapter 4	BP estimation for all BP estimation models	The university of Queensland	30
Chapter 4	Sensitivity analysis	The university of Queensland	30
Chapter 4	Computational complexity	The university of Queensland	30
Chapter 5	BP estimation based on IBI, calibration and PPG morphology	The university of Queensland	30
Chapter 5	Correlation between BP estimation based on IBI, calibration and PPG morphology models	The university of Queensland	30
Chapter 5	BP estimation based on IBI and different PPG morphology methods	UCI	200
Chapter 5	Evaluation of the proposed method on never seen test data	UCI	25

B: Bland-Altman Plots for Chapters 3 & 4

Blood pressure estimation results from Chapters 3 and 4 along with their corresponding Bland-Altman plots are presented below. The Bland-Altman method is used to compare two different measurement techniques by quantifying the agreement between measurements using a graphical method. It is different from correlation analysis, which can sometimes lead to incorrect or uncertain conclusions when comparing two measurement methods (Shimada, et al., 2015).

Table B-1. Blood pressure estimation performance using IBI features from 390 normalized arterial pulse waveforms. 5 features are used for systolic BP and 6 features for diastolic BP. The results are averaged over the 390 patients.

	ME (mmHg)	SDE (mmHg)	MAE (mmHg)
Diastolic BP	-0.7	7.16	5.85
Systolic BP	-1.17	16.86	13.97

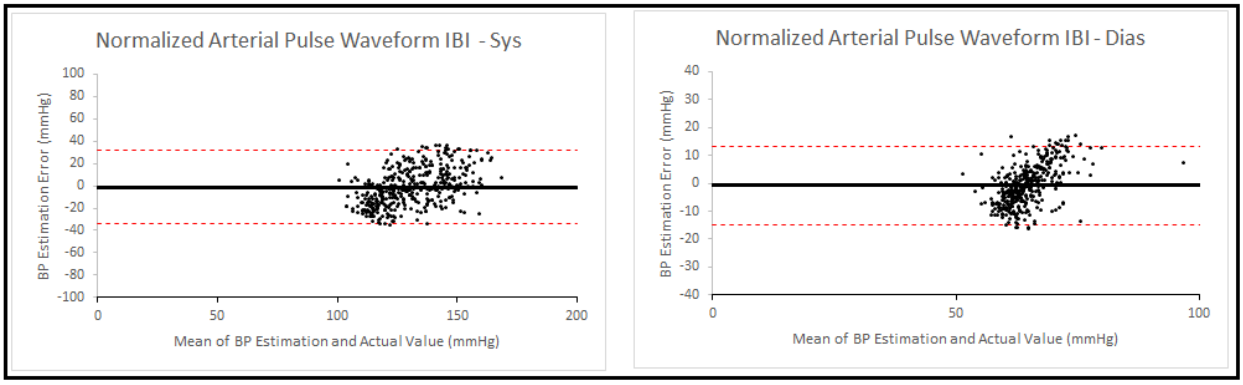

Figure B-1. Bland–Altman plots presenting systolic and diastolic blood pressure estimations using IBI features from 390 normalized arterial pulse waveforms based on the proposed estimation method in Chapter 3. This plot corresponds to Table B-1.

Table B-2. Blood pressure estimation performance using IBI features from 200 PPG waveforms. Five and six features are used for systolic BP and diastolic BP respectively. Results are averaged over the 200 patients.

	ME (mmHg)	SDE (mmHg)	MAE (mmHg)
Diastolic BP	0.03	7.91	5.75
Systolic BP	0.09	18.81	14.49

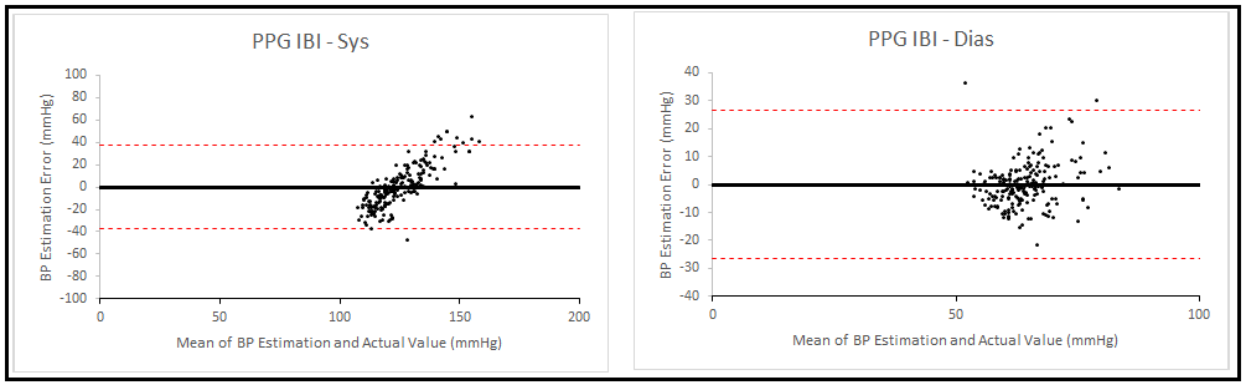

Figure B-2. Bland-Altman plots presenting systolic and diastolic blood pressure estimations using IBI features from 200 PPG waveforms based on the proposed estimation method in Chapter 3. This plot corresponds to Table B-2.

Table B-3. Blood pressure estimation performance using IBI features from 30 PPG waveforms. Five features are used for DBP and four are used for SBP. Estimation is carried out using the ANN described in the text, and the results are averaged over the 30 patients.

Dynamics			
	ME (mmHg)	**SDE (mmHg)**	**MAE (mmHg)**
Diastolic BP	0.14	10.97	7.54
Systolic BP	-0.39	22.16	15.26

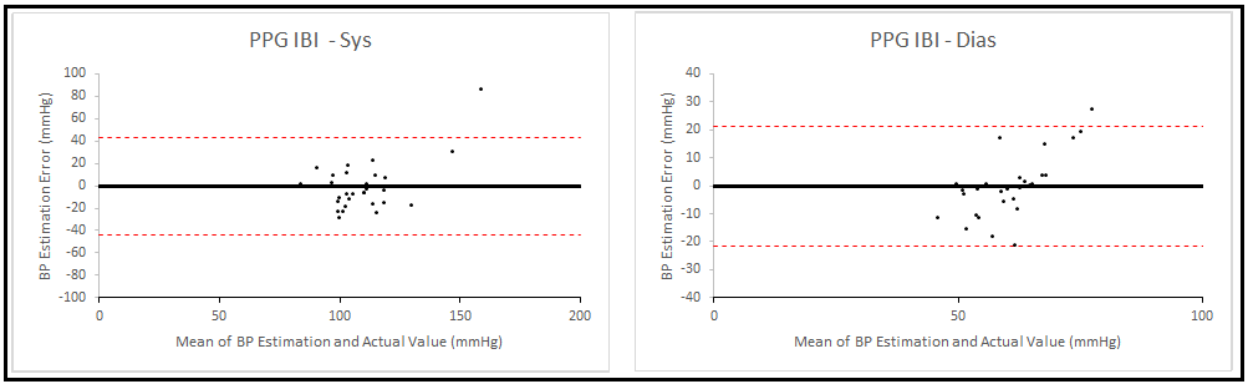

Figure B-3. Bland-Altman plots presenting systolic and diastolic blood pressure estimations using IBI features from 30 PPG waveforms based on the proposed estimation method in Chapter 4. This plot corresponds to Table B-3.

Table B-4. Blood pressure estimation performance using reflective PTT in a calibrated mathematical model with 30 PPG waveforms. The results are averaged over the 30 patients.

Modeling			
	ME (mmHg)	**SDE (mmHg)**	**MAE (mmHg)**
Diastolic BP	0.45	8.36	5.47
Systolic BP	3.18	12.49	9.11

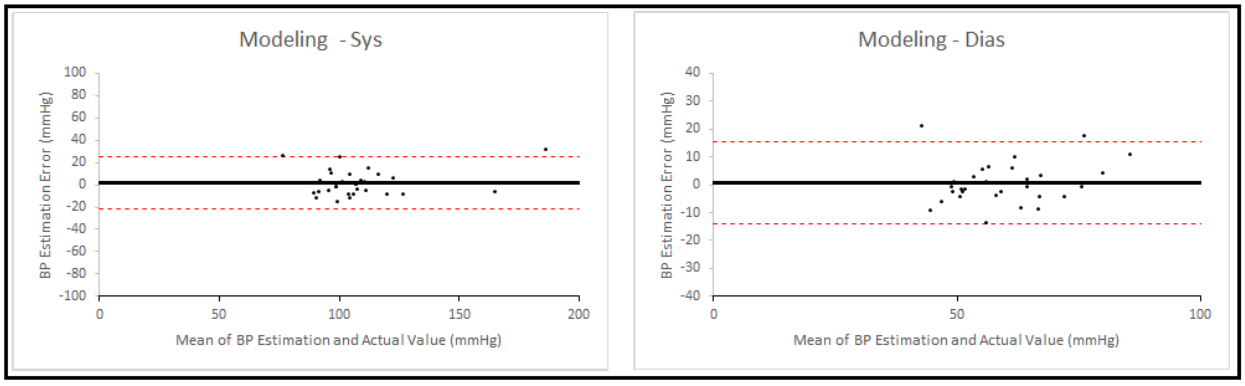

Figure B-4. Bland-Altman plots presenting systolic and diastolic blood pressure estimations using reflective PTT in a calibrated mathematical model with 30 PPG waveforms based on the proposed estimation method in Chapter 4. This plot corresponds to Table B-4.

Table B-5. Blood pressure estimation performance using IBI features and estimation from a calibrated mathematical model from 30 PPG waveforms. Three features are used for SBP and DBP. Estimation is carried out using the ANN described in the text, and the results are averaged over the 30 patients.

Dynamics + Modeling			
	ME (mmHg)	**SDE (mmHg)**	**MAE (mmHg)**
Diastolic BP	0.59	7.07	4.92
Systolic BP	2.52	12.15	8.89

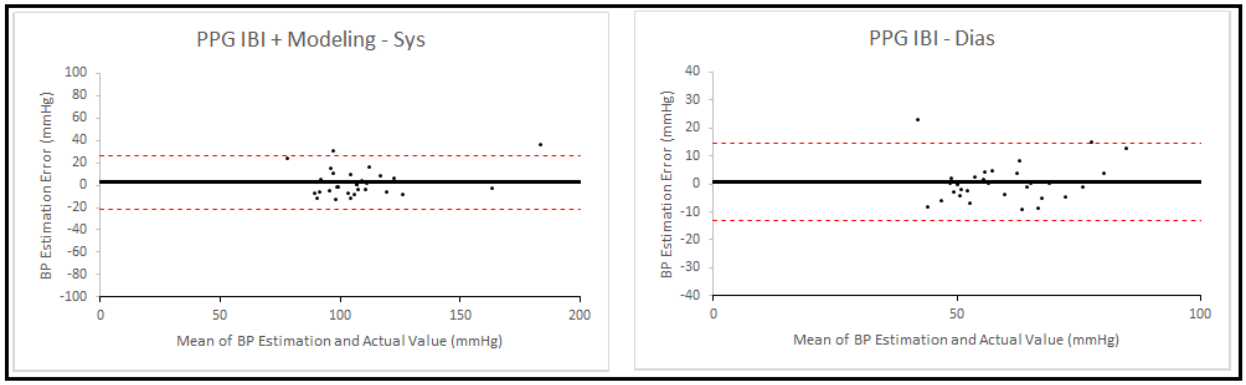

Figure B-5. Bland-Altman plots presenting systolic and diastolic blood pressure estimations using IBI features and estimation from a calibrated mathematical model from 30 PPG waveforms based on the proposed estimation method in Chapter 4. This plot corresponds to Table B-5.

The results from some of the Bland-Altman analysis above show a tendency for the difference between estimated and the reference blood pressure values to increase as the mean of the two BP values increases. This can be due to differences in interindividual variability obtained with the two methods as was mentioned in Section 5.4. When the Bland-Altman plot is generated for data A and B, if standard deviation of A and B are the same, the slope of the regression line will be zero. If standard deviation of A is greater than B, then there is an upward slope for the regression line and if standard deviation of B is greater than A then the regression slope will be downward.

C: Clarification on Chapter 4 Sensitivity Analysis

To clarify the sentence "Since the mathematical model was found to be sensitive to this parameter, effort should be made in carefully choosing its value during experimentation." in Section 4.3, we need to add that the coefficient that has the highest sensitivity in the model

is directly associated with SBP, DBP and R-PTT based on Equation 4-13. During calibration stage, when the coefficient value is determined, all three parameters of SBP, DBP and R-PTT can be measured. Therefore, it is crucial to pay close attention to collecting accurate measurements of these parameters, as even a small error in any of them can lead to variations in the coefficient and consequently have a significant impact on the output.

D: Statistical Significance of Improvement for Test Data in Chapter 5

We performed the student's t-test to investigate the statistical significance of the improvement that the proposed method in Chapter 5 made on blood pressure estimation for the test data from 25 patients that was never seen by the algorithm before. Since we hypothesized that using IBI dynamics improved the accuracy, one-tailed paired t-tests were performed to compare the Means of Absolute Errors (i.e. MAE) between the proposed estimation method (using IBI and PPG morphology) and the BP estimation method based on the PPG IBI alone and the PPG morphology alone for both SBP and DBP.

The result from the Student's t-test is presented in Tables D-1 and D-2. Based on Table D-1 there is a significant difference in MAE of SBP between the proposed method (mean = 7.41, standard error = 1.65) and the PPG IBI method (mean = 12.1, standard error = 1.65); with a $p = 0.023$ and a strong trend towards significance in MAE of DBP of the proposed method (mean = 3.33, standard error = 0.71) and the PPG IBI method (mean = 4.63, standard error = 0.65); with a $p = 0.054$. Table D-2 reveals a strong trend towards significance in MAE of SBP between the proposed method (mean = 7.41, standard error = 1.65) and the PPG morphology method (mean = 9.37, standard error = 1.26); with a $p = 0.054$ and insufficient evidence towards significance in MAE of DBP of the proposed method (mean = 3.33, standard error = 0.71) and the PPG morphology method (mean = 3.54, standard error = 1.04); with a $p = 0.35$.

Table D-1. T-test results comparing MAE between the proposed BP estimation method in Chapter 5 and our original PPG IBI method discussed in Chapter 3. Blood pressure estimation is based on the results from the test data from 25 never-seen-before patients that was discussed in Section 5.3.3. the sub-table on the left is the result of the t-test for SBP and the one on the right is for DBP.

t-Test: Paired Two Sample for Means - SBP		
	Absolute Error (ibi)	Absolute Error (ibi+morphology)
Mean	12.1	7.4128
Standard Error (SE)	1.65	1.65
P-Value	0.023	

t-Test: Paired Two Sample for Means - DBP		
	Absolute Error (ibi)	Absolute Error (ibi+morphology)
Mean	4.63	3.33
Standard Error (SE)	0.65	0.71
P-Value	0.054	

Table D-2. T-test results comparing MAE between the proposed BP estimation method in Chapter 5 and the PPG morphology method. Blood pressure estimation is based on the results from the test data from 25 never-seen-before patients that was discussed in Section 5.3.3. the sub-table on the left is the result of the t-test for SBP and the one on the right is for DBP.

t-Test: Paired Two Sample for Means - SBP		
	Absolute Error (morphology)	Absolute Error (ibi+morphology)
Mean	9.37	7.41
Standard Error (SE)	1.26	1.65
P-Value	0.054	

t-Test: Paired Two Sample for Means - DBP		
	Absolute Error (morphology)	Absolute Error (ibi+morphology)
Mean	3.54	3.33
Standard Error (SE)	1.04	0.71
P-Value	0.346	

It is therefore seen that in both comparisons for SBP and one of the comparisons for DBP, combining IBI dynamics and morphology produced an improvement in accuracy over IBI dynamics alone or morphology alone that is either statistically significant or very close to the standard threshold for statistical significance of $p = 0.05$. It is noteworthy that 1) these results were obtained with a relatively small value of N ($N = 25$), and 2) it is important to distinguish between statistically significant differences and "physically" significant differences in that a method may show a statistically significant improvement (e.g. if N is large), but not a

physically significant improvement (where for BP estimation, the physical improvement corresponds to the reduction in error in mmHg).

E: Clarification on Equation 4-16

It is important to emphasize that although there exist other methods to obtain more precise values for MBP, Equation 4-16 serves as an approximation of MBP that enables us to model the behavior of blood pressure.

F: BP Estimation Tracking Over Time

In this section, we investigated the ability of our proposed method to track changes in blood pressure (BP) over time. To achieve this, we required long recordings of PPG signals. Since the longest available signals in our dataset were from the University of Queensland Vital Signs database, we used the PPG signals as test data and non-invasive BP measurements as reference blood pressure. We visually inspected all the data and selected recordings with minimal or no interruptions throughout the entire duration. Additionally, we chose recordings that were longer than 40 minutes, resulting in a dataset from 17 patients.

Next, we divided the signals into sections of 10 minutes and used the same methodology as described in Section 5.3.3 for feature extraction and estimation such as averaging parameters for each feature and averaging the non-invasive reference BP values over 10 minutes, and using leave-one-out method during development of the ANN and evaluation process.

The results of the experiment are presented in Figure F-1 for systolic blood pressure and Figure F-2 for diastolic blood pressure. As shown in these figures, our proposed method generally follows the same trend of increases or decreases in the reference BP for both systolic and diastolic blood pressure estimations. However, it is noteworthy to mention here that the recordings were relatively short, and were all obtained from patients in operating rooms at the hospital. As a result, changes in cardiovascular dynamics, on which our method depends,

may not have been large over the duration of the recording. Future work should investigate whether our proposed method can track changes in BP over longer periods of time and over different daily activities that would be expected to involve more significant changes in cardiovascular dynamics.

Figure F-1. Systolic blood pressure estimation for 17 patients compared to the corresponding reference BP. The estimation is based on the proposed method in Section 5.3.3 that uses features from the PPG IBI and estimation from PPG morphology, and the reference values are from non-invasive BP measurements.

Figure F-2. Diastolic blood pressure estimation for 17 patients compared to the corresponding reference BP. The estimation is based on the proposed method in Section 5.3.3 that uses features from the PPG IBI and estimation from PPG morphology, and the reference values are from non-invasive BP measurements.